Simultaneous Optimisation of Composite Wing Structures and Control Systems for Active and Passive Load Alleviation

Binder, S.

DOI
10.4233/uuid:fac93ccf-7e0b-4971-a797-d2617e378a1d

Publication date
2021

Document Version
Final published version

Citation (APA)
Binder, S. (2021). *Simultaneous Optimisation of Composite Wing Structures and Control Systems for Active and Passive Load Alleviation*. [Dissertation (TU Delft), Delft University of Technology]. https://doi.org/10.4233/uuid:fac93ccf-7e0b-4971-a797-d2617e378a1d

Important note
To cite this publication, please use the final published version (if applicable).
Please check the document version above.

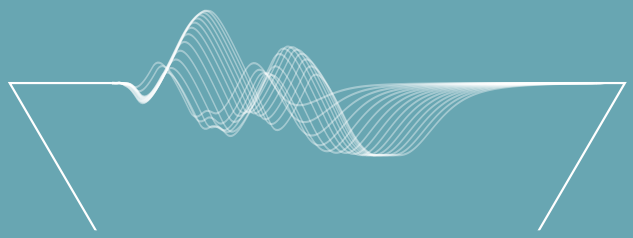

Simultaneous Optimisation of Composite Wing Structures and Control Systems for Active and Passive Load Alleviation

S. Binder

Simultaneous Optimisation of Composite Wing Structures and Control Systems for Active and Passive Load Alleviation

Simultaneous Optimisation of Composite Wing Structures and Control Systems for Active and Passive Load Alleviation

Dissertation

for the purpose of obtaining the degree of doctor
at Delft University of Technology
by the authority of the Rector Magnificus, Prof. dr. ir. T.H.J.J. van der Hagen,
chair of the Board for Doctorates
to be defended publicly on
Tuesday 6 July 2021 at 15:00 o'clock

by

Simon Binder

Diplom-Ingenieur, Technische Universität München, Germany,
born in Filderstadt, Germany.

This dissertation has been approved by the promotors.

Composition of the doctoral committee:

Rector Magnificus,	chairperson
Dr. ir. R. De Breuker,	Delft University of Technology, promotor
Prof. dr. C. Bisagni,	Delft University of Technology, promotor
Independent members:	
Prof. dr. N. Bartoli,	SUPAERO-ISAE/ONERA, France
Prof. dr. ir. W.R. Krüger,	Technische Universität Berlin, Germany
Prof. dr. P. Marzocca,	Royal Melbourne Institute of Technology, Australia
Prof. dr. ir. R. Benedictus,	Delft University of Technology
Prof. C.A. Dransfeld,	Delft University of Technology, reserve member
Other members:	
Dr. A. Wildschek,	Airbus Operations S.A.S., France

Keywords: Aeroelasticity, Aircraft Design, Active Load Control, Aeroelastic Tailoring, Model Order Reduction

Printed by: Ipskamp Drukkers B.V., Enschede, The Netherlands

Front & Back: Design by Simon Binder.

ISBN 978-94-6421-412-3

An electronic version of this dissertation is available at
http://repository.tudelft.nl/.

CONTENTS

SUMMARY

Simultaneous Optimisation of Composite Wing Structures and Control Systems for Active and Passive Load Alleviation

The aviation industry has made ambitious commitments to drastically reduce the environmental impact of civil aviation over the next 30 years. The increased utilisation of composite materials allows more than only weight savings due to the high strength to weight ratio. Further improvements can be made by exploiting the anisotropic material properties and thereby steering the aeroelastic deformations to alleviate the loads. This method is known as aeroelastic tailoring. Another method that enables the design of lighter weight aircraft structures is the use of active load control. Load peaks which occur during manoeuvres or under gust flight conditions can be reduced by control surface deflections which are commanded by control laws. The combination of these active control methods with the aforementioned passive method of aeroelastic tailoring is promising. However, possibly undesired interaction between the two technologies may lead to reduced overall performance. The integrated design of active load control and passive structural tailoring for civil transport aircraft wings represented a research gap. Therefore, the research outlined in this work focused on the investigation of the interaction between both technologies. Furthermore, the impact on the preliminary design of active adaptive wing structures for future civil transport configurations is examined.

A framework was first developed, which allows the rapid integrated preliminary design of actively controlled and structurally tailored wings. Due to the high model order, the simulation of unsteady aerodynamics is decisive for the computational efficiency of the overall framework. The generation of reduced order unsteady aerodynamic models that can be used throughout an entire aeroservoelastic optimisation posed one of the major challenges. These models must have high robustness against structural modifications and changes of the control surface layout that occur in the optimisations or studies carried out in the preliminary aircraft design phases. A suitable model order reduction method for linear aerodynamic models was presented using the concept of synthetic mode shapes. The proposed method allows a reduction of the model order of about two orders of magnitude while still preserving enough accuracy for the intended preliminary design optimisations. Furthermore, a 77% reduction in order was achieved compared to the models resulting from a model order reduction without prior input and output transformation on the synthetic mode shapes. Also, only a few synthetic mode shapes were required to set up the reduced order aerodynamic model that could be used throughout an entire aeroservoelastic optimisation.

The examination of the interaction between active and passive load alleviation in the

preliminary design of a typical transport aircraft configuration required the aerodynamic modelling of spoilers. A correction law of the spatial distribution of the boundary condition was proposed to improve the accuracy of panel-based aerodynamic modelling of spoiler control surfaces by using simulation data of higher fidelity. With the formulation of a generalised spatial distribution law of the boundary condition, this methodology allows the study of control surface layouts comprising spoiler devices.

To accomplish the integrated optimisation, the principal stiffness direction of the wing skins were used as a design parameter to allow for aeroelastic tailoring. Manoeuvre load alleviation was introduced in the design space in the form of static control surface deflections which redistribute the aerodynamic loads during critical manoeuvres. Finally, gust load alleviation was added to the design problem in terms of a feed-forward control law whose filter gains are used as design variables. The weight optimisation problem was then stated by the formulation of various constraints, such as the nonlinear constraints of the actuation system, namely rate and deflection saturation.

Based on the results of several optimisations, a thorough analysis was then conducted to draw conclusions about the interaction between active and passive load alleviation. The optimisations differ concerning the selection of the simultaneously designed parameters. Both the individual and combined application of manoeuvre load alleviation, gust load alleviation and structural tailoring were considered and compared to an optimisation that does not involve any of the three load alleviation technologies. It was confirmed that most weight reduction is achieved by simultaneously considering all three load alleviation approaches. Also, it was shown that the load alleviation technologies adapt to the prevailing load hierarchy and active constraints. Consequently, their impact on the design can only be adequately assessed, and possible synergies can only be exploited if the technologies are optimised in a combined manner.

Due to the use of advanced materials and manufacturing processes, a tendency towards wing structures with increased structural flexibility can be observed in recent aircraft generations. In order to investigate the influence of this trend on the previously drawn conclusions, a continuous variation of the material allowables was carried out. The study revealed that increased structural flexibility promises significant gains in the effectiveness of aeroelastic tailoring, while the effectiveness of active control is compromised. In particular, it was emphasised that the added value of active gust load control in an active adaptive wing design is diminished with increased structural flexibility due to the increased material allowables. The findings supported the previously drawn conclusion that the assessment of structural tailoring without taking into account active control is producing incorrect results, as the increased structural flexibility further intensifies this.

Since the advantages of the integrated design are counterbalanced by considerable computational effort and intensive cross-divisional cooperation, alternative optimisation approaches were also examined: In addition to a separate design approach, a semi-sequential design approach was proposed in which subspaces are iteratively optimised focusing on either active or passive load alleviation. The comparison with the results from the simultaneous optimisation confirmed that a separate design approach is inferior in the realisation of the potentials. The proposed semi-sequential design approach, however, allows to decouple the disciplines partially and to develop active and passive technologies

in parallel with iterative updates.

With the examination of two configuration changes, another problem relevant to preliminary design is addressed in this thesis. The configuration changes include, on the one hand, a change in the control surface layout and on the other hand, the investigation of the installation of an active winglet. While the change of the control surface layout did not substantially affect the previously drawn conclusions, the active winglet caused the flutter speed to be reduced significantly. With the results, it was shown that the integrated design allows the adaptation of the technologies to the respective active constraints since structural tailoring contributed to the improvement of flutter characteristics in case they are relevant for the design. The example proved the necessity of integrated optimisation as flutter was only critical when active load control was considered in the design problem.

In summary, including parameters of active manoeuvre and gust load control systems in the multidisciplinary design optimisation of the aeroelastically tailored composite wing structures as presented and demonstrated in this thesis has two major advantages. On the one hand, the use of synergies between the load alleviation technologies is enabled, and on the other hand, mechanisms that cannot be intuitively grasped that are beneficial for the overall concept can be identified. However, in terms of the future development of active adaptive wing structures, further work is needed to include more control functions as well as more detailed constraint functions concerning the manufacturability of the resulting structural designs.

SAMENVATTING

Simultane optimalisatie van composieten vleugelconstructies en besturingssystemen voor actieve en passieve belastingsreductie

De luchtvaartindustrie heeft ambitieuze doelstellingen om het milieueffect van de burgerluchtvaart in de komende 30 jaar drastisch te verminderen. Het toegenomen gebruik van composietmaterialen maakt een gewichtsbesparing mogelijk door de hoge sterkte-gewichtsverhouding. Verdere verbeteringen kunnen worden bereikt door gebruik te maken van de anisotrope materiaaleigenschappen en zo de aëro-elastische vervormingen te beheersen om de belasting te verminderen. Deze methode staat bekend als aëro-elastisch maatwerk. Een andere methode die het ontwerpen van lichtere vliegtuigconstructies mogelijk maakt, is het gebruik van actieve belastingsreductie. Belastingspieken die optreden tijdens manoeuvres of verticale windbelasting kunnen worden verminderd door stuurvlakuitslagen die worden bepaald door een besturingssysteem. De combinatie van deze actieve controlemethoden met de reeds genoemde passieve methode van aëro-elastisch maatwerk is veelbelovend. Een mogelijk ongewenste interactie tussen de twee technologieën kan echter leiden tot een verminderde algemene prestatie. Het geïntegreerde ontwerp van actieve belastingscontrole en passieve structurele aanpassing van de vleugels van burgerluchtvaartuigen was nog niet terdege onderzocht in de literatuur. Het onderzoek in deze thesis richtte zich daarom op het onderzoek naar de interactie tussen de twee technologieën. Bovendien worden de gevolgen voor het voorontwerp van actieve adaptieve vleugelstructuren voor toekomstige civiele luchttransportconfiguraties onderzocht.

Allereerst is er een methode ontwikkeld dat het mogelijk maakt om snel een geïntegreerd voorontwerp te maken van actief gecontroleerde en structureel op maat gemaakte vleugels. Door de hoge vliegsnelheid is de simulatie van de transsone aërodynamica cruciaal voor de rekenkundige efficiëntie van de methode. Daarom was het genereren van dynamische aërodynamische modellen van gereduceerde orde, die kunnen worden gebruikt tijdens een volledige aëroservo-elastische optimalisatie, één van de grootste uitdagingen. Deze modellen moeten zeer robuust zijn tegen structurele aanpassingen in de lay-out van de stuurvlakken tijdens optimalisaties of studies in de voorontwerpfasen van het vliegtuigontwerp. Een geschikte methode om complexiteit van lineaire aërodynamische modellen te reduceren werd gepresenteerd aan de hand van het concept van de synthetische modusvormen. De voorgestelde methode maakt een reductie van de complexiteit met ongeveer twee ordegroottes mogelijk, met behoud van voldoende

nauwkeurigheid voor de beoogde voorlopige ontwerpoptimalisaties. Bovendien werd een 77% reductie in ordegrootte van het systeem bereikt in vergelijking met modellen zonder transformatie van de in- en uitvoer. Verder waren slechts enkele synthetische vormen nodig om het gereduceerde aërodynamische model te creëren dat in een volledige aëroservo-elastische optimalisatie kon worden gebruikt.

Het onderzoek naar de interactie tussen actieve en passieve belastingsvermindering in het voorontwerp van een typische transportvliegtuigconfiguratie vereiste de aërodynamische modellering van spoilers. Een correctiemethode van de randvoorwaarde werd voorgesteld om de nauwkeurigheid van de op panelen gebaseerde aërodynamische modellering van spoilers te verbeteren door gebruik te maken van complexere simulaties. Met de formulering van veralgemeende randvoorwaarde maakt deze methodiek het mogelijk om willekeurige besturingsoppervlakte-indelingen inclusief spoilers te onderzoeken.

Om de geïntegreerde optimalisatie uit te voeren, werd de hoofdstijfheidsrichting van de vleugelhuiden als ontwerpparameter gebruikt om een aëro-elastische aanpassing mogelijk te maken. De vermindering van de manoeuvrebelasting is in de ontwerpruimte geïntroduceerd in de vorm van statische stuurvlakuitslagen die de aërodynamische belastingen tijdens kritische manoeuvres herverdelen. Tot slot werd het ontwerpprobleem aangevuld met de vermindering van de verticale windbelasting in de vorm van een feedforward controle wet, waarvan de filtereigenschappen worden gebruikt als ontwerpvariabelen. Het probleem van de gewichtsoptimalisering werd vervolgens aangevuld met de formulering van verschillende randvoorwaarden, zoals de niet-lineaire randvoorwaarde van het aandrijfsysteem, namelijk de verzadiging van de snelheid en de verplaatsing van de actuator.

Op basis van de resultaten van een aantal optimalisaties is vervolgens een grondige analyse uitgevoerd om conclusies te trekken uit de interactie tussen actieve en passieve belastingsverlaging. De uitgevoerde optimalisaties verschillen in de selectie van de ontwerpparameters die al dan niet gelijktijdig worden meegenomen. Zowel de individuele als de gecombineerde toepassing van manoeuvrebelastingsvermindering, verticale windbelastingsvermindering en structurele aanpassing zijn beschouwd en vergeleken met een optimalisatie waarbij geen van de drie technologieën meegenomen is. Er werd ontdekt dat de meeste gewichtsvermindering wordt bereikt door alle drie de technologieën voor gewichtsvermindering mee te nemen. Ook werd aangetoond dat het belang van elk van de technologieën voor de vermindering van de belasting verandert naar mate de actieve randvoorwaarden van de optimalisatie veranderen. Bijgevolg kan hun impact op het ontwerp alleen adequaat worden beoordeeld en kunnen mogelijke synergieën alleen worden benut als de technologieën in combinatie met elkaar worden geoptimaliseerd.

Door het gebruik van geavanceerde materialen en productieprocessen worden vleugels flexibeler. Om de invloed van deze trend op de eerder getrokken conclusies te onderzoeken, is een continue variatie van materiaaleigenschappen uitgevoerd. Uit het onderzoek bleek dat een grotere structurele flexibiliteit een aanzienlijke verbetering van de effectiviteit van aëro-elastisch maatwerk laat zien, terwijl de effectiviteit van actieve controle vermindert. In het bijzonder werd benadrukt dat de toegevoegde waarde van actieve verticale windbelastingsreductie in een actief adaptief vleugelontwerp afneemt met een toenemende structurele flexibiliteit als gevolg van veranderende materiaaleigen-

schapen. De resultaten ondersteunen de eerder getrokken conclusie dat de evaluatie van de structurele aanpassing zonder rekening te houden met actieve controle tot verkeerde resultaten leidt, aangezien de toegenomen structurele flexibiliteit dit versterkt.

Aangezien de voordelen van een geïntegreerd ontwerp worden gecompenseerd door een aanzienlijk toegenomen rekentijd en een intensieve interdepartementale samenwerking, werden ook alternatieve optimalisatiebenaderingen onderzocht: naast een aparte ontwerpbenadering werd een semi-sequentiële ontwerpbenadering voorgesteld, waarbij subruimtes iteratief worden geoptimaliseerd, met de nadruk op ofwel actieve ofwel passieve belastingreductie. De vergelijking met de resultaten van de gelijktijdige optimalisatie bevestigt dat een aparte ontwerpbenadering inferieur is aan de simultane. De voorgestelde semi-sequentiële ontwerpbenadering maakt het echter mogelijk om de disciplines gedeeltelijk te ontkoppelen en actieve en passieve technologieën te ontwikkelen, parallel aan iteratieve updates.

Met het onderzoek naar twee configuratiewijzigingen wordt in dit proefschrift een ander probleem aangepakt dat relevant is voor het voorontwerp. De configuratiewijzigingen bestaan enerzijds uit een wijziging van de lay-out van de sturvlakken en anderzijds uit het onderzoek naar de installatie van een actieve winglet. Hoewel de verandering van de lay-out van het stuurvlak geen significante invloed had op de eerder getrokken conclusies, leidde de actieve winglet tot een significante vermindering van de fluttersnelheid. Met de resultaten zou kunnen worden aangetoond dat het geïntegreerde ontwerp het mogelijk maakt de technologieën aan te passen aan de respectievelijke actieve technologieën, aangezien structurele aanpassingen bijdragen aan de verbetering van de flutterkarakteristieken, voor zover deze relevant zijn voor het ontwerp. Het voorbeeld bewees de noodzaak van een geïntegreerde optimalisatie omdat flutter alleen kritisch was als er in het ontwerpprobleem rekening werd gehouden met actieve belastingsvermindering.

Samenvattend kan worden gesteld dat het opnemen van de parameters van actieve manoeuvre- en windbelastingsregelsystemen in de multidisciplinaire optimalisatie van aëro-elastisch op maat gemaakte composieten vleugelconstructies, zoals in dit proefschrift wordt aangetoond, twee grote voordelen heeft. Met betrekking tot de toekomstige ontwikkeling van actieve adaptieve vleugelconstructies is echter verder werk nodig om meer controlemethoden en meer gedetailleerde randvoorwaarden met betrekking tot de produceerbaarheid van de resulterende constructieontwerpen op te leggen.

Academic Contribution of this Dissertation

Current processes employed for the preliminary design of aircraft structures do not allow the analysis and optimisation of the interaction between active and passive load alleviation. While the presence of a control law can be considered in structural sizing processes, integrated design of the active control system and composite structures is not a functionality in conceptual design tools. Furthermore, the interaction between the three technologies of active gust load alleviation, active manoeuvre load alleviation and aeroelastic tailoring has not been investigated in the setting of preliminary wing design.

This dissertation aims to relocate the border of knowledge to shed light on the interaction between active and passive means for manoeuvre and gust load alleviation. The contributions listed in this section are split in (i) the development of a framework that allows the integrated analysis and optimisation of the said technologies and (ii) the study of the synergies and interaction of active and passive method for load alleviation:

Aeroservoelastic Modelling and Optimisation Framework

- An object-oriented framework was developed, allowing the co-design of control systems for load alleviation and tailored composite wing structures. By the combination of two existing toolchains, the open-source optimisation framework was created efficiently reusing existing capabilities such as the realisation of passive aeroelastic tailoring by exploiting the anisotropic properties of composite materials. New features have been implemented, such as the consideration of active aeroelastic control for static and dynamic load alleviation, including nonlinear constraints of the actuation system, namely rate and deflection saturation.

- A novel method for modelling aerodynamics of spoiler controls has been developed. Aerodynamic models created with panel-based potential flow methods are improved by changing the spatial distribution of the boundary condition. The proposed generalized distribution law was derived from higher-fidelity numerical flow simulation data. As the method allows the modelling of any spoiler geometry and position, it is particularly suitable for design studies in the context of preliminary and conceptual aircraft design.

- A procedure for the generation of reduced order aerodynamic models based on a combination of the concepts of balanced proper orthogonal decomposition and synthetic mode shapes has been developed. Due to their robustness to structural and control surface layout variation, the resulting reduced order models are suitable for the application in aeroservoelastic optimisation problems where the

design space is spanned by structural parameters and parameters of the control surface layout. The proposed method improves the accuracy per order of reduced order models resulting compared to the sole application of the balanced proper orthogonal decomposition.

- Alongside the model order reduction method, three different types of synthetic mode shapes were formulated for complete aircraft configurations based on zonal partitioning, Chebyshev polynomials and radial basis functions to transform the spatially distributed inputs and outputs of the full-order aerodynamic models. An analysis of the influence of type and dimension of the set of synthetic mode shapes has been carried out. Both parameters are identified as critical tuning parameters for the achievable accuracy in aeroservoelastic analyses carried out with the reduced order models and the computational effort required for the generation of the reduced order models. Two sets of parameters are found that are (i) optimal concerning the accuracy per order of the resulting model and (ii) optimal in terms of computational effort required for the model generation.

The Interaction of Active and Passive Methods for Load Alleviation

- A series of simultaneous design optimisations have been carried out with the developed framework. The frontier of the state of the art was shifted by (i) the use of a long-haul transport aircraft configuration with a conventional control surface layout comprising spoiler controls that are used for load alleviation and roll control, and (ii) the simultaneous optimisation of the three technologies of active gust load alleviation, active manoeuvre load alleviation and structural tailoring. To reveal possible design differences in the optimisations and synergies between the technologies, all possible combinations of the three technologies were examined.

- By a gradual variation of the allowable material properties, it was demonstrated that the results mentioned in the previous point are highly dependent on the structural flexibility. The increased structural flexibility associated with future innovative materials and lightweight construction methods was achieved by varying the knockdown factor applied to the material properties.

- An optimisation algorithm is proposed in which subspaces of the overall parameter space are iteratively optimised. The algorithm proves to be useful if only limited computational resources are available or fast turnaround times are required, as is the case in the preliminary design.

- The applicability of the developed tools and methods for the preliminary design of future aircraft wings was demonstrated by the investigation of two configuration changes characteristic for the preliminary design: an alternative control surface layout and the use of an active winglet.

1

Introduction

The dream of flying is as old as humankind itself. Within the last century, civil aviation has experienced a journey from the dreams of bold pioneers to the daily life of most of us. This growth was accelerated by the development of civil jet-powered aircraft in the mid-50s and continues today, mainly due to the progressing globalisation. In the recently published global market forecast, Airbus estimates the traffic will double in 15 years with an average growth of 4.3% per year throughout the next 20 years [1]. Similarly, Boeing predicts a traffic growth of 4.6% per year in its current market outlook [2]. While traffic growth is economically promising, the numbers are alarming in terms of impact on nature and the environment. At 2.4%, the share of global CO_2 emissions was already disproportionately high in 2019 compared to the relative size of the industry [3]. As part of the "flightpath 2050" program, the European Commission, together with the European aviation industry, has set high goals to contain the consequences of this growth for the climate [4]. To protect the environment and energy supply, CO_2 emissions per passenger kilometre are to be reduced by 75% and NO_x emissions per passenger kilometre by 90% compared to the capabilities of aircraft from 2000.

In the past decades, tremendous improvements in fuel efficiency have been achieved by increasing the bypass ratio of jet engines. This trend is not only approaching technological limits, but the ever-increasing engine diameters are also causing significant integration problems for aircraft manufacturers: For example, the landing gear size has to be adjusted due to the required ground clearance. In other cases, complex active systems must be designed to counteract non-linear aerodynamic phenomena caused by the size of the engines, such as pitch-up dynamics due to flow separation. Concerning the potential of individual technologies, aerodynamic improvements and new materials or lightweight designs offer more significant potential in the future [5]. Radical configuration changes, e.g. blended wing bodies, are not planned for the generations of civil aircraft entering the service within the next ten years [6]. The potential for the improvement of those aircraft is primarily limited to technologies applied in wing design which are introduced in the following paragraph.

1

Wing of the (near) Future The driving factors of overall aircraft fuel efficiency are, in addition to the specific fuel consumption of the engine, aerodynamic performance and weight. A significant portion of the drag that drives the aerodynamic performance is the lift-induced drag, which has long been motivating the development of wings with a high aspect ratio. The importance of increasing the aspect ratio for the development of efficient aircraft is demonstrated by the recent maiden flight of the 777X where a complex folding mechanism allows the outer wing to be folded upwards at the airport to meet the span limiting box constraints [7]. While the high aspect ratio allows the intensity of the tip vortices causing the induced drag to be reduced, the resulting large deformations that occur in flight also might cause detrimental aeroelastic phenomena. Furthermore, the bending loads, which govern the structural weight of the wing, are increased especially near the wing root. An alternative approach to reduce the induced drag is the use of winglets. However, the additional weight attached to the wingtip has equally adverse effects on the aeroelastic behaviour.

Due to their excellent properties, carbon fibre reinforced plastics, also referred to as carbon composites or composites in the following, have quickly established a strong position in the aviation and aerospace industry. In addition to a strength-to-weight ratio that is superior to that of aluminium, which has been the industry standard for many years, the directional stiffness properties allow the realisation of so-called tailored structures. The directional stiffness properties can be adjusted by placing the fibre in a specific direction within the matrix. Tailoring refers to the advantageous use of directional stiffness either to optimally distribute a given load or to achieve a specific deformation for a given load. In the case of aerodynamic loads, the latter is also called aeroelastic tailoring. This technology, which was already patented in the times of wooden propellers over 70 years ago [8], is now experiencing a renaissance in civil aircraft construction with the increased use of carbon fibre reinforced plastics and the associated further development of automated production processes. In wing structural design, usually, a bending-torsion coupling is generated, which causes a downward pitch of the leading edge when the wing is bent up. A deflection of the wing upwards due to manoeuvring or flight through turbulence then leads to a lift reduction at the outer wing. Since this redistribution of the loads reduces the bending loads in the wing, the method is also known as passive load alleviation.

The counterpart, active load alleviation, is based on the redistribution of aerodynamic loads by static and dynamic control surface deflections. The original idea behind the control surfaces, in general, was to assign a specific function to each type of control surface. Elevators were primarily designed to control pitch, ailerons to control attitude about the longitudinal axis, rudder to yaw and spoilers to slow down the aircraft. For active manoeuvre load alleviation, not only the primary control surfaces are used during manoeuvring, but the other control surfaces are also deflected so that an optimal load distribution is achieved during the different phases of the respective manoeuvre. These additional control surface deflections are usually predetermined and proportional to the pilot commands, i.e. load factor or roll rate.

For the mitigation of detrimental effects resulting from gusts or turbulence, the control surface deflections are computed by a dedicated controller. The most common approach is to dampen the vibrational motion that is causing the loads by feeding back acceleration

measurements to the controller. The feedback of the acceleration signals to the deflections of the control surfaces alters the overall aircraft dynamics. The influence of the control laws on other important dynamic properties such as handling qualities or closed-loop flutter characteristics must, therefore, be closely monitored during their synthesis. An alternative approach is to measure the disturbance, i.e. the gust or turbulence, in front of or at the nose of the aircraft. The control surface deflections that mitigate the detrimental effects resulting from the disturbance are then determined by an optimised filtering of the measured signal. The main advantage of this feed-forward architecture is that the gust load controller function does not influence the inherent dynamics of the aircraft and thus, other properties related to stability or handling. An essential advantage of active control compared to passive load alleviation techniques is the ability to adapt the mechanism and the strength of the control to the phase and state of flight. Not only the promising results but also the rapidly advancing development of the respective sensor technology, such as laser-based measurement techniques, will make it possible to utilise this type of gust load alleviation to future civil aircraft.

The concept of active control was already applied to novel wing configurations in the form of large active winglets, as intensively investigated in the research project Smart Intelligent Aircraft Structures (SARISTU) [9], or active and passive folding wingtips as recently demonstrated in a scaled flight test by Wilson et al. [10]. A logical consequence of the developments described is the combination of both approaches, active control and structural tailoring in one integrated active adaptive wing concept.

Future Preliminary Wing Design The simultaneous implementation of the technologies presented in the previous section in a single wing design poses various challenges for the preliminary design. The similar effect of active and passive load alleviation achieved with different mechanisms leads to a strong and possibly undesired interaction among both technologies. Since the application of both technologies enables highly flexible wing designs with high aspect ratio, the static and dynamic aeroservoelastic behaviour needs careful monitoring early in the design process. Furthermore, the simultaneous application of active and passive load alleviation leads to conflicting requirements on the stiffness properties of the underlying primary wing structure: while passive aeroelastic tailoring tends to reduce the torsional stiffness in favour of the load alleviating bending torsional coupling, active control requires torsional stiffness to strengthen the effectiveness of the employed control surfaces. The resulting complex design synthesis problem requires not only an integrated optimisation process even to find feasible solutions, but also to get the best out of each of the applied technologies. The integrated aeroservoelastic analysis also enables the identification of non-intuitive concepts and the advantageous usage of the interaction between active and passive load alleviation by exploiting synergistic effects.

In addition to climate goals, the relentless competition between airlines dominates the air transport business, so that other direct operating costs are relevant in addition to fuel costs. Aircraft depreciation and amortisation costs increase with the introduction of the innovative technologies described above as the complexity of the aircraft increases. Design freedom must be maintained as long as possible during the design process in order to be able to react to possible problems and change requests in later design stages to counteract this effect and reduce costs throughout the value-creation chain. This can be

done by increasing design knowledge and gaining valuable insights and design experience in early design phases. The previously mentioned multidisciplinary design optimisation methods should, therefore, be incorporated into the overall design process as early as possible in order to maximise the available design freedom as long as possible. However, the opposite is the case in the industrial environment, especially in the conceptual design of control surfaces: Even though they are already used in a highly multifunctional manner (primary function, cruise performance control, load alleviation and secondary functions as vibration damping for ride comfort), control surfaces long have been conceptually designed based on an experience-based largely mono-functional breakdown [11].

In order to design and develop new and innovative concepts in the field of aviation in the future, it is not only necessary to merely combine or link the respective disciplines. It is also essential to develop a thorough understanding of the interaction between the various disciplines and technologies and to establish comprehensive collaboration between the physical departments dealing with the individual fields. The launch of various intensive, multidisciplinary research projects in recent years, such as the biggest ever research and technology project within Airbus, the Wing of Tomorrow Programme, underlines this demand [12].

One of the most significant shortcomings of integrated design synthesis is still the enormous computational effort required to perform the analyses and optimisations. In contrast to the increasing complexity of the processes and computational effort due to the consideration of more and more disciplines, there is still the need for rapid turnaround times in preliminary design. Efficient aeroservoelastic modelling for optimisation in the context of preliminary design, therefore, represents a field of its own. Typically, a first step is to efficiently model each discipline required for integrated design separately. The efficiency, i.e. the ratio between accuracy and computational effort, can be further increased by the use of model order reduction methods. The primary source of the overall complexity of aeroservoelastic models is unsteady aerodynamics. In addition to efficient aerodynamic modelling itself, the current research focuses in particular on modelling and subsequent model reduction, which is suitable for multidisciplinary optimisation problems.

1.1. RESEARCH OBJECTIVE

The technologies and processes described in the previous section for the design of future aircraft wings promise significant progress towards achieving the ambitious fuel efficiency targets. The integrated design of future wing structures including active and passive load alleviation and the analysis of the interaction between both technologies is the subject of this work. The research question underlying the dissertation is formulated as follows:

> *What is the benefit of including parameters of active manoeuvre and gust load control systems in the multidisciplinary design optimisation of aeroelastically tailored composite wing structures in the preliminary phases of aircraft design?*

Different subtasks are defined to find answers to the research question:

- A framework needs to be developed that enables the rapid integrated pre-design of tailored composite wing structures, including control systems for load alleviation during manoeuvres and gust encounters.

- Next, the interaction between active and passive load alleviation needs to be thoroughly studied on the example of a conventional long-haul aircraft configuration.

- The third component of the work should deal with further studies relevant to the preliminary design of aircraft. It needs to be investigated how the optimisation process can be accelerated to be suitable for preliminary aircraft design and how configuration changes affect the previously gained knowledge about the interaction between active and passive load alleviation.

1.2. APPROACH AND ORGANISATION OF THE THESIS

The introduction is followed by the main body of the thesis being structured according to the previously described subtasks that must be completed to answer the research question.

The first of the three main parts is concerned with the development of the toolchain that allows the integrated preliminary design of tailored composite wing structures, including active control systems for load alleviation. The foundation of the framework is based on the combination of two existing toolchains to avoid a time-consuming re-implementation: dAEDalus [13], a tool initially developed as an analysis tool to study the influence of aeroelasticity on handling characteristics during preliminary aircraft design, and Proteus [14], a tool developed for the structural optimisation of aeroelastically tailored wing structures.

The elimination of the performance bottleneck of the toolchain by efficient modelling and simulation of unsteady aerodynamics is the subject of Chapter 2. The technique of model order reduction implemented in Proteus is further developed for the use in aeroservoelastic optimisations. The target is the generation of one reduced order model that can be used throughout an entire optimisation of the wing structure and the control system for load alleviation. First, an overview of conventional model order reduction methods is given, after which the balanced proper orthogonal decomposition is combined with the concept of synthetic mode shapes. Three different methods for generating synthetic mode shapes are then formulated for complete aircraft configurations including wing, horizontal and vertical tail and subsequently used in the process of the aerodynamic model order reduction. The chapter continues with extensive studies to determine (i) the optimal type and (ii) the optimal number of synthetic mode shapes used to generate the training data required for the model order reduction. The subsequent optimal setup selection is based on the accuracy of the resulting aerodynamic models in aeroservoelastic analyses. These quantitative analyses include flutter speed prediction, continuous turbulence loads and control surface transfer function analysis. Structural and control surface layout variations are considered to ensure the usability of the aerodynamic reduced order models in the targeted, integrated optimisation workflow.

The developed framework is applied in Chapter 3 to investigate the interaction between active and passive load alleviation.

In this chapter, first, the detailed setup and architecture of the optimisation workflow are described. Furthermore, the exemplary case of a typical transport aircraft configuration with a conventional control surface layout is introduced. In order to enable the use of the control surface layout consisting of spoilers and ailerons, a method for efficient aerodynamic modelling of spoilers is proposed next, which is particularly suitable for the preliminary design context.

The chapter continues with a description of how the technologies used for active and passive load alleviation expand the design space of the optimisation problem. This includes the definition of the design variables allowing the optimiser to exploit the stiffness direction for passive load alleviation in the form of structural tailoring. Furthermore, it is described how the active manoeuvre load alleviation is realised by the scheduled control surface deflections in symmetrical and asymmetrical flight conditions, which represent additional design variables. Finally, the design space is supplemented by the parameters of the feed-forward active control system for gust load alleviation.

The formulation of the optimisation problem is then completed with the definition of the objective function and the formulation of static and dynamic aeroelastic constraints resulting from manoeuvre and gust flight simulations. What follows is a thorough discussion of the results of optimisations with the individual load alleviation technologies and all their combinations. It is analysed to what extent the optimisation results differ and how the different technologies interact with each other.

The chapter ends with an analysis of the extent to which the results hold in case of structural flexibility variations. Also, the observed results and the general conclusions about the interaction between active and passive load alleviation are reassessed.

The third part of the main body of the present work, Chapter 4, presents further studies on the impact of the results found on the work in the field of aircraft preliminary design.

First, alternative optimisation approaches are investigated and compared to the results of simultaneous optimisation, which seem to be more suitable for early design studies due to their better computational efficiency. In addition to a separate design of the technologies, an approach is proposed in which different subspaces of the overall parameter space are iteratively optimised focusing on individual technologies.

In the further course of the chapter, two significant configuration changes are investigated, since the rapid evaluation of such changes is an additional important task of the preliminary design in addition to the initial conception of new aircraft configurations. First, the control surface layout is changed from the initial split aileron concept to a flaperon layout. Second, a non-planar wing configuration with an active winglet is examined. By comparison with the results presented in the previous chapter, the extent to which the interactions and synergies are configuration-specific is then determined.

The final part of this dissertation, Chapter 5, provides, on the one hand, a summary of the main findings and the conclusions drawn throughout the work. On the other hand, general conclusions are drawn concerning the research question and the overall objectives.

In the further course of the final chapter, suggestions for improvement are given for the framework developed in this thesis for the integrated optimization of wing structures and active control systems. Besides, recommendations are given on how the interaction between active control and structural design can be further investigated in order to utilize possible synergies better. Finally, the work is concluded with an outlook on the future of integrated active adaptive wing design.

2

Aerodynamic Model Order Reduction for Aeroservoelastic Optimisation

Abstract The combined optimisation of aircraft structures and active control systems in early design stages requires low-order unsteady aerodynamic models that are robust to structural and control surface layout modifications. A combination of the balanced proper orthogonal decomposition with the concept of synthetic modes is proposed and different formulations for the generation of synthetic modes are given. The models resulting from the proposed procedure are tested for their suitability and accuracy in aero(servo)elastic analyses (stability assessment, continuous turbulence loads and calculation of control surface transfer functions) of a tube-wing aircraft configuration. The results indicate that the number and type of synthetic modes have a significant influence on the achievable accuracy and the accuracy per order of the resulting reduced order model. At a required accuracy of 10^{-3}, the most suitable set of synthetic modes is based on radial basis functions and reduces the aerodynamic model order by about two orders of magnitude while still being able to handle structural and control surface layout modifications.

Publication A modified version of this chapter was published as: S. Binder, A. Wildschek, R. De Breuker, Unsteady Aerodynamic Model Order Reduction for Aeroservoelastic Optimisation by Balanced Proper Orthogonal Decomposition and the use of Synthetic Mode Shapes. *Journal of Aeroelasticity and Structural Dynamics,* Vol.6 No.1 pp. 43-72, 2018.

2.1. INTRODUCTION

The ever-increasing demand on cost and fuel efficiency are driving the development of aircraft with high aspect ratio wings, lightweight structures and technologies such as active control. The resulting increased influence of structural flexibility along with the increased interaction between structural dynamics and aerodynamics require new ways of working in early stages of aircraft design. Also, the growing use of active control methods such as gust load control or aeroelastic stability control must be considered as early as possible to achieve more optimal designs. One possibility to master this challenge is the use of computational methods and multidisciplinary design optimisation (MDO). The integration of a multitude of disciplines enables the uncovering of potentials that cannot be achieved through classical iterative design methods. A part of the integrated design of future aircraft is known as the field of aeroservoelasticity incorporating aero-, structural and control system dynamics. Integrated models for analysis and optimisation that originate in this field are often very complex and computationally costly to simulate. For the optimisation problems to be carried out in the conceptual and preliminary design stages, fast turnaround times are required to enable the assessment of many configurations, parameter variations and trade-offs. Typically, the modelling of transient aerodynamics involves the highest complexity (i.e. states in the resulting model) among the various disciplines of aeroservoelasticity and thus offers the highest potential regarding the reduction of turnaround times and computational effort. The present work is thus concerned with finding a solution to significantly reduce the dimensionality of the aerodynamic model while ensuring the required accuracy in aeroelastic analyses even in the presence of considerable parameter variations of the concept to be optimised. This solution shall enable the efficient integrated optimization of active control systems (e.g. for load alleviation or flutter suppression) along with the primary wing structure (i.e. layout and dimensions of wing skins, spars, stiffeners and ribs). Special focus is therefore placed on assuring the accuracy of aeroelastic analyses in the presence of parameter variations of the structure and the control systems. These variations include on the one hand the variation of the position and size of control surfaces and on the other hand the variation of the stiffness and mass distribution of the primary structure. In aircraft design, analyses of the aeroservoelastic model (stability, flight loads and control law synthesis) must be carried out at many flight points to verify a design point across the targeted flight envelope. The number of equations required for the generation of the models ranges from $10^3 - 10^4$ (potential flow based methods) to $> 10^6$ (higher order methods) solely for the aerodynamics. Order reduction before analysis is inevitable to enable the many studies in a reasonable time frame. On the global or system level, many conventional approaches exist which originated from control engineering. The most intuitive method is simply truncating certain states that are not significantly influencing the dynamics. The selection, however, requires precise knowledge of the individual states and how they contribute to the overall dynamics. A selection might be based on Another method for the reduction of a dynamic model is the modal truncation. Here the selection is based on an eigenanalysis of the model and a transformation on a selected subset of eigenmodes yields the reduced order model. While the eigendynamics of the full order model might be contained in the reduced order model, the input-state and state-output behaviour of the dynamic system are not considered during the selection of the subset of eigenmodes.

An important and widely used method that considers the input-state and the state-output behaviour is the Balanced Truncation (BT). Here, the system is first transformed in a balanced form so that the resulting states are equally controllable as observable [15]. Then the model order is reduced by keeping only the most controllable and observable states. The method has proven to be very efficient while producing models which closely match the input-output behaviour of the full order models. However, for large systems as in aeroservoelasticity, this kind of methods are often not directly applicable due to limited computational resources. Besides, after transforming the integrated model, the individual equations can no longer be associated with the different disciplines. Thus, usually, an order reduction on the discipline level is performed before the global reduction with methods suitable for the different properties of the models (e.g. Guyan and modal reduction for structural models) [16].

In the field of fluid dynamics, several methods were developed in the past decades. Three of the most prominent examples are the Proper Orthogonal Decomposition (POD), also known as Karhunen–Loève decomposition, the Balanced Proper Orthogonal Decomposition (BPOD) and the Eigensystem Realization Algorithm (ERA).

The mentioned methods fall into the category of snapshot-based methods in which a limited collection of data from simulations or experiments is used. In the POD, the snapshots are used to compute a vector basis which optimally approximates the collected state snapshot data [17]. A combination of the POD and the balanced truncation has been presented by Rowley forming the BPOD [18]. To overcome the limitation that the POD based models can only reflect the input-state behaviour and not the state-output behaviour, both, snapshot simulations of primal and the adjoint or dual system are used to compute a transformation that approximately balances the system. The ERA algorithm tries to find a state-space realisation of a system reflecting the collected input-output snapshot data in a balanced form. Ma et al. compare the BPOD and the ERA algorithm yielding that theoretically, both methods produce identical ROMs [19]. However, an advantage of the BPOD is that it produces a set of bi-orthogonal vectors with which the full order model can be reconstructed from the reduced order model, while the ERA algorithm produces only the ROM without information about the relation of the resulting states to the original states. In other words, in case the full order system is given including its adjoint form, less information gets lost during the model order reduction by BPOD. The BPOD was successfully applied in reducing aerodynamic models of airfoils, cascades and wings [20], [21].

For the generation of aerodynamic reduced order models used in aeroelastic applications, all the previously described methods require the structural and flight dynamic degrees of freedom to be reduced to a finite set of generalised coordinates to reduce the number of in- and outputs of the aerodynamic model. Thus, the resulting model is only valid and accurate for these structural degrees of freedom. In sizing-type aeroelastic optimisation (i.e. for a fixed topology and shape), the mass and stiffness distribution and thus the structural mode shapes change during the design. It is therefore desirable to create one ROM which is robust enough to capture all expected variations in the structural and flight dynamic degrees of freedom. Fenwick et al. presented a study in which the resulting reduced order model was interpolated from a previously created data basis across the structural parameter range [22]. In optimisations with a large number of structural pa-

rameters such as aircraft structure optimisations, this requires a large amount of models to be created before the optimisation. A suggestion to account for arbitrary structural modifications is to use significantly more mode shapes of the basis model for the generation of the reduced order model than used in the aeroelastic analysis [23]. This approach requires the basis mode shapes to represent all structural modifications occurring during the optimisation. Another method is to augment the basis mode shapes by the introduction of fictitious masses [24]. The modal basis of the overall structure is enriched by the integration of modes of the substructure where structural modifications are expected or planned. The method has been especially useful in augmenting dynamic models of fighter aircraft to enable the efficient flutter analysis of numerous loading conditions [25]. Furthermore, the method was successfully applied to include local deformations of actuators and their attachment structure in low dimensional modal representations of the overall structure [26]. However, it is required that all possible structural modifications and their locations are known beforehand to ensure the required robustness.

Instead of utilising the mode shapes of the basis model, artificial mode shapes (also referred to as prescribed or synthetic mode shapes) may be used which are not related to the basis structural model. Voss et al. compared the use of different functions and polynomials for generation of synthetic mode shapes finding that only ten synthetic mode shapes are required to approximate the first 50 structural eigenmodes of a transport aircraft regarding the Modal Assurance Criterion (MAC) [27]. However, the different types used have not been compared concerning their suitability to approximate the aeroelastic behaviour. With respect to snapshot based model order reduction techniques, Zhang et al. reproduced the snapshot data for the current mode shapes by reprojecting them on the snapshot data generated with Radial Basis Function (RBF) based synthetic mode shapes [28]. Winter et al. created mode shapes based on Chebyshev polynomials and RBFs to establish a ROM which is robust to structural variations [29]. Their studies include a qualitative comparison of the two different methods for basis mode shape generation concerning the accuracy of generalised aerodynamic forces generated with the resulting ROM.

The mentioned examples study the accuracy of the resulting ROMs concerning their frequency response or flutter point of an isolated wing. All the examples deal with purely structural modifications of the basis model. In aeroservoelastic optimisations carried out in early design stages of aircraft, also the position and size of control surfaces may be varied. The robustness of ROMs to changes of the control surface layout has not been studied so far.

In this chapter, first, the basic concept of BT, POD and BPOD are reviewed. The BPOD is then combined with the concept of synthetic mode shapes. Therefore, three different methods for synthetic mode shape generation based on RBF, Chebyshev polynomials and zonal subdivision are formulated for full aircraft configurations including wings, horizontal and vertical tail. These synthetic modal bases are used in the process of the aerodynamic model order reduction. After the reduction process, the aerodynamic ROMs are combined with the flight dynamic and structural equations of motion forming the integrated aeroelastic model. Subsequently, flutter point, continuous turbulence loads and control surface transfer functions are computed in the presence of structural (mass and stiffness distribution) and control surface layout variations (size and location of the

control surfaces). The influence of the number of synthetic mode shapes used for the generation of training data on the accuracy of the resulting ROMs is studied. Finally, a quantitative comparison of the accuracy is made between the different approaches for synthetic mode shape generation used for the training data generation.

2.2. METHODOLOGY

Each component or discipline involved in the field of aeroservoelasticity (aero-, flight- and structural dynamics as well as sensors and actuators) can be modelled as a dynamic system. The term modelling refers to the derivation of mathematical equations describing the behaviour of those systems. The result is mostly a set of coupled ordinary differential equations (ODE) or partial differential equations (PDE). In the latter case, the conversion to systems of ODEs is often done with discretisation methods as finite elements, volumes, differences or boundary element methods. As the solution of non-linear ODEs is complex and linear approximations can be obtained around a specific equilibrium point. For each component in aeroservoelasticity, eventually, the result is a set of homogeneous, linear ODEs (also known as Linear Time-Invariant (LTI) system) which can be cast into a state space representation of the form:

$$\begin{aligned} \dot{\mathbf{x}} &= \mathbf{A}\mathbf{x} + \mathbf{B}\mathbf{u} \\ \mathbf{y} &= \mathbf{C}\mathbf{x} + \mathbf{D}\mathbf{u} \end{aligned} \tag{2.1}$$

with the state vector $\mathbf{x} \in \mathbb{R}^n$, the output vector $\mathbf{y} \in \mathbb{R}^q$ and the input vector $\mathbf{u} \in \mathbb{R}^p$ where n, p and m are the number of states, outputs and inputs of the state space system. The physical interpretation of inputs to an aerodynamic model used in aeroelastic applications are variations of boundary conditions due to surface motion or external disturbances. The outputs correspond to the variation in pressure distributions across the surfaces. The exact interpretation of the states depends on the underlying numerical modelling technique. For potential flow methods as they are most commonly used in subsonic aero(servo)elastic applications, the states can be associated to the unsteady interaction between the wake and the lifting surfaces (also known as lag states). Models representing the unsteady aerodynamics of full aircraft configurations can be large and costly to simulate. Techniques reducing the number of states are referred to as model order reduction methods. All methods target the realisation of models that reproduce the behaviour of interest as precisely as possible with a lower number of states and equations. The fundamental model order reduction methods have their origin in the field of control engineering in the late last century [30]. The methods forming the basis of this work are the BT and the POD. Both methods are projection based methods that reduce the space in which the differential equations are solved by projection on a new set of basis vectors:

$$\mathbf{x}_r = \Phi_r \mathbf{x} \tag{2.2}$$

with the reduced state vector $\mathbf{x}_r \in \mathbb{R}^{k<n}$ and the reduction basis $\Phi_r \in \mathbb{R}^{k \times n}$. The resulting ROM is then given by:

$$\begin{aligned} \dot{\mathbf{x}}_r &= \tilde{\mathbf{A}}\mathbf{x}_r + \tilde{\mathbf{B}}\mathbf{u} = \Phi_r^{-1}\mathbf{A}\Phi_r\mathbf{x}_r + \Phi_r^{-1}\mathbf{B}\mathbf{u} \\ \mathbf{y} &= \tilde{\mathbf{C}}\mathbf{x}_r + \mathbf{D}\mathbf{u} = \mathbf{C}\Phi_r\mathbf{x}_r + \mathbf{D}\mathbf{u} \end{aligned} \tag{2.3}$$

In order to outline the basis for the present work, the following section (2.2.1) presents a quick review of the concepts of BT and POD followed by the introduction of the combined BPOD. In Section 2.2.2 the use of synthetic mode shapes for the reduction of large aerodynamic systems used in aeroservoelastic applications is proposed and three different types of synthetic mode shapes are formulated for full aircraft configurations. A summary of the resulting combined procedure is presented in Section 2.2.3.

2.2.1. MODEL REDUCTION BY BALANCED PROPER ORTHOGONAL DECOMPOSITION

Balanced Truncation The concept of balancing was initially developed by Moore in the balanced truncation with the idea to reduce the state space onto a subspace spanned by the most controllable and observable states [15]. Therefore, Gramians are computed which can be used to quantify the contribution of the individual states to the input-state and state-output behaviour. The controllability Gramian $\mathbf{W}_c$ used for the quantification of the input-state contribution of a stable system is given by:

$$\mathbf{W}_c = \int_0^\infty e^{\mathbf{A}t}\mathbf{B}\mathbf{B}^T e^{\mathbf{A}^T t}\, dt \tag{2.4}$$

An interpretation of Eq. 2.4 is that the controllability Gramian equals the infinite integral of the outer product of impulse state responses for every input to the system. The actual quantification is done by computing the Singular Value Decomposition (SVD) of the Gramian:

$$\mathbf{W}_c = \mathbf{U}_c \Sigma_c \mathbf{V}_c^T \tag{2.5}$$

where Σ_c contains the singular values σ_c on its diagonal ($\Sigma_c = \text{diag}(\sigma_{c,1} ... \sigma_{c,n})$ with $\sigma_{c,1} \geq \sigma_{c,2} \geq ... \geq \sigma_{c,n}$) and $\mathbf{U}_c$ as well as $\mathbf{V}_c$ the corresponding left and right-singular vectors as columns. The singular value σ_i then quantifies the controllability of the state described by the i-th column of $\mathbf{U}_c$.

The observability Gramian $\mathbf{W}_o$ for determination of the relative state-output importance is given similarly:

$$\mathbf{W}_o = \int_0^\infty e^{\mathbf{A}^T t}\mathbf{C}^T\mathbf{C} e^{\mathbf{A}t}\, dt \tag{2.6}$$

According to the principle of duality, the observability Gramian equals the controllability Gramian of the adjoint $(\bar{\cdot})$ or dual system whose state equation is given by:

$$\dot{\bar{\mathbf{x}}} = \mathbf{A}^T\bar{\mathbf{x}} + \mathbf{C}^T\bar{\mathbf{u}} \tag{2.7}$$

with $\bar{\mathbf{x}}$ being the dual system state vector.

A system is in its balanced form when the resulting reduced states are equally observable as controllable, i.e. the singular values of the Gramians coincide. The transformation that balances the system is found by an eigenanalysis of the product $\mathbf{W}_c\mathbf{W}_o$. When the system is in its balanced form, a reduced order model is obtained by truncation of the least controllable and observable states. For further information, the reader is referenced to [15], or to [31] for the numerically more reliable Square Root Balanced Truncation.

Usually, the Gramians are computed by solving the Lyapunov equation. However, the algorithm used for the solution is computationally expensive, and the effort grows cubically with the number of states [32]. Thus, for large systems, the standard balanced truncation is practically not feasible. In the past decades, many methods have been developed with the aim to realise approximately balanced ROMs for such large-scale systems. Many of those methods make use of simulation snapshots as they can be obtained for all kinds of underlying dynamical systems. One of those methods is the use of empirical Gramians based on simulation data for the computation of the balancing transformation. Assuming the empirical Gramians represent a good approximation of the exact Gramians, the resulting truncated balanced realisation models are very close to the models obtained by using exact Gramians. Moore already used time sampled simulation data for the computation of the Gramians instead of a numerical solution of the Lyapunov equation[15]. Lall et al. proposed to use this way of Gramian estimation to reduce the dimension of complex, controlled non-linear systems by balanced truncation [33]. For linear systems, the integral for the computation of the controllability Gramian in Eq. 2.4 can be approximated by the sum of the outer product of m state snapshots at equally spaced time steps $(1t_s, 2t_s, ..., mt_s)$:

$$\mathbf{W}_c \approx \sum_{i=1}^{m} \sum_{j=1}^{p} \mathbf{x}_{i,j} \mathbf{x}_{i,j}^T t_s \tag{2.8}$$

Herein, $\mathbf{x}_{i,j}$ is the i-th snapshot of the state response to a unit Dirac impulse at input j. The observability Gramian is similarily approximated by the help of the adjoint system defined in Eq. 2.7:

$$\mathbf{W}_o \approx \sum_{i=1}^{m} \sum_{j=1}^{q} \bar{\mathbf{x}}_{i,j} \bar{\mathbf{x}}_{i,j}^T t_s \tag{2.9}$$

Here, $\bar{\mathbf{x}}_{i,j}$ denotes the i-th snapshot of the state response to a unit Dirac impulse at input $\bar{\mathbf{u}}_j$ of the adjoint system. With the obtained approximated Gramians, first an aproximately balanced transformation is made, followed by an truncation of the least controllable and observable states. The main drawback of using empirical Gramians is that many simulation snapshots are needed for a sufficiently high accuracy of the approximation. For aerodynamic systems which usually have many inputs and outputs, the number of simulations required is particularly high.

Proper Orthogonal Decompostion Especially in the area of fluid dynamic simulation, the POD has proven itself in the past as an effective method for model reduction. The original concept of the POD was presented by Pearson as a method for finding the "best-fitting" straight line or plane for 2D or 3D point clouds [34]. With respect to large systems, one of the most important advancements is the POD by the method of snapshots presented by Sirovich [35]. The principal idea behind the POD is to perform a Galerkin projection of the vector space onto a subspace spanned by orthonormal basis vectors so that the approximation of a given set of simulation snapshots is optimal in a least square sense [30]. Therefore, a set of m state snapshots at different time steps resulting from simulations with the full order model is collected in the snapshot matrix $\mathbf{X}$:

$$\mathbf{X} = \frac{1}{m} [\mathbf{x}(t_1), \ ... \ , \mathbf{x}(t_m)] \tag{2.10}$$

It can be shown that, in the finite-dimensional space, the solution for the optimal approximation are the eigenvectors of the correlation matrix $\mathbf{X}\mathbf{X}^T$ [36]. The largest eigenvalues correspond to the most suitable POD mode shapes regarding approximating the given dataset $\mathbf{X}$. Hence, a reduced order model is formed by using only the eigenvectors belonging to the k largest eigenvalues.

The method of snapshots proposed by Sirovich makes use of the positive semidefiniteness of the correlation matrix $\mathbf{X}\mathbf{X}^T$ [35]. When the number of snapshots m is smaller than the number of states n, the size of the eigenvalue problem can be reduced from $n \times n$ to $m \times m$ by computing the eigenvalues of $\mathbf{X}^T\mathbf{X}$.

The resulting m POD modeshapes $\Phi_{\text{POD}} = [\phi_1, ..., \phi_m]$ are then found by:

$$\phi_j = \frac{1}{\sqrt{\lambda_j}} \mathbf{X}\mathbf{v}_j \quad , j = 1, ..., m \tag{2.11}$$

where λ and $\mathbf{v}$ are the eigenvalues and eigenvectors of $\mathbf{X}^T\mathbf{X}$.

As the resulting modes are optimal in approximating a given dataset, the question remains if the same modes are suitable for the representation of the system dynamics.

Balanced Proper Orthogonal Decompoistion As the POD is based on snapshots of states, only the input-state behaviour is reflected in the resulting model. When empirical Gramians are used for a BT, additional snapshots of the impulse responses of the adjoint system have to be computed. This results in a large number of simulations required, especially when the number of outputs is large. To overcome these issues, Rowley suggested a combination of the BT and the POD which will be outlined in the following[18].

In the BPOD, first the m state snapshots $\mathbf{x}$ obtained from p impulse response calculations at time steps $t_1, ..., t_m$ are stored in the matrix $\mathbf{X} \in \mathbb{R}^{n \times pm}$ together with their appropriate quadrature coefficients $\delta_1, ..., \delta_m$, which are equal to the time interval between the individual snapshots (e.g. $\delta_i = t_i - t_{i-1}$):

$$\mathbf{X} = [\mathbf{x}_{1,1}\sqrt{\delta_1}, \ ... \ , \mathbf{x}_{1,m}\sqrt{\delta_m}, \ ... \ , \mathbf{x}_{p,m}\sqrt{\delta_m}] \tag{2.12}$$

When the number of outputs is large, it is recommended to first project the system output on POD modes generated from a dataset of input-output trajectories. As the input-state snapshots $\mathbf{X}$ are already computed, multiplication with the matrix $\mathbf{C}$ generates a set of input-output snapshots $\mathbf{Y}$:

$$\mathbf{Y} = \mathbf{C}\mathbf{X} \tag{2.13}$$

The eigenvectors and eigenvalues of $\mathbf{Y}^T\mathbf{Y}$ are used to define the POD output mode shapes $\Phi_{\text{POD,o}}$ as it is shown in Eq. 2.11. The number of POD modes used for output projection h is given by the desired approximation error defined as:

$$\epsilon_{\text{proj}} = \sum_{j=h+1}^{q} \lambda_j \tag{2.14}$$

in which λ are the eigenvalues of $\mathbf{Y}^T\mathbf{Y}$.

Subsequently the input vector of the adjoint system $\bar{\mathbf{u}}$ in Eq. 2.7 is projected on the POD output modeshapes ($\bar{\mathbf{u}} = \Phi_{\mathrm{POD,o}}\check{\mathbf{u}}$):

$$\dot{\bar{\mathbf{x}}} = \mathbf{A}^T\bar{\mathbf{x}} + \mathbf{C}^T\Phi_{\mathrm{POD,o}}\check{\mathbf{u}} \tag{2.15}$$

Now, impulse response snapshots of the transformed adjoint system are taken at l time steps and stored in the matrix $\bar{\mathbf{X}} \in \mathbb{R}^{n\times hl}$

$$\bar{\mathbf{X}} = [\bar{\mathbf{x}}_{1,1}\sqrt{\delta_1},\ \dots,\bar{\mathbf{x}}_{1,l}\sqrt{\delta_l},\ \dots,\bar{\mathbf{x}}_{h,l}\sqrt{\delta_l}] \tag{2.16}$$

The transformation that approximately balances the system is then found by an SVD of $\bar{\mathbf{X}}^T\mathbf{X}$:

$$\bar{\mathbf{X}}^T\mathbf{X} = \mathbf{U}_b\Sigma_b\mathbf{V}_b^T \tag{2.17}$$

$$\Phi_{\mathrm{bal}} \approx \Phi_{\mathrm{bal,a}} = \mathbf{X}\mathbf{V}_b\Sigma_b^{-0.5} \tag{2.18}$$

$$\Phi_{\mathrm{bal}}^{-1} \approx \Phi_{\mathrm{bal,a}}^{-1} = \Sigma_b^{-0.5}\mathbf{U}_b^T\bar{\mathbf{X}}^T \tag{2.19}$$

The ROM is then found by using only the first k columns of $\Phi_{\mathrm{bal,a}}$ and the first k rows of $\Phi_{\mathrm{bal,a}}^{-1}$. Compared to the simple use of empirical Gramians, the method is especially useful when the number of states and outputs is large. The computation of the POD mode shapes for output projection requires only little extra computational effort as no additional impulse response simulations are necessary. However, during the analyses run for this work, it has been observed that the matrices $\mathbf{X}$ and $\bar{\mathbf{X}}$ can get very large and the product $\bar{\mathbf{X}}^T\mathbf{X}$ may get prohibitively expensive when it comes to memory usage. In this case and more specifically when $pm > n$ or $hl > n$, it is more efficient to compute a form of approximated Gramians by:

$$\mathbf{W}_c \approx \mathbf{X}\mathbf{X}^T \tag{2.20}$$

$$\mathbf{W}_o \approx \bar{\mathbf{X}}\bar{\mathbf{X}}^T \tag{2.21}$$

Similar to the empirical Gramians discussed earlier, the accuracy of the Gramians strongly depends on the number of snapshots used in the impulse response simulation. The accuracy of the approximated observability Gramian additionally depends on the chosen projection error ϵ_{proj} used for the determination of POD modeshapes h used in the output projection (Eq. 2.14). With the use of these approximated Gramians, the balanced transformation and the reduced order model can be computed as described in the BT.

Contrary to the POD, the BPOD takes into account the input-state as well as the state-output dynamics for the selection of states that are kept in the reduced order model. In addition, it has been found that the BPOD shows higher robustness with regard to preserving stability compared to the POD [37]. Compared to the use of empirical Gramians, the BPOD reduces the amount of required impulse response simulations of the adjoint system by reducing the number of outputs prior to the training data generation process.

2.2.2. SYNTHETIC MODE SHAPES FOR SNAPSHOT DATA GENERATION IN AEROSERVOELASTIC APPLICATIONS

In aeroservoelastic applications, the aerodynamic model is responsible for calculating distributed forces among the surfaces given the boundary conditions imposed at the

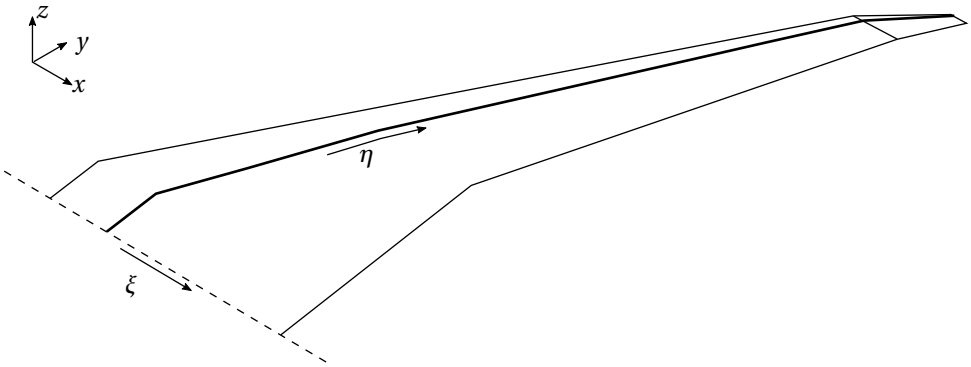

Figure 2.1: Location and definition of the introduced reference coordinate directions used for the formulation of the synthetic mode shapes on a lifting surface. The spanwise direction η follows the local one -quarter chord line and the chordwise direction ξ is placed along the primary flightpath.

same surfaces by structural, flight dynamic and control surface degrees of freedom. When the aerodynamic and structural models are initially set up, the number of inputs to the aerodynamic model depends on the number of stations at which the force and displacement transfer between the aerodynamic and the structural model is facilitated. Using all possible stations as inputs for the aerodynamic model order reduction by the BPOD, a large number of simulations needs to be carried out to estimate the Gramians. Transforming the inputs to the aerodynamic model on generalised coordinates reduces the number of inputs. Typically, the eigenmodes of the in vacuo structural model are used for the generalised coordinate basis alongside with the control surface modes for the given control surface layout. As the targeted application of the proposed method is sizing type aeroservoelastic optimisation, generalised coordinates in terms of structural mode shapes and the control surface layout are unknown at the time of the generation of the reduced order model, i.e. before the optimisation.

In this work, synthetic mode shapes are used for the reduction of the number of inputs to the aerodynamic model. In the following, three different methods for the synthetic mode shape generation for full aircraft configurations are proposed. It is assumed that the surface on which the aerodynamic forces are computed and the boundary conditions are imposed, is given as a spatially discretised domain as is usual for finite difference, element or volume methods. For the sake of simplicity, the following description is limited to surface representations of the wings only, i.e. no fuselage aerodynamics are modelled.

Synthetic mode shapes based on Subdivision The first method used in this work is to divide each lifting surface into zones by spanwise as well as chordwise subdivision. To divide the lifting surfaces into zones, first, two reference coordinate directions per lifting surface are defined as shown in Fig. 2.1. A spanwise coordinate direction η is defined along the one-quarter chord line of each lifting surface ranging from one tip ($\eta = -1$) to the other ($\eta = 1$) for symmetric lifting surfaces and from the root ($\eta = -1$) to the tip ($\eta = 1$) for non-symmetric lifting surfaces. The chordwise coordinate direction ξ is defined along the primary flight direction and ranges from the local leading edge ($\xi = -1$)

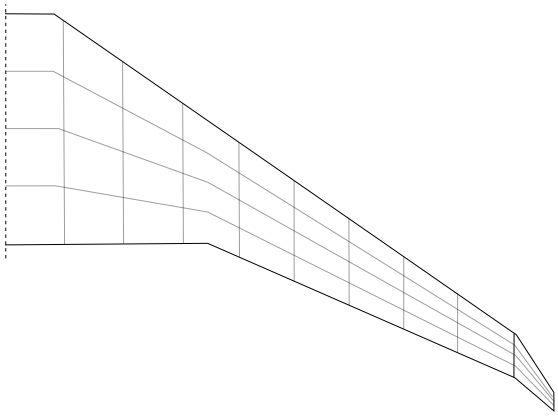

Figure 2.2: Example of the resulting zones for a division of the lifting surface $n_{z,\xi} = 4$ zones per chord and $n_{z,\eta} = 20$ zones per reference span.

to the trailing edge ($\xi = 1$). The zones are then defined by dividers which are equally spaced along the two defined directions. As an example, Fig. 2.2 shows the resulting subdivisions for $n_{z,\eta} = 20$ zones per reference span as well as $n_{z,\xi} = 4$ zones per chord. For each zone, a synthetic mode shape is then defined by a vector with zeros for the boundary condition points which are outside and ones for the points which are inside the respective zone. Stacked horizontally, the mode shapes form the synthetic modal basis for the lifting surface. For the full aircraft configuration, the modal bases for each lifting surface are block-diagonally stacked. Depending on the number of subdivisions chosen, the transformation of the aerodynamic system results in a reduced number of inputs.

Gillebaart and De Breuker also used this approach to reduce the amount of impulse response simulations required to carry out the BPOD for a panel-based aerodynamic model. However, only one chordwise zone has been used while the spanwise number was chosen to be the number of spanwise panels used in the underlying aerodynamic full order model [21]. In this work, the influence of the number of zones used on the resulting accuracy of the reduced order model is studied in Section 2.3.

Synthetic mode shapes based on Chebyshev Polynomials Another way of generating synthetic mode shapes is the use of spatial weighting functions. Ideally, the weighting functions form an orthogonal basis. One of the most prominent sets of orthogonal vectors are the Chebyshev polynomials of the first kind as shown in Fig. 2.3. An explicit definition of the one-dimensional polynomial in dependence of the order j is given as [38]:

$$U_j(\eta) = \frac{(\eta + \sqrt{\eta^2 - 1})^j + (\eta - \sqrt{\eta^2 - 1})^j}{2} \tag{2.22}$$

Again the two reference coordinate directions defined in Fig. 2.1 are used to formulate the mode shapes:

$$\begin{aligned} \phi_{c,(i-1)j+i}(\xi,\eta) = & U_i(\xi) U_j(\eta) \\ & \text{with } i = 0,...,n_{c,\xi} - 1 \text{ and } j = 0,...,n_{c,\eta} - 1 \end{aligned} \tag{2.23}$$

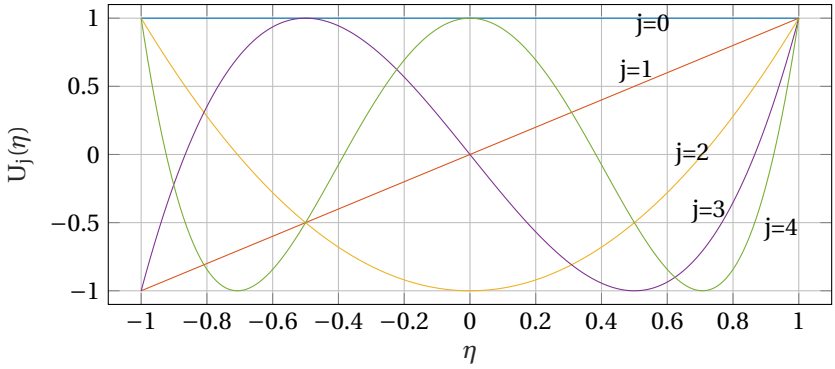

Figure 2.3: Chebyshev polynomials of the first kind as a function of η evaluated for various orders j.

For a typical wing geometry, the resulting synthetic mode shapes for various orders are shown in Fig. 2.4. Again, the modes are horizontally stacked for each wing and block-diagonally arranged for the full aircraft configuration.

Winter et al. used a similar description for the generation of mode shapes [29]. However, in their formulation, the polynomials have been defined along global coordinate directions. As a result, the polynomial boundaries lie outside of the wings surface for tapered or swept wings. Hence, not the full weighting functions are used, and consequently, higher order polynomials are required to achieve the same distributions.

Synthetic mode shapes based on Radial Basis Functions The third set of synthetic mode shapes used in this work is based on radial basis functions. Here, the magnitude of the mode shapes depend on the distance to a centre node. The underlying formulation used in this work has been described by Zhang et al., however, adapted to be used for complex wing geometries [28]. First, the $n_{r,\xi}$ chordwise and $n_{r,\eta}$ spanwise centre nodes are placed equidistantly along each of the two reference coordinate directions defined in Fig. 2.1. The resulting centre nodes form a mesh in total consisting of $n_r = n_{r,\xi} n_{r,\eta}$ centre nodes. The i-th RBF is defined in dependence of the spanwise reference coordinate η as:

$$R_i(\eta) = (1 - d_\eta)^4 (4 d_\eta + 1) \tag{2.24}$$

Herein, d_η denotes the distance to the respective centre node in spanwise direction η defined as:

$$d_\eta = \max\left(\frac{|\eta - \eta_i|}{r_\eta}, 1\right) \tag{2.25}$$

with η_i being the spanwise station of the i-th centre node. The radius r is a function of a scaling factor f and the number of spanwise centre nodes:

$$r_\eta = \frac{f}{n_{r,\eta}} \tag{2.26}$$

The resulting RBFs of $n_r = 3$ centre nodes are shown in Fig. 2.5 for different scaling factors f. Similarly, the RBF is defined in chordwise direction. One mode shape per centre node

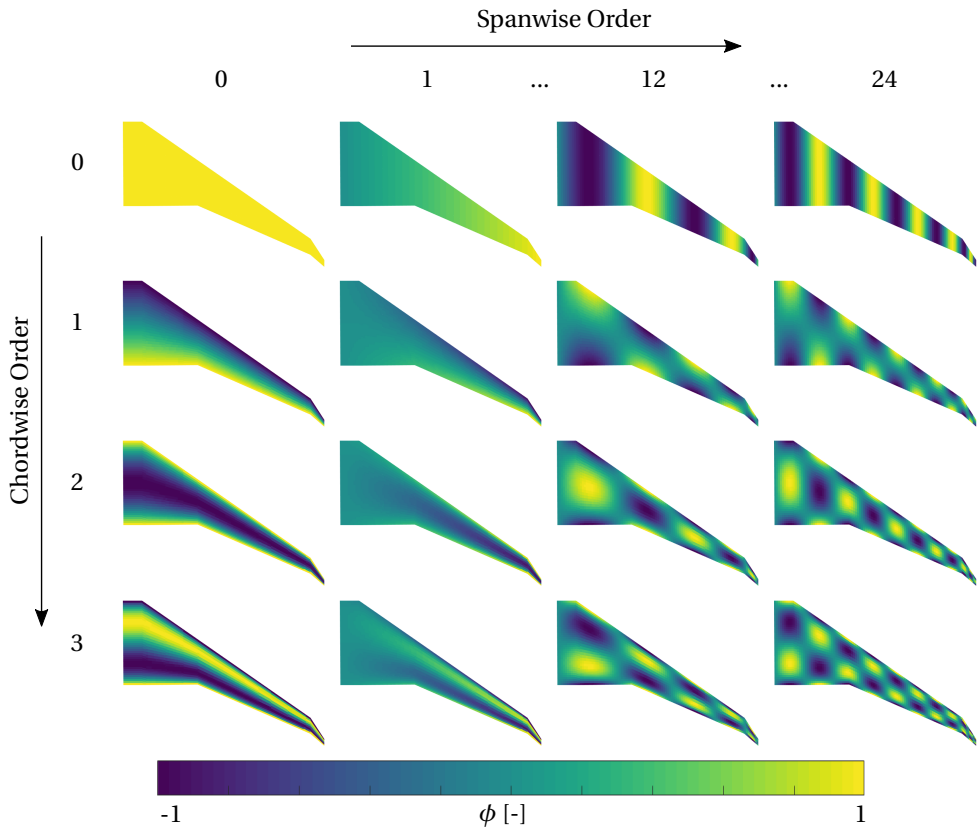

Figure 2.4: Synthetic mode shapes for a typical wing geometry based on Chebyshev polynomials of the first kind for various number of chordwise $n_{c,\xi}$ and spanwise polynomials $n_{c,\eta}$.

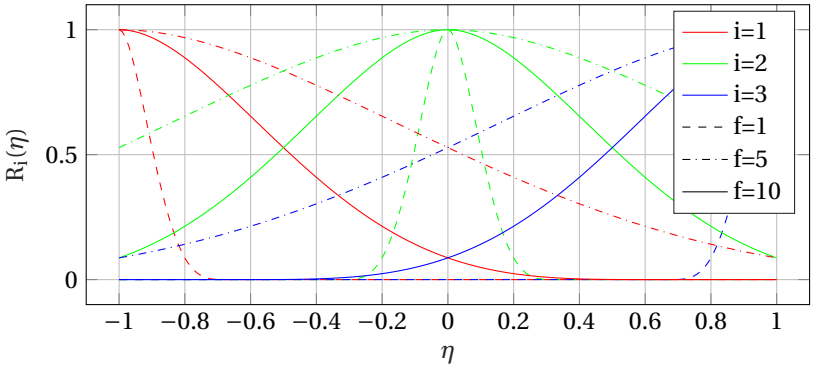

Figure 2.5: The resulting radial basis functions for a number of $n_r = 3$ centre nodes placed along the coordinate η for three different radius scaling factors f.

is then calculated by:

$$\phi_{r,i} = R_i(\xi) R_i(\eta) \quad \text{with } i = 1, ..., n_{r,\xi} n_{r,\eta} \tag{2.27}$$

An example mode shape is shown in Fig. 2.6 alongside with the positions of the centre nodes for this case. Again, the mode shapes are stacked horizontally to form the transformation basis as for the other two methods described.

2.2.3. RESULTING PROCESS FOR AERODYNAMIC MODEL ORDER REDUCTION

The proposed process to create the reduced order aerodynamic model is summarised in the following steps:

1. Create a set of synthetic mode shapes Φ_{syn} for the surfaces on which the aerodynamic model inputs are defined.

2. Project the input space of the aerodynamic model from Eq. 2.1 onto the chosen set of synthetic mode shapes to obtain the transformed ($\hat{\cdot}$) system with the input vector $\hat{\mathbf{u}}$:

$$\begin{aligned} \dot{\mathbf{x}} &= \mathbf{A}\mathbf{x} + \hat{\mathbf{B}}\hat{\mathbf{u}} = \mathbf{A}\mathbf{x} + \mathbf{B}\Phi_{\text{syn}}\hat{\mathbf{u}} \\ \mathbf{y} &= \mathbf{C}\mathbf{x} + \hat{\mathbf{D}}\hat{\mathbf{u}} = \mathbf{C}\mathbf{x} + \mathbf{D}\Phi_{\text{syn}}\hat{\mathbf{u}} \end{aligned} \tag{2.28}$$

3. Calculate the transformation $\Phi_{\text{bal,a}}$ and $\Phi^{-1}_{\text{bal,a}}$ that approximately balances the transformed system using the BPOD described in Sec. 2.2.1.

4. Select a subset of the balancing transformation to construct the reduction basis Φ_r and Φ_r^{-1} by keeping the firt k columns of $\Phi_{\text{bal,a}}$ and the first k rows of $\Phi^{-1}_{\text{bal,a}}$.

5. Transform the state space of the aerodynamic model with the reduction basis to obtain the k-th order ROM using Eq. 2.3.

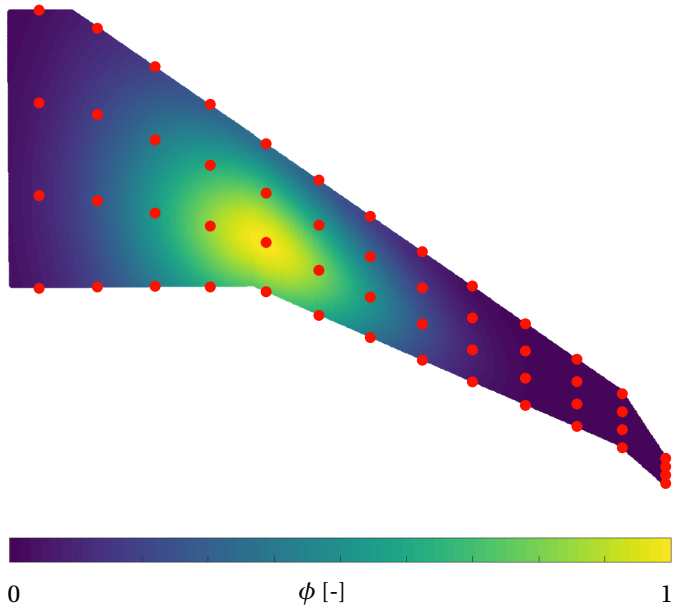

Figure 2.6: Example of a synthetic mode shape for a typical wing geometry based on radial basis functions alongside with the respective centre nodes.

Note, that no information concerning the structural or control surface properties is required for the generation of the aerodynamic ROM. In the following, the aerodynamic ROMs resulting from the proposed process are integrated with the structural and flight dynamic equations of motion and subsequently tested for their accuracy in aero(servo)elastic analyses. The synthetic mode shapes are only required for reducing the aerodynamic model and are not used in the integration of the aeroelastic model or the aero(servo)elastic analyses shown in the following.

2.3. APPLICATION AND RESULTS

In this section, first, the example case is introduced by describing the aeroservoelastic full order model with the structural and control surface variations used for benchmarking the resulting reduced order models (see Section 2.3.1). In Section 2.3.2, the aeroelastic analyses are introduced and appropriate error measures are defined to quantify the accuracy of the reduced order models in an objective comparison. The application of the BPOD without previous input transformation is described in Section 2.3.3. The main results produced with the proposed combination of the BPOD with input projection on synthetic mode shapes are presented in Section 2.3.4.

2.3.1. MODEL DESCRIPTION

As an illustrative example, a twin-engine tube wing aircraft configuration as depicted in Fig. 2.7a is examined. Since the resulting ROMs are to be used wit hin aeroservoelastic

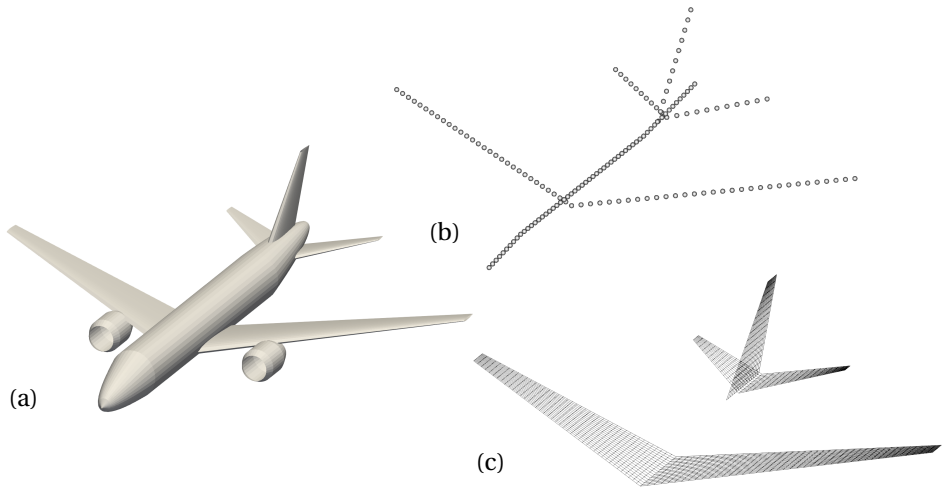

Figure 2.7: (a) The twin-engine tube wing aircraft configuration used as example. (b) The nodes representing the stick model used for the structural representation. (c) Panel mesh used for the generation of the full order unsteady aerodynamic model.

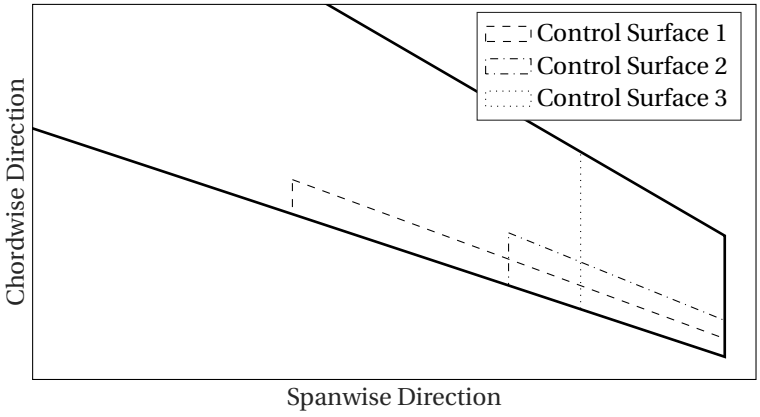

Figure 2.8: Schematic description of the three control surfaces used to test the robustness of the resulting ROMs regarding control surface layout variations.

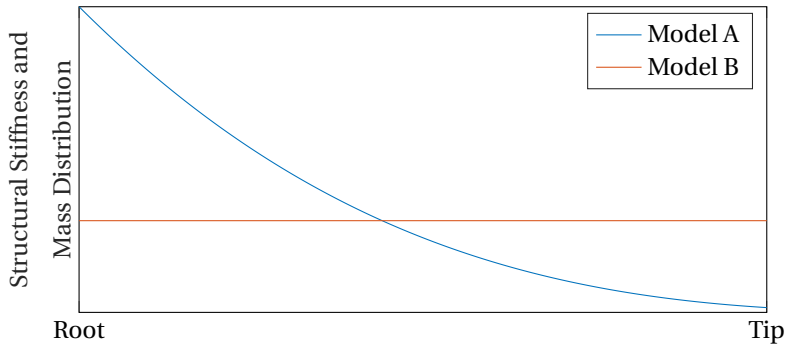

Figure 2.9: Primary stiffness and mass distributions of the two structural models used to test the robustness of the resulting ROMs regarding structural modifications.

optimisation, they must be robust to structural and control surface parameter variations. Therefore, threie control surfaces are defined at the tip of the main wing, see Fig. 2.8), with chordwise lengths of 15, 30 and 100 % of the local chord and spanwise lengths of 30, 15 and 10 % of the span of the main wing.

The aerodynamic model is based on a continuous time state space formulation of the UVLM [39], [40]. The panel model consists of 2180 surface bound panels, see Fig. 2.7c, and 8580 wake panels. The resulting linear state-space model has 2180 inputs for the boundary conditions imposed at the panels, 8580 wake vorticity states and 2180 outputs for the pressures on the surface-bound panels. Deflection of the control surfaces is facilitated by rotation of the normal vectors in the area of the control surface. By appropriate weighting, the boundaries of the control surface do not need to coincide with the panels and can be moved without regenerating the panel mesh.

A practical mean axis formulation is used for the formulation of the equations of motion that introduce the flight dynamic rigid body degrees of freedom [41]. The structural model is based on Euler Bernoulli beam elements placed at the elastic axis of the wings and the fuselage. The nodes representing the structural beam model are shown in Fig. 2.7b. Two different structural models are defined for the aircraft configuration to evaluate the accuracy of the resulting ROMs in the presence of structural modifications. As shown in Fig. 2.9, Model A has cubic mass and stiffness distributions and for Model B, linear distributions are used for the wing and tail structure. Mass and stiffness along the fuselage are assumed to be constant for both models. These distributions were solely chosen to obtain different eigenmodes and are not comparable to any realistic designs. Large system masses (engine and landing gear) are modelled as concentrated masses with rigid lever arms. A total of 20 structural mode shapes is retained in the aeroelastic analyses. The frequencies of the first ten in vacuo structural modes are shown in Table 2.1 for both structural models.

2.3.2. ANALYSES AND ACCURACY MEASURES

The targeted sizing-type optimisation problem consists of objective and constraint functions that depend on the results of analyses carried out using the integrated aeroservoe-

	Frequency [Hz]	
Mode	Model A	Model B
1	1.16	0.72
2	2.24	1.75
3	3.72	2.60
4	4.04	2.91
5	4.08	3.45
6	6.36	4.33
7	7.50	6.19
8	8.35	7.89
9	10.99	7.95
10	11.79	8.25

Table 2.1: In vacuo structural mode frequencies of both structural models without the rigid body modes.

lastic model. In addition to flutter point and gust loads assessment, aeroservoelastic analyses include the analysis of dynamics involved by control surface motion. In the following, these analyses are described in more detail, and error measures for each aeroelastic analysis are derived which will be used for the evaluation of the accuracy of the resulting ROMs.

Flutter Point With both structural models, the testcase shows a flutter instability at subsonic speeds. A flutter analysis is performed for a constant Mach number of Ma = 0.5 at sea level. Frequency ω and damping ζ of the first four structural modes over the velocity V are shown in Fig. 2.10 for model A and in Fig. 2.11 for model B.

The ROMs resulting from the proposed procedure shall be able to predict the flutter point (i.e. flutter speed and frequency) accurately for both structural models. In this work, the relative error in flutter speed V_f and frequency ω_f between every ROM $(\tilde{\cdot})$ and the unreduced, full order model is determined as:

$$\epsilon_{V_f} = \frac{\tilde{V}_f}{V_f} - 1 \tag{2.29}$$

$$\epsilon_{\omega_f} = \frac{\tilde{\omega}_f}{\omega_f} - 1 \tag{2.30}$$

The test case used shows a form of bending-torsion flutter with a high damping gradient near the flutter point. For flutter mechanisms in which the damping gradient is significantly lower, the flutter speed may vary strongly with small changes in the aeroelastic behaviour. For such flutter mechanisms, an error definition based on the damping of the aeroelastic modes of interest at a given speed should be used.

Gust Loads In this work, the root-mean-square (RMS) values of the dynamic response to a gust signal generated with the one dimensional von Kármán turbulence spectrum are used as a measure of the ROMs ability to predict gust loads. The parameters of the gust model are chosen according to the certification specifications for large aeroplanes

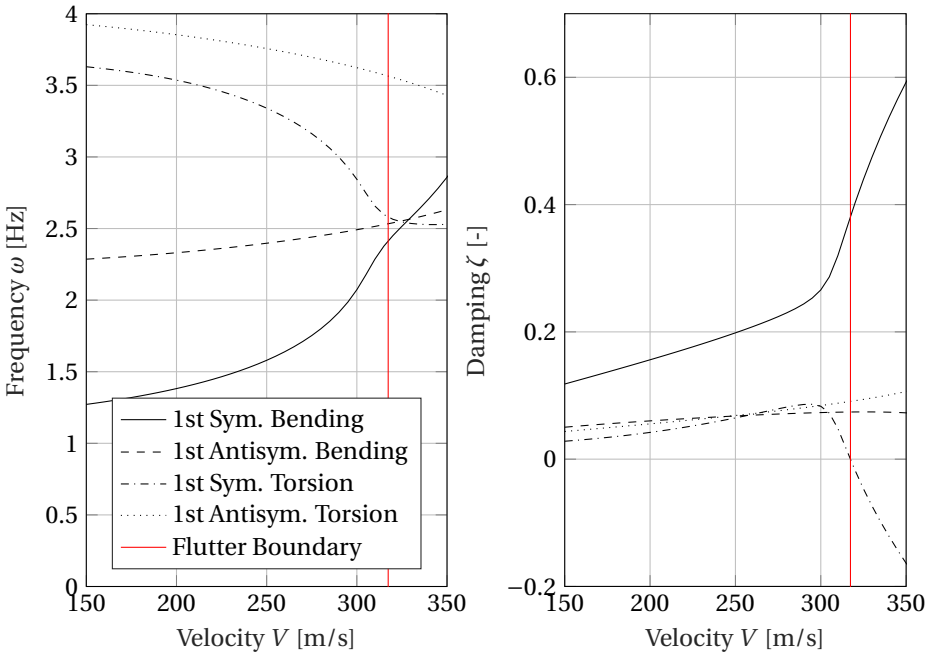

Figure 2.10: Flutter analysis results of the integrated aeroelastic model using structural Model A. The flutter boundary at a speed of $V = 317.37$ m/s is highlited.

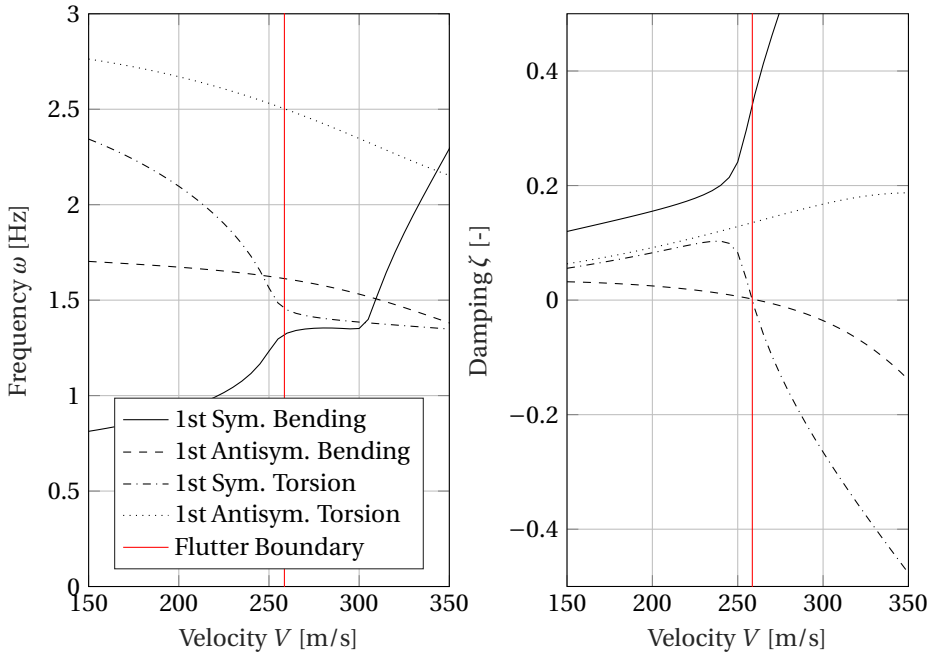

Figure 2.11: Flutter analysis results of the integrated aeroelastic model using structural Model B. The flutter boundary at a speed of $V = 258.55$ m/s is highlited.

[42]. A turbulence length scale of 2500 ft (762 m) is used, and the chosen flight condition corresponds to a Mach number of Ma = 0.5 at sea level which results in a turbulence intensity of 27.43 m/s. Gust zones are defined dividing the entire aircraft into 30 segments along the primary flight path to account for the time delay required as the vehicle passes through the gust. The error in the gust load prediction is defined as the relative difference in the RMS of the wing root bending moment $M_{x,\mathrm{wr}}$ between the ROM ($\tilde{\cdot}$) and the full order model:

$$\epsilon_{\mathrm{Gust}} = \frac{\mathrm{rms}(\tilde{M}_{x,\mathrm{wr}})}{\mathrm{rms}(M_{x,\mathrm{wr}})} - 1 \tag{2.31}$$

Control Surface Transfer Function As the intended application is an aeroservoelastic optimisation, the ROM used for the aerodynamics needs to accurately reproduce the influence of control surface motion on structural deflection and loads. Here, the influence is characterised by the transfer function from a symmetric control surface rotation input to an acceleration of the wingtip. The influence of actuation and sensor dynamics is not included in this transfer function. Error norms, such as the $\mathscr{H}_2$ norm, have been derived to measure the deviation of a given transfer function from a desired transfer function in the frequency domain. A frequency-limited formulation of the $\mathscr{H}_2$ norm is used which is given for a dynamical system G as [43]:

$$\|G\|_{\mathscr{H}_2,\omega,j} = \left(\frac{1}{\pi}\int_{\omega_1}^{\omega_2} |H_j(\nu)|^2 d\nu\right)^{\frac{1}{2}} \tag{2.32}$$

herein, H denotes the complex-valued transfer function from the control surface input j to the vertical tip acceleration. The frequencies ω_1 and ω_2 usually result from the targeted aeroelastic control law as well as the sensor and actuator bandwidth. The frequencies considered in this work range from 1 to 250 rad/s. The transfer function (from the rotational input of control surface 2 to the wingtip vertical acceleration) of the aeroelastic model with the full aerodynamic model is shown in Fig. 2.12 in the frequency range considered for the error computation. It is noted, that for accurate reduced order modelling for lower frequencies of interest, the singular perturbation technique should be favoured over a simple truncation as used in this work. For more information on the singular perturbation technique, the reader is referred to [44].

To quantify the deviation between the transfer function resulting from the ROM $\tilde{G}$ and the full order model transfer function G, the control surface transfer function error ϵ_{CS} is calculated by:

$$\epsilon_{\mathrm{CS}} = \frac{\|G - \tilde{G}\|_{\mathscr{H}_2,\omega}}{\|G\|_{\mathscr{H}_2,\omega}} \tag{2.33}$$

2.3.3. BPOD WITHOUT INPUT PROJECTION

Before applying the proposed combination of the BPOD with input projection on synthetic modes, a model reduction with the BPOD alone is presented in this section. Therefore all available inputs are used for the generation of the training data. With the presented test case, this results in 2850 input-state impulse response simulations required for the estimation of the controllability Gramian. The resulting state snapshots contain all possible characteristics that can be excited by the aerodynamic model inputs. To ensure

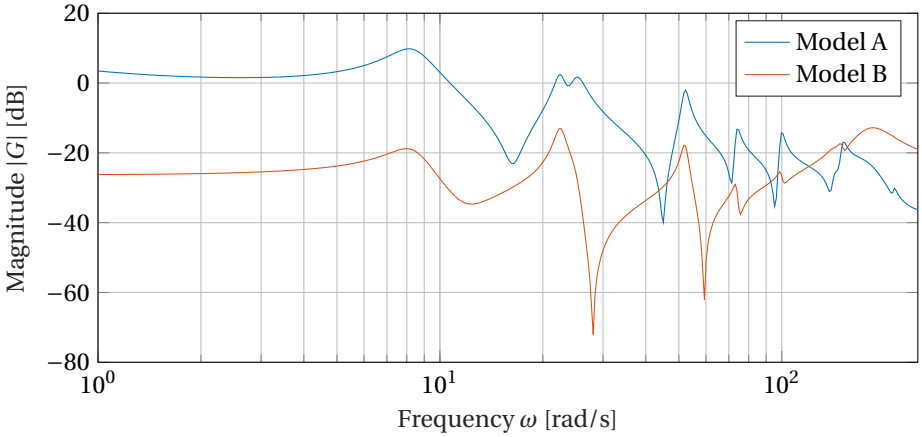

Figure 2.12: Transfer function from the rotational input of control surface 2 to the wingtip vertical acceleration. The transfer function is shown for both structural model variants and in the frequency range considered in the error computation.

that the subsequently calculated base of the POD modes contains all the relevant state characteristics, the projection error given in Eq. 2.14 is limited to $\epsilon_{\text{proj}} < 10^{-9}$. The approximately balancing transformation is computed with the approximation of the observability Gramian. In the following, aerodynamic ROMs are realised for various truncated model orders k and afterwards integrated with the structural and flight dynamic equations. These models are then used to perform the aeroelastic analyses described in the previous section. The calculation of the flutter point and gust loads results in two errors per structural model variant. Together with the three errors in the control surface transfer functions of the three control surfaces, this results in five errors for each structural model variant or in a total of ten errors for both structural models investigated. The maximum among these errors ϵ_{max} over the truncated model order k is shown in Fig. 2.13. As usual for the balanced truncation, the maximum error decreases rapidly with increasing model order k. However, the maximum error is not necessarily decreasing monotonically. Instead, oscillations are possible, and therefore a monotonic decreasing envelope is calculated to improve the readability of all following plots. At low truncated model orders (less than $k = 50$), the aerodynamic ROMs do not contain enough dominant flow characteristics leading to high maximum errors in the aeroelastic analyses. With increasing truncated model order, the error decreases to $\epsilon_{\text{max}} = 4 \cdot 10^{-4}$ corresponding to the maximum achievable accuracy.

It is noted that contrary to a balanced truncation using exact gramians, the BPOD cannot yield the exact results even if the full order balancing transformation is used. The error can be explained by its three sources. First, the data used in the BPOD is based on discrete snapshots of continuous time signals. Second, the impulse responses are calculated for a finite time horizon. And Third, the inputs of the adjoint system are projected on a set of POD modes before the determination of the observability Gramain. Consequently, if higher accuracy is desired, one may take more snapshots, increase the

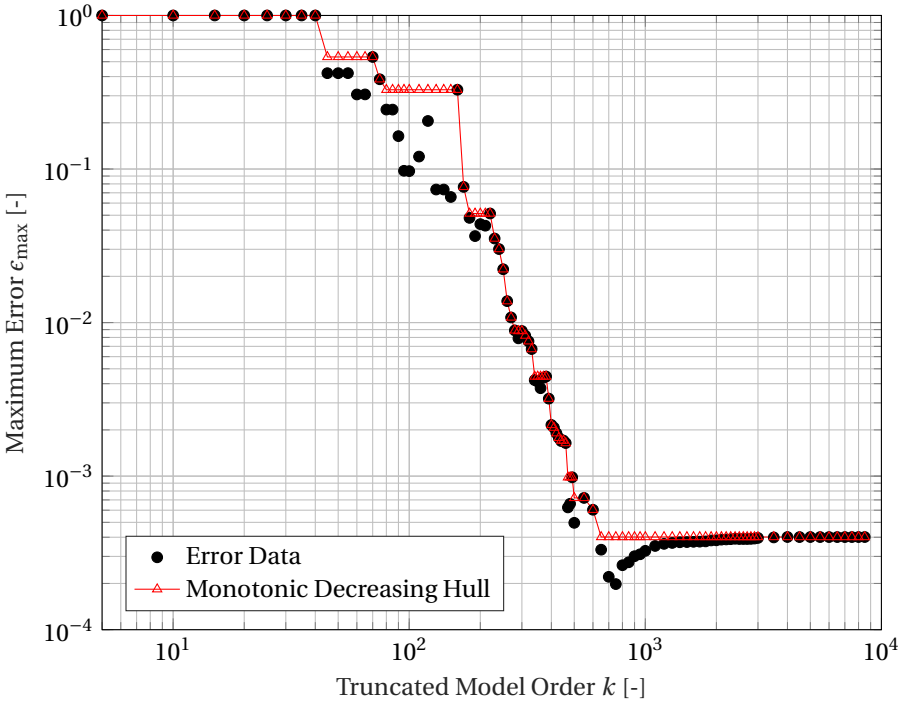

Figure 2.13: The maximum error (among the ten errors in the aeroelastic analyses) of the models resulting from a BPOD without input projection over the truncated model order. The monotonic decreasing envelope represents the upper expected error bound of the ROM.

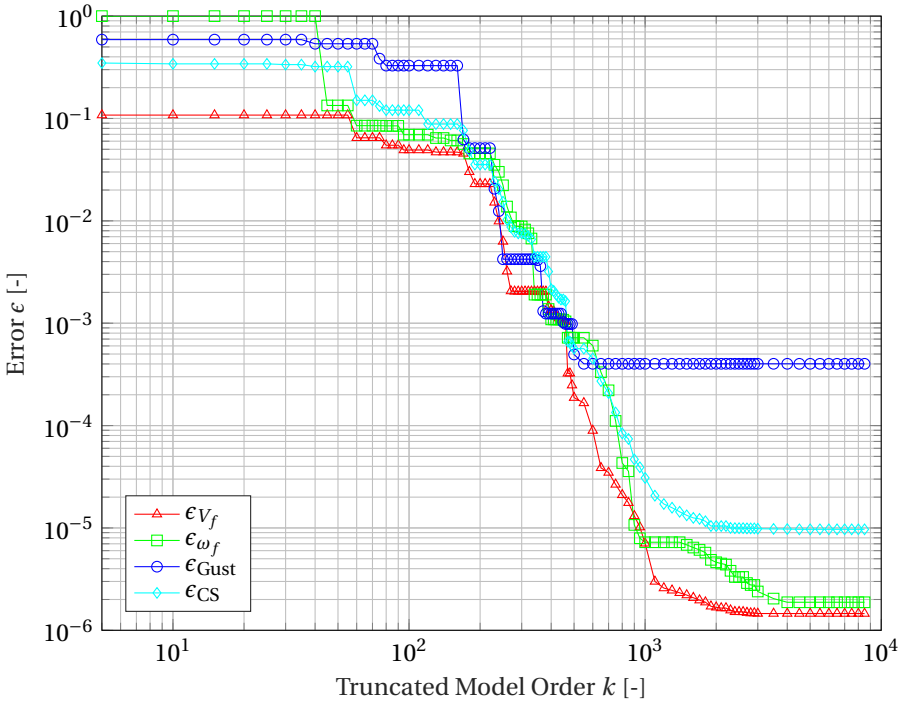

Figure 2.14: The analysis-specific error of the models resulting from a BPOD without input projection over the truncated model order.

simulation time horizon and limit the output projection error ϵ_{proj} to lower values. The maximum achievable accuracy is sufficient for the studies in the present work.

The error in the different analyses in dependency of the truncated model order k is shown in Fig. 2.14. Depending on the truncated model order, the highest error is caused by different analyses. While the highest error for low truncated model orders is observed in the flutter frequency, the maximum achievable accuracy is dominated by the gust load analysis. Without further studies, it is not evident whether the error is caused by the number of snapshots or by the end time of the impulse response simulations. The maximum achievable accuracies in all analyses with both structural models and all three control surfaces are listed in Table 2.2 together with the truncated model order required to achieve a given desired accuracy of $\epsilon < 10^{-3}$. For both structural models, the maximum achievable accuracy is driven by the gust load analysis. The required model order to achieve the desired accuracy is driven by the analysis of flutter frequency and control surface transfer functions both requiring a model order of $k = 470$.

2.3.4. BPOD WITH INPUT PROJECTION ON SYNTHETIC MODES

The idea of the proposed method is to capture more relevant flow characteristics in less balancing modes by an input projection on a suitable set of synthetic modes before the BPOD. Thereby, the required model order to achieve the desired accuracy is minimised

Structural Model	Analysis		Achievable Accuracy	Required Order ($\epsilon < 10^{-3}$)
A	Flutter Speed		$1.46 \cdot 10^{-6}$	340
	Flutter Frequency		$7.86 \cdot 10^{-8}$	**470**
	Gust Loads		$1.46 \cdot 10^{-5}$	460
	Transfer Func.	Ctrl. Surf. 1	$2.33 \cdot 10^{-6}$	340
		Ctrl. Surf. 2	$2.39 \cdot 10^{-6}$	340
		Ctrl. Surf. 3	$2.18 \cdot 10^{-6}$	390
B	Flutter Speed		$1.14 \cdot 10^{-6}$	400
	Flutter Frequency		$1.88 \cdot 10^{-6}$	**470**
	Gust Loads		$\mathbf{4.01 \cdot 10^{-4}}$	370
	Transfer Func.	Ctrl. Surf. 1	$5.81 \cdot 10^{-6}$	**470**
		Ctrl. Surf. 2	$9.22 \cdot 10^{-6}$	**470**
		Ctrl. Surf. 3	$9.69 \cdot 10^{-6}$	**470**

Table 2.2: Maximum achievable accuracy and minimum model order required to achieve the desired accuracy of 0.1% in the different analyses and for the different structural models. The minimum achievable accuracy as well as the highest required minimum order are highlited. The models result from a BPOD without input projection.

compared to the case without prior input projection.

For this, first, the optimal number of synthetic mode shapes is determined for each type of mode shapes separately in Section 2.3.4. In Section 2.3.4 the different types of mode shapes are then compared to each other concerning their suitability for the use in aerodynamic model order reduction. The results are also compared to the results without input transformation shown in the previous section.

THE OPTIMAL NUMBER OF SYNTHETIC MODES

It is evident that with a larger number of orthogonal synthetic mode shapes, a closer approximation of the actual mode shapes can be obtained by linear combination. However, when more characteristics are included in the snapshot data used for the BPOD, the resulting singular values show a lower rate of decay, and thus less energy will be concentrated in or captured by the selected subset of balancing modes. As a result, for higher accuracy, larger subsets must be taken, and the resulting required model order is higher. Besides, a larger number of synthetic mode shapes results in more simulations that must be carried out leading to a higher computational effort required during the ROM generation phase. At the same time, a certain number of synthetic mode shapes is required to capture a sufficient variety of flow characteristics in the training data. The resulting reduced order model can only reflect characteristics which are available in the training data. In the following, ROMs are generated with varying numbers of synthetic mode shapes used in the process of snapshot data collection. The goal is then to find the right amount of synthetic modes needed to achieve a given desired accuracy in the aeroelastic analyses ($\epsilon_{\max} < 10^{-3}$) while keeping the computational effort for the model order generation and the required model order as low as possible.

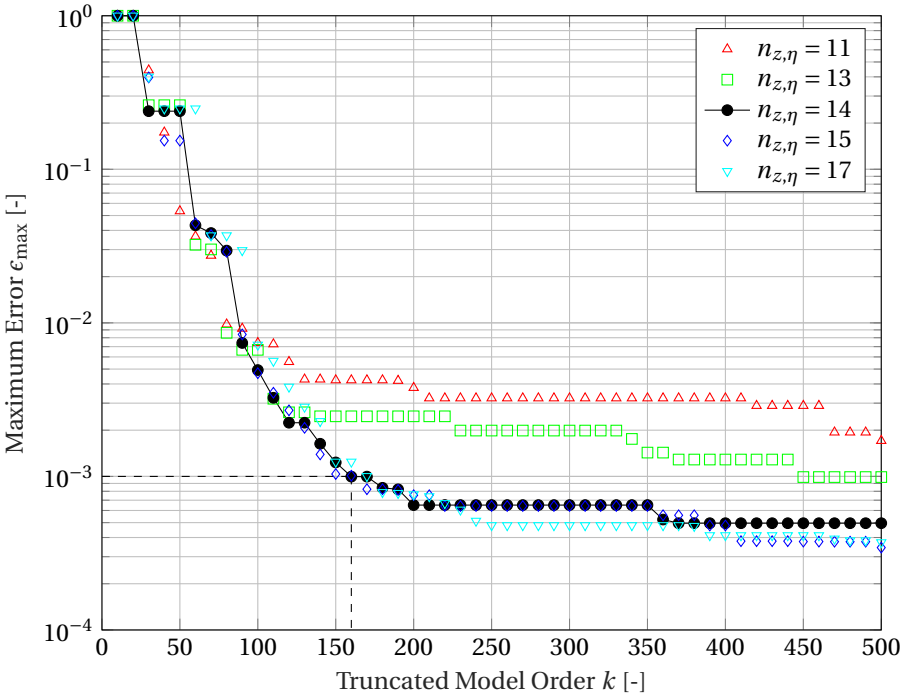

Figure 2.15: The maximum error in the aeroelastic analyses over the truncated model order for various number of zones per reference span $n_{z,\eta}$ at a fixed number of chordwise zones of $n_{z,\xi} = 2$.

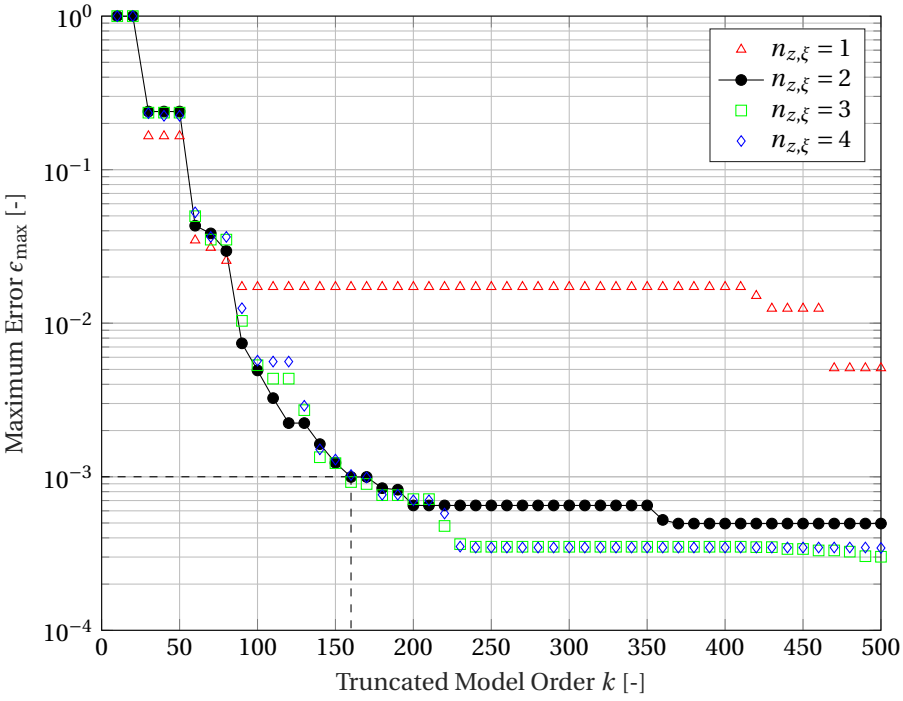

Figure 2.16: The maximum error in the aeroelastic analyses over the truncated model order for various number of chordwise zones $n_{z,\xi}$ at a fixed number of zones per reference span of $n_{z,\eta} = 14$.

Input Projection on Synthetic Modes based on Zonal Aggregation The maximum error over the truncated model order for the various number of zones per reference span $n_{z,\eta}$ at a fixed number of chordwise zones of $n_{z,\xi} = 2$ is shown in Fig. 2.15. As expected, the maximum error decreases rapidly with increasing truncated model order, i.e. the number of balancing modes kept in the transformation. The cases differ mainly in the maximum achievable accuracy within the analysed range of truncated model orders. More zones and thus more synthetic mode shapes result in a bigger and more complex set of data which contains a broader variety of state snapshots and therefore the rate at which the maximum error decreases, i.e. the accuracy per model order, is lower. It is furthermore observed, that if the number of synthetic mode shapes is too small, the captured characteristics are insufficient to achieve the desired accuracy.

For the given desired accuracy of $\epsilon_{\max} < 0.1\%$, both the cases $n_{z,\eta} = 14$ and $n_{z,\eta} = 15$ can be seen as optimal as both require the lowest truncated model to achieve the desired accuracy. However, a number of zones per reference span of $n_{z,\eta} = 14$ is chosen as a less computational effort is required for the generation of the ROM.

A similar behaviour can be observed when varying the chordwise number of zones $n_{z,\xi}$ at a fixed number of spanwise zones of $n_{z,\eta} = 14$. The resulting maximum error in the aeroelastic analyses over the truncated model order is shown in Fig. 2.16. Again, the case is identified which requires the lowest truncated model order to achieve the desired

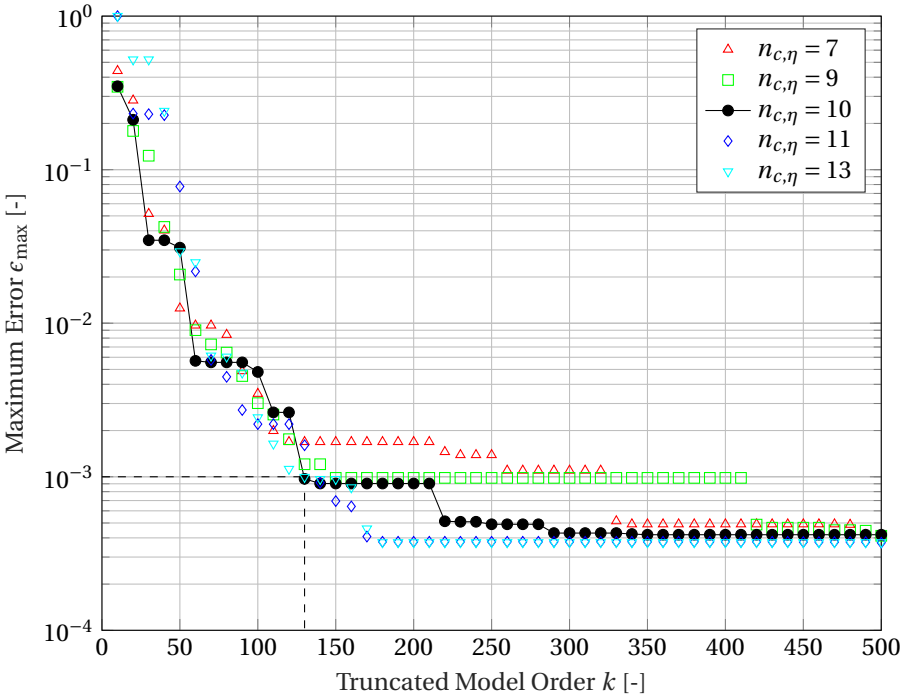

Figure 2.17: The maximum error in the aeroelastic analyses over the truncated model order for various number of Chebyshev polynomials per reference span $n_{c,\eta}$ at a fixed number of chordwise Chebyshev polynomials of $n_{c,\xi} = 4$.

accuracy. With the additional constraint of keeping the number of synthetic modes as low as possible, a number of chordwise zones of $n_{z,\xi} = 2$ is identified as the most favourable case.

Input Projection on Synthetic Modes based on Chebyshev Polynomials The optimal number of Chebyshev modes is determined in the same way. The maximum error over the truncated model order for the various number of spanwise and chordwise Chebyshev polynomials is shown in Fig. 2.17 and Fig. 2.18. A similar trend is observed as in finding the optimal number of zones, and the optimal setup is chosen to be $n_{c,\eta} = 10$ and $n_{c,\xi} = 4$.

Input Projection on Synthetic Modes based on Radial Basis Functions Besides the number of RBF centre nodes, the formulation used for the generation of RBF modes requires the definition of the radius scaling factor f in Eq. 2.26. The maximum error over the truncated model order for different radius scaling factors is shown in Fig. 2.19. Here, both the spanwise as well as the chordwise number of RBF centre nodes are fixed. Similar to the previously described way of determining the optimal number of synthetic mode shapes, the optimum radius scaling factor is found by identifying for which radius scaling factor f the lowest truncated model order is required. The maximum error over

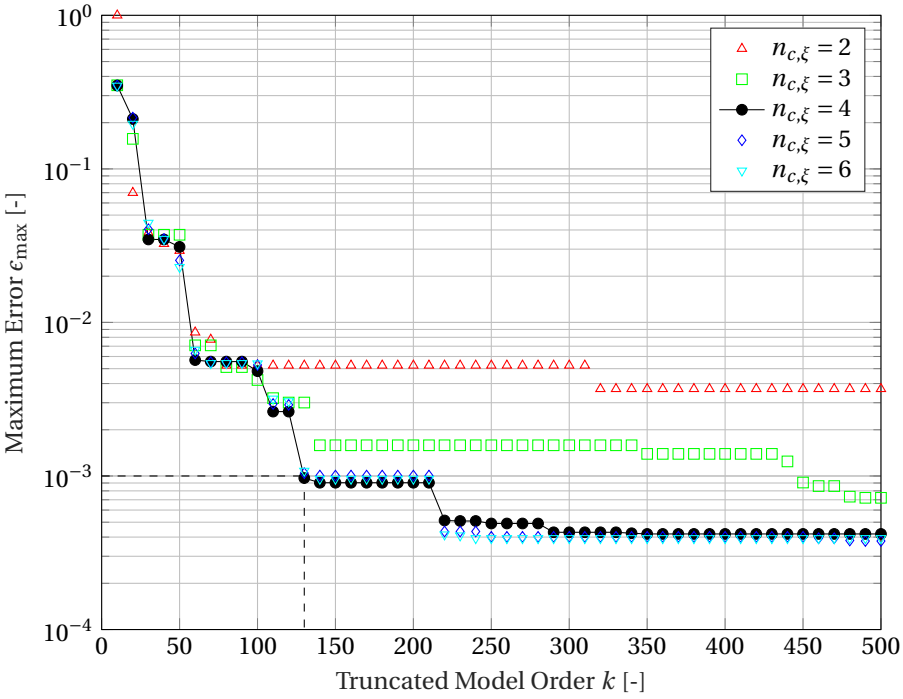

Figure 2.18: The maximum error in the aeroelastic analyses over the truncated model order for various number of chordwise Chebyshev polynomials of $n_{c,\xi}$ at a fixed number of Chebyshev polynomials per reference span of $n_{c,\eta} = 10$.

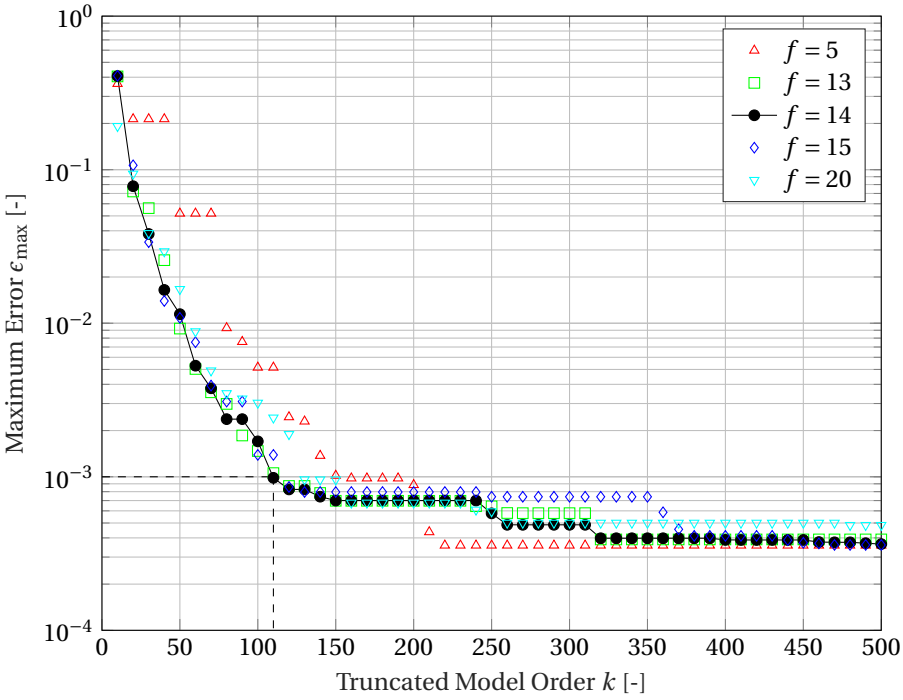

Figure 2.19: The maximum error in the aeroelastic analyses over the truncated model order for various radius scaling factors f at a fixed number of centre nodes per reference span of $n_{r,\eta} = 10$, and at a fixed number of chordwise centre nodes of $n_{r,\xi} = 4$.

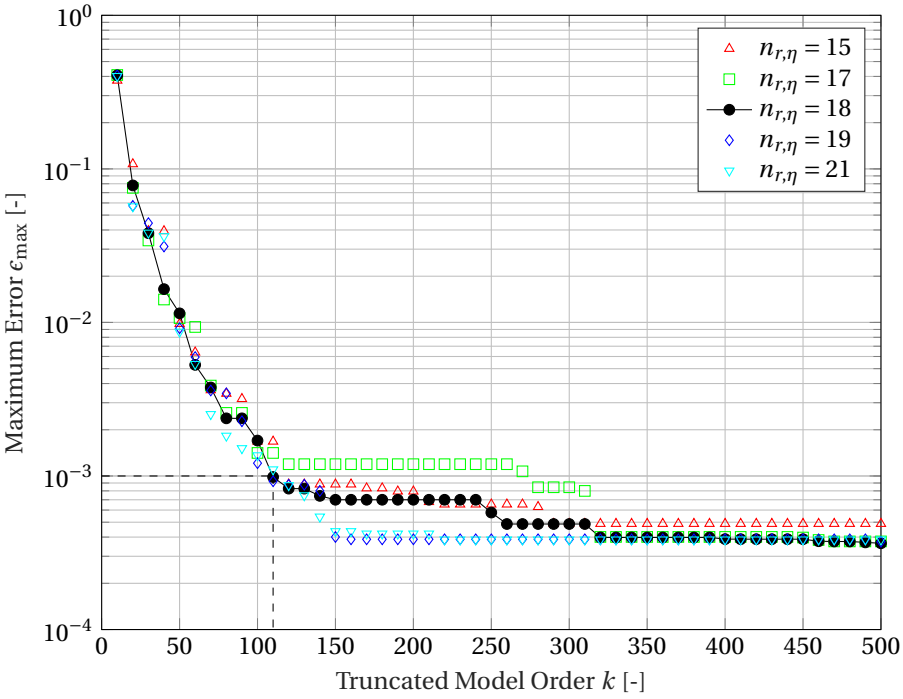

Figure 2.20: The maximum error in the aeroelastic analyses over the truncated model order for various number of centre nodes per reference span $n_{r,\eta}$ at a fixed number of chordwise centre nodes of $n_{r,\xi} = 3$ and a fixed radius scaling factor of $f = 14$.

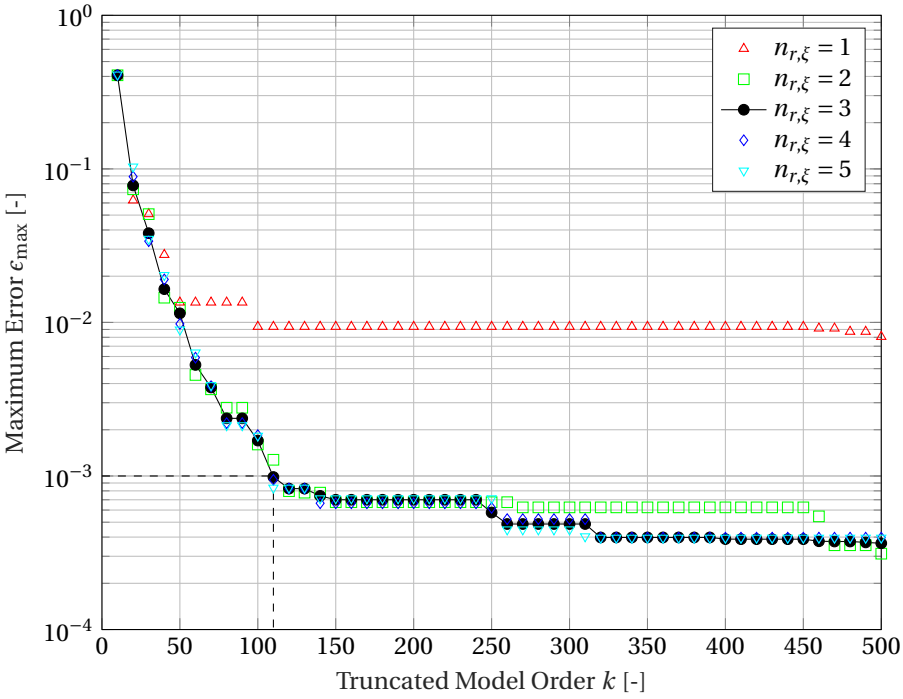

Figure 2.21: The maximum error in the aeroelastic analyses over the truncated model order for various number of chordwise centre nodes $n_{r,\xi}$ at a fixed number of centre nodes per reference span of $n_{r,\eta} = 18$ and a fixed radius scaling factor of $f = 14$.

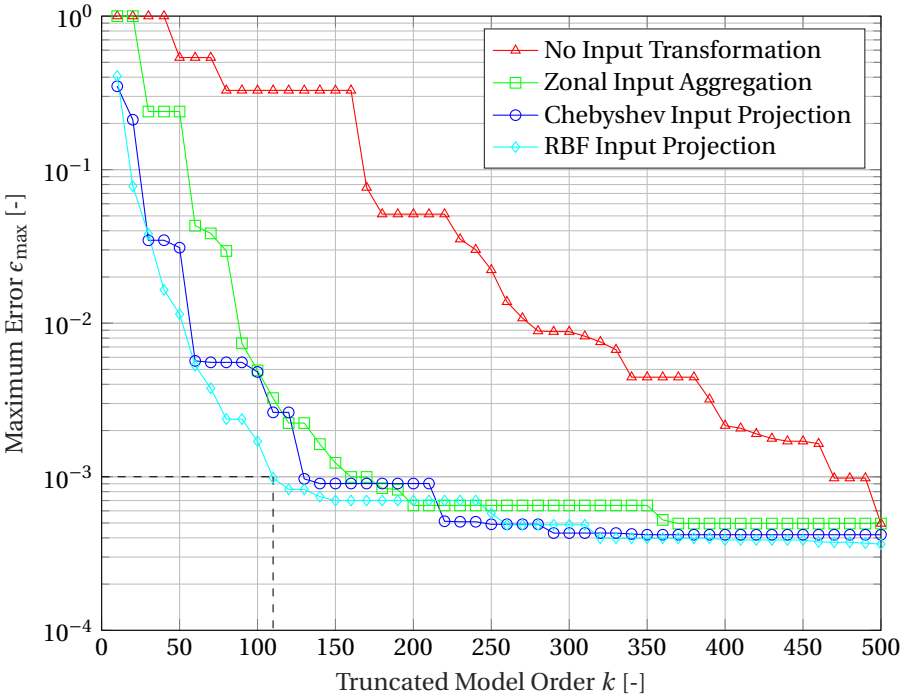

Figure 2.22: The resulting maximum error over the truncated model order for the different types of synthetic mode shapes used and a case without input transformation.

the truncated model order for the various number of spanwise and chordwise RBF centre nodes is shown in Fig. 2.20 and Fig. 2.21. The optimal setup is chosen to be $n_{r,\eta} = 18$ spanwise RBF centre nodes, $n_{r,\xi} = 3$ chordwise RBF centre nodes and a radius scaling factor of $f = 14$.

THE OPTIMAL TYPE OF SYNTHETIC MODESHAPES

The individually chosen parameters for the synthetic mode shapes are optimal in terms of the compactness of the resulting ROMs for the given desired accuracy. In the following, the different sets are compared to each other to find the most suitable type of synthetic modes.

Accuracy per Order The resulting maximum error over the truncated model order is shown in Fig. 2.22 for the different types of synthetic mode shapes used. For comparison, results are also shown in which the balancing transformation is determined without prior input transformation as presented in Section 2.3.3. It can be immediately seen that with an input projection by each of the types of synthetic mode shapes, models can be established showing a higher accuracy per order in the analysed range of truncated model orders compared to the method without prior input transformation. Among the three methods employing synthetic mode shapes, the use of RBF modes shows the

highest rate of decrease in the maximum error. Furthermore, the models created by using RBF modes show fewer oscillations in the error which can be seen by the fact that the monotonically decreasing envelope has fewer areas in which the error is constant over a range of truncated model orders. This shows that synthetic mode shapes based on RBFs are less sensitive to the choice of the truncated model order.

The model orders required to achieve the desired accuracy in the different aeroelastic analyses are summarised in Table 2.3. The order required to achieve the desired accuracy in all analyses ranges from 110 to 160 for the different types of synthetic mode shapes used. Compared to the case without input transformation, this corresponds to a reduction in the required model order of 66-77%. Depending on the type of synthetic modes, the required order is driven by different analyses. Using zonal modes, gust loads and flutter analysis (depending on the structural model) drive the required model order. When using modes based on Chebyshev polynomials or RBF functions, the required order is determined by the analysis of the control surface transfer functions.

Putting the results in relation to the unreduced, full order model, the BPOD results in a significant total reduction of the states ranging from 98.1% combined with zonal modes to 98.7% combined with RBF modes while the maximum error in the aeroelastic analyses being less than 0.1% in the presence of significant structural and control surface parameter variations.

Computational Effort Not only the accuracy per order of the ROM can be improved, but also the computational effort required for the generation of the balancing transformation can be reduced using synthetic mode shapes. In Table 2.4, the number of required impulse response simulations is listed for the different synthetic mode shapes used in their optimal setups. The reduction in required impulse response simulations is comparable for all the methods and lies in the range of 95% compared to the process without input transformation. Among the methods that use synthetic modes, the most significant reduction in computational effort can be achieved with zonal modes. Compared to RBF modes, about 22% fewer simulations are needed. Depending on the number of analyses carried out with the reduced order model and the complexity of the full order model, the choice of the type of synthetic mode shapes has to be done based on the available generation time and the desired accuracy of the reduced order model.

Correlation of the Results to the Modal Assurance Criterion The MAC is widely used to quantify the similarity of two mode shapes. The MAC value between two mode shapes ϕ_1 and ϕ_2 is given by [45]:

$$\mathrm{MAC} = \frac{|\phi_1^T \phi_2|^2}{(\phi_1^T \phi_1)(\phi_2^T \phi_2)} \tag{2.34}$$

The more correlation, the higher the MAC value. A MAC value of 1 indicates full similarity, i.e. ϕ_1 and ϕ_2 are the same vector except for a possible scaling.

To use the MAC values as an approximation quantification, first, the approximated mode shapes are calculated with the respective set of synthetic modes by finding the linear combination. In Fig. 2.23 the resulting mean MAC Values are depicted for the different synthetic modal bases used in the prior analyses (i.e. in their optimal setup). While

Structural Model	Analysis		No Input Projection	Zonal Modes	Chebyshev Modes	RBF Modes
A	Flutter Speed		340	90	50	60
	Flutter Frequency		**470**	140	100	70
	Gust Loads		460	**160**	80	70
	Transfer Func.	Ctrl. Surf. 1	340	120	90	80
		Ctrl. Surf. 2	340	140	**130**	100
		Ctrl. Surf. 3	390	150	100	**110**
B	Flutter Speed		400	120	80	60
	Flutter Frequency		**470**	**160**	70	100
	Gust Loads		370	120	80	70
	Transfer Func.	Ctrl. Surf. 1	**470**	140	**130**	100
		Ctrl. Surf. 2	**470**	150	**130**	**110**
		Ctrl. Surf. 3	**470**	150	110	**110**
Maximum			**470**	**160 (-66%)**	**130 (-72%)**	**110 (-77%)**

Table 2.3: Comparison of the required truncated model order in the different aeroelastic analyses for the different types of synthetic mode shapes used for input transformation and the case without input transformation. The highest required model order for each type is highlighted indicating the minimum required order to obtain $\epsilon_{\max} < 10^{-3}$.

	No Input Transformation	Zonal Modes	Chebyshev Modes	RBF Modes
$n_{\text{sim, primal}}$	2180	52	72	96
$n_{\text{sim, dual}}$	391	64	66	53
$n_{\text{sim, total}}$	2571	**116 (-95%)**	138 (-95%)	149 (-94%)

Table 2.4: Number of required impulse response simulations for the different types of synthetic mode shapes used for input transformation and the case without input transformation.

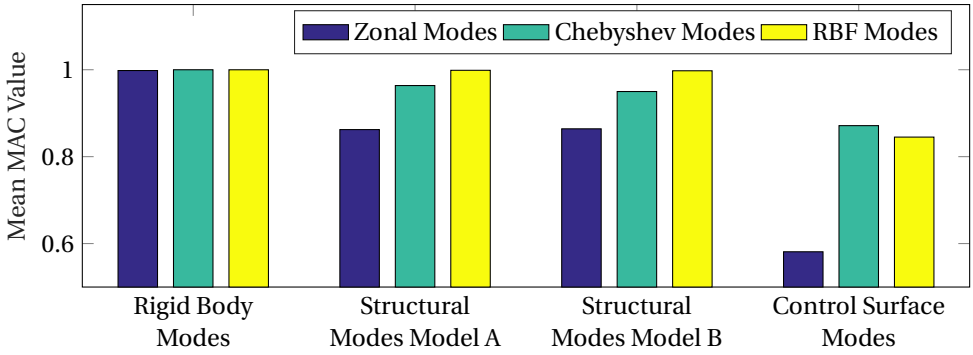

Figure 2.23: Mean MAC values between the actual mode shapes and the approximations resulting from the different sets of synthetic mode shapes in their optimal setup for model order reduction.

all types of synthetic mode shapes successfully approximate the rigid body modes, the RBF modes outperform the other methods in approximating the structural mode shapes of both structural models. This correlates to the result of the previous section where the models created using RBF modes produce the highest accuracy per order. However, considering the MAC values of the control surface modes, no correlation is observed to the results shown in Table 2.3. Although the approximation of the control surface modes by RBF modes is not as accurate as by Chebyshev polynomials, the ROM produced using RBF modes still shows the highest accuracy per order in the control surface transfer functions. This becomes even clearer in the case of zonal modes. The MAC analysis shows a relatively poor consistency of the control surface modes compared to the structural and flight dynamic modes. In turn, the accuracy per order of the control surface transfer functions is comparable to the accuracy per order in the other aeroelastic analyses. In general, it can be said that evaluating the suitability of synthetic modes for the purpose of model reduction by the MAC value can be misleading and should be avoided.

2.4. CONCLUSION

In this work, a procedure for the generation of ROMs has been outlined which is suitable for the use in aeroservoelastic optimisation. The concepts of BPOD and synthetic mode shapes are combined to facilitate ROMs which are robust to structural and control surface layout variations. Three different types of synthetic mode shapes based on zonal subdivision, Chebyshev polynomials and RBFs have been formulated for full aircraft

configurations. The resulting algorithm has been applied to an aeroservoelastic model of an exemplary aircraft configuration. Besides an analysis of the optimal number of synthetic mode shapes, the different types have been compared to each other concerning their accuracy in aeroservoelastic analyses, computational effort during the generation of the ROM and resulting MAC values.

It was shown that all methods are improving the accuracy per order of the resulting ROM compared to a BPOD without the use of synthetic mode shapes. Next, the influence of the number of synthetic modes used for the ROM generation was examined, with the result that the number of synthetic modes has a considerable impact on the achievable accuracy and the accuracy per order of the resulting ROM. The maximum error in the aeroelastic investigations (stability, gust loads and control surface transfer functions) caused by the model order reduction in the presence of structural and control surface layout variations has been constrained to be less than 0.1%. With this requirement, the optimal setup was determined for each type of mode shapes individually.

The use of RBF based mode shapes in combination with the BPOD resulted in the highest reduction of the states of 98.7% compared to the full order model and 77% compared to a BPOD without prior input transformation. To approximate the input space to the aerodynamic model, 96 RBF based synthetic mode shapes have been used. These mode shapes have been generated on a grid of ten points per reference span and four points per reference chord. The computational effort required for the generation of the ROM is reduced by 94% compared to the BPOD without input transformation. This generation time can be further reduced when using synthetic mode shapes based on zonal subdivision. The lowest required order for the desired accuracy was achieved with 14 zones per reference span and two zones per reference chord resulting in a total of 52 synthetic mode shapes used to approximate the input space of the aerodynamic model. The optimal type and number of synthetic mode shapes is thus depending on the envisaged number of simulations carried out with the reduced order model and the available time required for its generation.

The presented method was applied in the reduction of a linear, incompressible aerodynamic model based on the unsteady vortex lattice method. Analysing the capabilities of the method in reducing higher order aerodynamic models capturing complex flow effects (e.g. transonic effects) is subject to further research. However, since the excitation of the aerodynamic model is purely based on the structural and control surface motion, it is believed that the synthetic mode input projection still enhances the results and efficiency of model order reduction techniques based on simulation snapshot data.

3

The Interaction of Active Control and Passive Structural Tailoring

Abstract This chapter presents an analysis of the interaction and trade-off between active aeroelastic control and passive structural tailoring on a free-flying fully flexible aircraft model. Both technologies are included in the preliminary design of a typical transport aircraft configuration with a conventional control surface layout containing trailing edge control surfaces and spoilers. The passive structural tailoring is facilitated by exploiting the anisotropic properties of composite materials to steer the static and dynamic aeroelastic behaviour. Active aeroelastic control is implemented by scheduled control surface deflections redistributing the aerodynamic loads during manoeuvres to achieve manoeuvre load alleviation and a feed-forward control law for gust load alleviation. The panel-based aerodynamic modelling of spoiler deflections is improved by a correction of the spatial distribution of the boundary condition derived from higher fidelity simulation data. The optimisation of active control laws requires the consideration of constraints of the actuation system, namely rate and deflection saturation, in a nonlinear manner. The interaction of manoeuvre load alleviation, gust load alleviation and passive structural tailoring is investigated on the basis of results of different aeroservoelastic optimisations. Therefore the primary wing structure is simultaneously optimised with the individual technologies being activated or deactivated, resulting in eight different wing structures. The results of the individual and combined optimisations reveal significant design differences. The potentials of the different technologies can only be optimally exploited by simultaneous optimisation. The chapter concludes with a study of the sensitivity of the major findings with respect to the knockdown factor for failure applied to the material properties. A substantial shift of effectiveness from active aeroelastic control to passive structural tailoring is observed with increased allowables resulting in more flexible and hence less stiff wing designs.

Publication A modified version of this chapter was published as: S. Binder, A. Wildschek, R. De Breuker, The Interaction Between Active Aeroelastic Control and Structural Tailoring in Aeroservoelastic Wing Design. *Aerospace Science and Technology*, Vol.110, No. 106516, 2021.

3.1. INTRODUCTION

The introduction of composite materials was an important milestone in the development of lightweight wing structures. However, costly manufacturing, high repair costs and complex recycling processes put the advantages of the high strength to weight ratio into perspective. In fact, full exploitation of the material properties is required for composite materials to compete with well established metallic structures [46]. An important step in fully exploiting the anisotropic material properties of carbon fibre reinforced plastics has been the industrial utilisation of automated processes for producing tow-steered composites. While the method allows improving the aeroelastic behaviour by introducing beneficial aeroelastic couplings passively, the interaction with active control systems is affected. The analysis thereof is the subject of this work.

In aviation, the exploitation of anisotropic material properties has its origin 70 years ago in the development of wooden propellers in which the fibre direction was utilised to create the desired aeroelastic behaviour [8]. This method, also known as structural tailoring, is defined as the steering of the aeroelastic behaviour by structural design so that it is favourable for the particular performance target. In terms of wing development, structural tailoring by the embodiment of directional stiffness promises various enhancements of the aircraft performance. The early studies have concentrated on the beneficial effects of the induced stiffness cross-coupling on static and dynamic aeroelastic stability, control surface effectiveness and load redistribution for manoeuvre load alleviation and lift efficiency [47]. Further studies also revealed the positive influence of structural tailoring on the dynamic characteristics relevant for gust encounters [48], [49]. Motivated by the promising results, directional stiffness was included as a parameter in the field of multidisciplinary aircraft wing optimisations. While most optimisation studies aim to reduce the mass of the primary structure [50] [51], others seek to further increase the fuel efficiency of aircraft by additionally improving the lift-to-drag ratio in static trim conditions [52]. In recent years, the investigation of the influence of directional stiffness on the dynamic behaviour of box-like wing structures has received more attention [53], [54].

Stodieck et al. [55] recently investigated the application of tow-steering in the design of composite wing boxes. With the inclusion of control surface effectiveness constraints, it became apparent that depending on the design driving constraints, different mechanisms occur. While load alleviation for manoeuvre and gusts requires wash-out, control surface effectiveness and flutter speed were raised by inducing a wash-in behaviour by structural tailoring.

Contrary to passive methods for influencing the aeroelastic behaviour, active means have been investigated since decades. An important distinction from passive methods results from the ability of the active control methods to adapt to the particular flight conditions such as fuel state, payload configuration or centre of gravity position. The active control systems considered in this work are Manoeuvre Load Alleviation (MLA) and

Gust Load Alleviation (GLA).

Both technologies have been applied to various aircraft [56] and target the alleviation of aerodynamic loads by control surface deflections in a way that is beneficial for the structural design. Concerning MLA, the redistribution of aerodynamic loads by control surface deflections mostly involves a shift of the centre of pressure inboard and thus closer to the wing root resulting in a reduced bending moment. Gust Load Alleviation targets the reduction of the loads encountered during turbulent flight conditions by dynamic control surface deflections. Feeding back the signal of sensors as accelerometers to control surface actuators can artificially increase the damping of specific aeroelastic modes and thereby lower the structural loads. Instead of modifying the response, these control surface deflection commands can also be computed by feeding forward a filtered signal of a turbulence measurement taken upfront the aircraft. Both ways, the control surface deflections lead to redistributed aerodynamic loads when encountering turbulence.

Besides the influence that GLA has on the dynamic response of an aircraft, the similarity in the mechanisms of structural tailoring and MLA, as well as the conflicting requirements on the bending-torsion coupling, suggests that strong interaction is expected when using both technologies on a single wing. Weisshaar predicted that the designers of active control systems for composite wings would have not only to examine the effect of changing the gains but also the effects of structural tailoring on the resulting control law [57]. The interaction and the associated issues or synergies have led to a variety of studies and projects to address the so-called field of aeroservoelasticity. The general aspects of aeroservoelastic modelling, analysis and optimisation, as well as relevant applications, are summarised in [16].

Dealing with aircraft wings on a simplified and general level, the studies of Zeiler and Weisshaar [58], Librescu et al. [59] and Weisshaar and Duke [60] have been, amongst others, pointing the way. In the study performed by Zeiler et al. [58], the synergistic potential of integrated structural and control design was revealed in a wing optimisation with the objective of aeroelastic stability increase. More specifically, specific changes in the structural design showed an increase in the controllability of modes that were otherwise nearly uncontrollable [58]. This beneficial effect was also observed by Librescu et al. [59] when extending the concept to anisotropic, composite wing structures. It was shown that the combined optimisation outperforms either structural tailoring or active control alone [59]. Weishaar and Duke [61] investigated the combined use of active control and structural tailoring with the objective of drag reduction. With combined use, the induced drag can be minimised with smaller control surface deflections, but the determination of the deflections requires a combined optimisation with the structure.

Over the years and as the tools and methods for integrated aeroservoelastic analysis and optimisation have evolved, many applications have been presented that target the integrated preliminary design of transport aircraft wings.

Integrating active manoeuvre and gust load control in the preliminary aircraft design was shown to have a drastic impact on the resulting optimal overall design [62]. Many studies exist in which transport aircraft wing structures with isotropic material properties are optimised concurrently with flutter control, GLA, MLA and shape adaption by morphing [63], [64], [65], [66], [67].

The interaction of structural tailoring and active control was studied by Handojo

et al. [68] using the example of optimisation of a composite wing in the presence and absence of a fixed control law for manoeuvre and gust load alleviation. However, in the applied sequential optimisation, the optimiser couldn't fully utilize the directional stiffness properties as the sensitivity of the loads with respect to the structural design parameters was invisible to the optimiser. As a result, the optimiser was unable to exploit the potential of the directional stiffness properties to redistribute and alleviate the loads.

Integrated design of subsonic transport aircraft composite wings employing structural tailoring and active trailing edge morphing for manoeuvre load alleviation has been presented by Werter [69] finding that design difference occur both in the stiffness distribution as well as the morphing induced camber distribution whether or not the other technology is accounted for. A similar investigation was carried out by Krupa et al. [70], who simultaneously optimised a wing structure including the control surface deflections for active manoeuvre load alleviation. As expected, the wing employing both technologies outperformed the designs employing one of the two.

The previously given examples were focused either on single technologies or combinations of structural tailoring with manoeuvre load alleviation or flutter control. The interaction between active gust load alleviation and structural tailoring in the integrated optimisation of composite wings has not been studied on the example of transport aircraft configurations. The above-listed examples that include active control and structural tailoring consider either single control surfaces or distributed control surfaces located at the trailing edge. The following points differentiate the present work from the mentioned studies:

- Instead of individual considerations or pairwise combinations, an analysis of the interaction between the three technologies of structural tailoring, manoeuvre load alleviation, and gust load alleviation is presented as the tailored utilization of directional stiffness properties affects both, manoeuvre and gust loads.
- Instead of single control surfaces or idealised layouts, a typical transport aircraft configuration is used with a conventional control surface layout consisting of spoilers and ailerons that is compatible to the current state of the art.
- The influence of the structural flexibility on the observed interactions and the trade-off between active and passive load alleviation is analysed by a continuous variation of the material properties. This enables the assessment of the extent to which the results retain validity in case of variations.

Various optimisations of the wing structure are carried out with the individual technologies and their combinations to understand the mechanisms behind the three technologies. Optimisations are carried out including static and dynamic aeroelastic constraints including strength and buckling constraints resulting from manoeuvre and gust flight conditions. For the consideration of structural tailoring, a predefined laminate layup is used that complies with the usual composite design guidelines used in the industry. The actual parameter for including stiffness direction in the optimisation is the reference direction of the plies. The MLA is included by scheduled control surface deflections during the steady symmetric load conditions, i.e. pull-up or push-over manoeuvre, and antisymmetric load conditions, i.e. rolling manoeuvres. A stack of finite impulse response

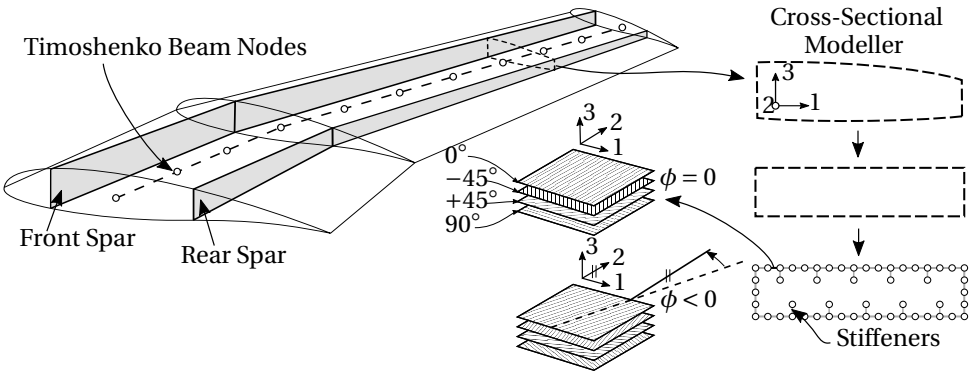

Figure 3.1: Structural modelling approach using Timoshenko beam elements with stiffness and mass properties obtained by the cross-sectional modeller. Explanation of the reference angle or principal stiffness direction ϕ.

filters are optimised alongside the other design parameters to emulate the presence of an optimal feed-forward gust load alleviation system. The chapter concludes by answering the remaining question whether the observed interactions are robust to variations in the selected material by a sensitivity analysis of the major findings with respect to the knockdown factor applied to the material properties.

3.2. AEROSERVOELASTIC MODEL

The integrated aeroservoelastic design studies carried out in this work are performed with the open-source toolchain dAEDalus that has been originally developed to investigate the effects of aeroelasticity on the handling qualities during preliminary aircraft design [13]. Among other developments, the capability of numerical optimisation was included in the course of this work. The following introduces the models of structural dynamics, aerodynamics and active control required for the aeroservoelastic optimisation.

3.2.1. STRUCTURAL MODEL

The equations of motion of the structural dynamics are based on the finite element method. Linear Timoshenko beam elements are used for the discretisation of the aircraft structure on a global level. The stiffness and mass properties of the thin-walled wing cross-sections are obtained by the cross-sectional modeller developed by Ferede and Abdalla [71]. The implementation used in the course of this work has been adopted from Proteus, a toolchain developed by Werter and De Breuker [14] for the structural optimisation of aeroelastically tailored wing structures.

On the cross-sectional level, the geometry of the cross-section is first discretised with two-dimensional shell elements, as shown in Fig. 3.1. The outer dimensions of the cross-sections result from predefined spar positions and airfoils. The height of the front and rear spar are assumed to be equal. On the laminate level, the layup is specified by the stacking sequence of the individual ply directions. The Timoshenko cross-sectional stiffness matrix is computed based on the discretised cross-section, the composite layup and the material properties consisting of longitudinal/transverse and in-plane shear

modulus as well as Poisson's ratio. The Timoshenko cross-sectional stiffness matrix $\mathbf{C}$ relates the strains ϵ and curvatures κ at the beam axis reference point to the applied stress resultants F and moments M:

$$\mathbf{C}\{\epsilon_{11},\epsilon_{12},\epsilon_{13},\kappa_1,\kappa_2,\kappa_3\}^T = \{F_1,F_2,F_3,M_1,M_2,M_3\}^T \tag{3.1}$$

The various elements of the cross-sectional stiffness matrix $\mathbf{C} = C_{ij}$ (with $i = 1..6$, $j = 1..6$) provide information about the kinematic mechanisms and couplings that occur in the deformation of the beam elements. The bending-torsion coupling C_{45} relating κ_1 to M_2 is of particular interest because it produces the mentioned wash-in or wash-out behaviour of the wing.

With the information obtained on the cross-sectional level, the Timoshenko beam element stiffness and mass matrices are obtained. The global stiffness and mass matrix are thereafter assembled. The full stiffness and mass matrix are used for the static structural analyses, whereas a representation based on modal coordinates is employed in the dynamic structural model. A mean-axis approach is utilised for the realisation of the equations of motion of the free-flying flexible body, as used by Seywald [13].

3.2.2. AERODYNAMIC MODEL

The steady aerodynamic model in dAEDalus is based on the well-known Vortex Lattice Method (VLM) [72]. The unsteady aerodynamic model is based on a continuous-time state-space formulation of the Unsteady Vortex Lattice Method (UVLM) that has been first described by Mohammadi et al. [73] for two-dimensional airfoils, formulated for three-dimensional lifting surfaces by Werter et al. [74], and extended for arbitrary motion and control surface deflections by the Binder et al. [75]. Both methods produce panel-based aerodynamic models based on linear potential flow theory. The flowfield is solved by a superposition of fundamental solutions to the linearised Laplace equation forming a linear system of equations. Flow tangency, i.e. zero normal flow, is imposed as a boundary condition on the lifting surface to solve the linear system of equations.

A deflection of a control surface is realised by a modification of the boundary conditions imposed on the respective control surface panels. The modification is equivalent to a rotation of the panels associated with the control surface around the hinge axis. The control surface deflection thereby leads to a different flow field in which mainly the circulation near the control surface is changed. By appropriate weighting of the rotation factors, the boundaries of the control surface do not need to coincide with the panel boundaries.

The control surface layout used in this work also includes spoilers for which this type of modelling, i.e. the mere modification of the boundary condition imposed on the spoiler panels, produces unsatisfactory results. The flow around a deployed spoiler, i.e. exhibiting large deflections, is highly dominated by effects that are not accounted for by potential flow methods, e.g. regions of separated flow behind the spoiler. In the following, the derivation of a correction method is shown to improve the accuracy of modelling spoilers with the vortex lattice method. The boundary condition is therefore modified for all panels in the spanwise region of the spoiler instead of only the spoiler panels.

The linearity of the vortex lattice model allows an inverse computation of the required incremental boundary condition $\mathbf{b}_{\text{req}}$ that results in a given incremental pressure

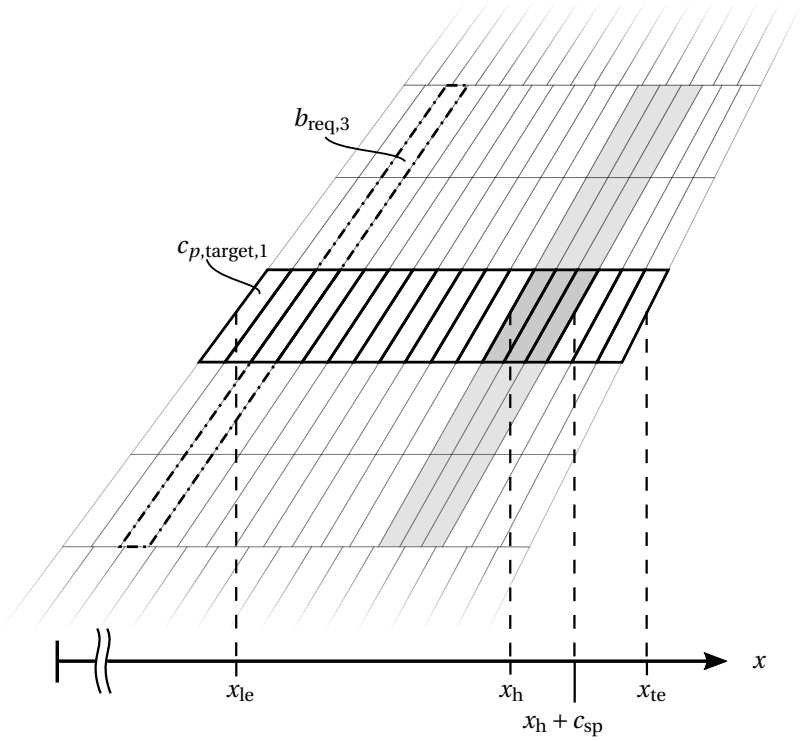

Figure 3.2: Aerodynamic panel mesh in the area of a spoiler control surface. The panels chosen for the derivation for a correction law are highlighted in bold. The dash-dotted line indicates the area in which the boundary condition is varied simultaneously.

distribution $\mathbf{c}_{p,\text{target}}$ by solving the linear system of equations:

$$\left(\frac{\partial c_{p,i}}{\partial b_j}\right)_{(i=1..n_p, j=1..n_p)} \mathbf{b}_{\text{req}} = \mathbf{c}_{p,\text{target}} \tag{3.2}$$

with $\partial c_{p,i}/\partial b_j$ being the influence that an increment in the boundary condition of the j-th panel has on the pressure coefficient of the i-th panel. These differentials are obtained by a transformation of the influence coefficients that are naturally available using the VLM.

To provide a correction that is usable for different shapes and positions of spoilers, the set of panels considered in the target pressure distribution is limited to a set of panels in the area of the midspan of the spoiler surface, which are the bold panels in Fig. 3.2. Furthermore, the boundary condition is varied simultaneously for all spanwise panels of a row in chordwise direction in the region of the spoiler. The combination of the panels of the third row, resulting in the combined boundary condition $b_{\text{req},3}$, is indicated by the dash-dotted line in Fig. 3.2.

The target pressure distribution used here is calculated from data obtained by a commercial CFD solver based on Reynolds Averaged Navier Stokes (RANS) equations.

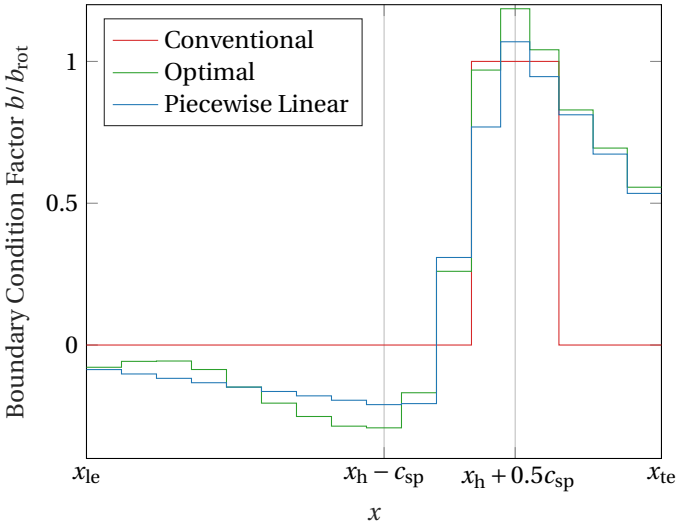

Figure 3.3: Comparison of the boundary condition required to match the pressure distribution obtained by CFD simulation with the conventional boundary condition. The piecewise linear approximation represents the simplified correction that is usable for different shapes and positions of spoiler control surfaces.

The CFD computations were carried out on the wing of the NASA Common Research Model (CRM [76]) for one flight condition with and without spoiler deflection. The target pressure distribution is calculated by mapping the data obtained by the CFD computations to an equivalent panel mesh.

The chordwise distributed boundary condition that matches a sectional pressure distribution obtained by the CFD calculation is shown in Fig. 3.3 and is indicated by the adjective optimal. The boundary condition is normalised to the equivalent boundary condition obtained by a conventional rotation of the panels resulting in the boundary condition factors b/b_{rot}. The chordwise distribution of a conventional rotation b_{conv} of the panels associated to the spoiler surface is shown for comparison.

A simplified distribution is obtained by an approximation of the optimal distribution by piecewise linear segments between the four chordwise stations indicated in Fig. 3.3 by the vertical lines:

$$\begin{aligned} b(x_{\text{le}}) &= -0.075 b_{\text{rot}} \\ b(x_{\text{h}} - c_{\text{sp}}) &= -0.2 b_{\text{rot}} \\ b(x_{\text{h}} + 0.5c_{\text{sp}}) &= 1.1 b_{\text{rot}} \\ b(x_{\text{te}}) &= 0.5 b_{\text{rot}} \end{aligned} \tag{3.3}$$

Herein, x_{le}, x_{te} and x_{h} denote the chordwise position of the leading edge, trailing edge and spoiler hinge axis, and c_{sp} denotes the chord of the spoiler control surface.

While the correction factors are obtained for one intermediate spoiler deflection of 15°, that this is expected to be sufficient for load alleviation functions, Fig. 3.4 shows the resulting integrated sectional lift and moment coefficient for various spoiler deflections. It can be seen that the VLM without correction produces unsatisfactory results.

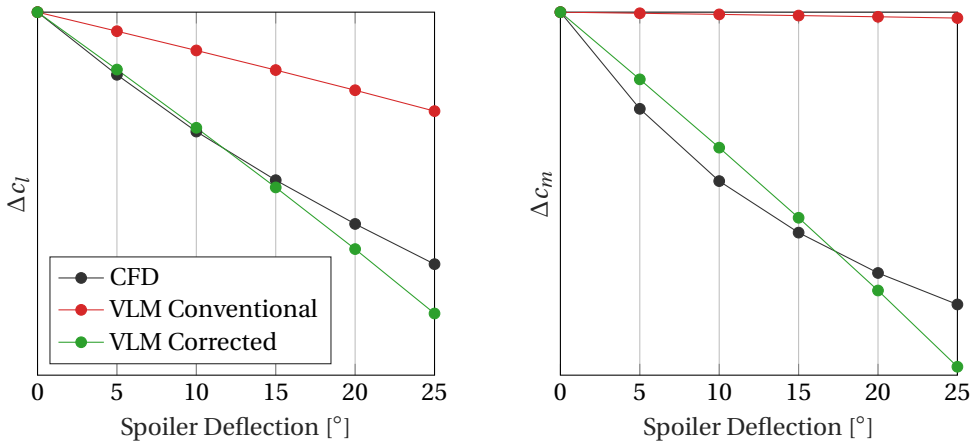

Figure 3.4: Spoiler induced increment in sectional lift Δc_l and sectional moment Δc_m for various spoiler deflections obtained by CFD, the conventional VLM without correction and the corrected VLM.

The resulting reduction in lift Δc_l due to a spoiler deflection is only nearly half of that observed in the CFD results. The change in the sectional moment coefficient Δc_m, which is essential for aeroelastic applications, can not be predicted at all. The correction method significantly improves the accuracy of the VLM in predicting the sectional lift and moment coefficient. However, the linear VLM cannot account for the nonlinear effects that are observed in the CFD results such as flow separation.

The derived piecewise linear correction law is implemented for all spoiler control surfaces in the aerodynamic models used in this work. However, due to the lack of appropriate simulation data, it was not investigated, to which extend the correction method found is applicable for unsteady aerodynamic models.

The models representing the unsteady aerodynamics of aircraft including wing, horizontal and vertical tail lifting surfaces are large and costly to simulate, i.e. the number of states is usually exceeding 10^4. During the aeroservoelastic optimisations envisioned in this work, many analyses have to be carried out using the unsteady aerodynamic model. Model order reduction methods target the realisation of models that reproduce a certain model behaviour of interest as precisely as possible with a lower number of states and equations, and whose simulation is possible with less computational effort. Among the most common methods for model order reduction, the balanced proper orthogonal decomposition was found to be most suitable in reducing aerodynamic state-space models that are based on the continuous-time UVLM [77]. By the combination with the use of synthetic mode shapes, the model order reduction can be carried out before the optimisation and thereby without knowledge of the structural dynamics [78]. In the course of this work, the method reduces the order of the aerodynamic state-space model by two orders of magnitude before the integration with the structural and flight dynamic equations of motion.

Coupling the aerodynamic model to the equations of motion of the free-flying flexible body requires the transformation of aerodynamic loads to structural loads and the

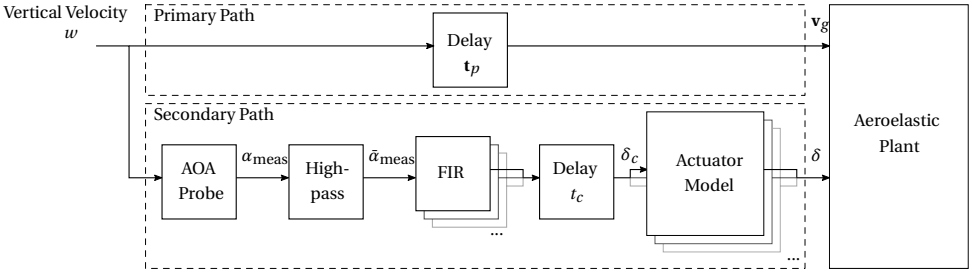

Figure 3.5: Control scheme used to emulate the presence of an optimal gust load control law during the structural optimisation.

transformation of structural motion to the motion of the panels. The generation of the required coupling matrices, as well as the integration of the models used in this work, is described by the author in detail in Ref. [79].

3.2.3. ACTIVE AEROELASTIC CONTROL

The presence of an MLA control law is simulated by commanding control surface deflections δ_{MLA} during the static analysis of the manoeuvre conditions. For push-over and pull-up manoeuvres, these control surface deflections are symmetric, i.e. the deflections on the right wing equal the deflections of the control surfaces on the left wing. In case of asymmetric load conditions, e.g. a roll manoeuvre, the symmetric deflections are additionally superimposed by a vector of antisymmetric control surface deflections $\delta_{\text{MLA,asym}}$.

The GLA control law is modelled by the secondary feed-forward path that is shown in Fig. 3.5. The vertical flow velocity w is sensed by an Angle Of Attack (AOA) sensor located at the nose of the aircraft. The measured variation in angle of attack α_{meas} is high pass filtered to prevent the feed-forward controllers from trying to alleviate the trim angle of attack. The resulting signal $\bar{\alpha}_{\text{meas}}$ is then passed to the stack of Finite Impulse Response (FIR) filters associated to the individual control surface pair. Thereby, one FIR filter is used per control surface pair consisting of left and right control surface. The z-transfer function of an FIR filter of order N can be written as [80]:

$$H_{\text{FIR}}(z) = \sum_{n=1}^{N} h_n z^{-n+1} \tag{3.4}$$

with h_n being the n^{th} element of the vector of FIR filter coefficients $\mathbf{h}$.

The subsequent delay t_c accounts for the time required by the fictitious controller for the computation of the control surface deflection commands δ_c. The actuators for each control surface pair are modelled as nonlinear second-order systems with rate and deflection limits. After the commanded signals δ_c have been processed by the actuator models of the individual control surfaces, the resulting actual deflections δ are forwarded to the aeroelastic model.

In parallel, the vertical flow velocity w is delayed before it is passed to the gust zone inputs $\mathbf{v}_g$ of the aeroelastic model, see the lower path in Fig. 3.5. The different delays

in the vector of time-delays $\mathbf{t}_p$ depend on the flight speed and the distance between the reference point, i.e. the aoa probe, and the aerodynamic centres of the individual gust zones.

It should be noted that in this work, the assumption of one-dimensional turbulence profiles results in an exact measurement of the gust velocity at only one spanwise station. Furthermore, no uncerntainty in the delay t_c and properties of the actuator transfer function are taken into account. Under these circumstances, the feed-forward path used here can be considered as a highly idealised gust load controller.

3.3. AEROSERVOELASTIC ANALYSIS AND OPTIMISATION

For the optimisations required in this work, static and dynamic aeroservoelastic analyses are performed after integrating the models of aerodynamics, structure and control described in the previous section. This section describes the principal methodology of steady manoeuvre and dynamic gust analysis as well as the general aspects of the optimisation problem formulation.

3.3.1. ANALYSIS

The analysis of quasi-steady manoeuvre conditions is done by finding the static equilibrium between inertial and aerodynamic forces acting on the aircraft. The iterative search of the required angle of attack, angle of sideslip and control surface deflections eliminates the need for the trim parameters to be design variables in the optimisation problem. For symmetric cases, the angle of attack and the elevator deflection are used as trim parameters to find the longitudinal equilibrium between weight forces and the required lift. The asymmetric roll manoeuvre condition also requires the equilibrium of lateral forces. Therefore, the trimming parameters additionally include antisymmetric control surface deflections $\delta_{\text{MLA,asym}}$ and the sideslip angle β. As multiple control surfaces can be used for roll control, the weights of the individual deflection are used as design variables defining the roll allocation $\bar{\delta}_{\text{MLA,asym}}$. A single amplification parameter r is then used within the trimming routine that is multiplied with the the vector of weights to find the actual individual control surface deflections:

$$\delta_{\text{MLA,asym}} = r\bar{\delta}_{\text{MLA,asym}} \tag{3.5}$$

For the dynamic analysis of gust encounters during horizontal flight conditions, the simulation of the free-flying flexible body is performed in the time domain in three steps:

1. The discrete transfer functions of the FIR filters, compare Eq. 3.4, are transformed in the time domain by a bilinear transformation, and the control surface commands δ_c due to the gust profiles are computed as depicted in Fig. 3.5.

2. The continuous-time signal of commanded control surface deflections is subsequently used in the nonlinear simulation of the actuator, including actuator rate limitations and deflection saturation.

3. The resulting actual control surface deflection histories δ are used alongside with the gust profiles in a linear time-domain simulation of the overall aircraft dynamics.

Subsequently, structural failure is assessed by the computation of strength and buckling reserve factors with the wing deformation resulting at the obtained equilibrium points of the steady cases and the time history of the dynamic analysis. Similar to the approach used by Werter [69], the strength failure criterion is based on the work of IJsselmuiden et al. [81], and the buckling reserve factors are computed by a buckling analysis based on the work of Dillinger et al. [82]. It should be noted that only local buckling is taken into account with the buckling panels being bounded by ribs and stiffeners. For computational reasons, the buckling reserve factors during gust encounters are computed only for the maximum principal strains obtained in the dynamic analysis.

3.3.2. OPTIMIZATION PROBLEM FORMULATION

The objective of all design optimisations carried out in the current work is the reduction of the mass of the primary wing-box structure, i.e. the skin and spars.

The design parameters include structural and control design variables. Four variables are used for the thickness of skins and spars in each beam element, i.e. no chordwise variation of the thickness is allowed and the stringer thickness is held constant. The local minimum allowable value for the material thickness is defined based on requirements resulting from manufacturing, handling and uncontained engine failure cases. While the layup is held constant throughout the optimisation process, only the ply thickness is varied to ensure a continuous design space. Besides the laminate thickness variables, the laminate principal stiffness direction is optimised in the form of a distribution of the reference angle ϕ for the 0° ply direction as shown in Fig. 3.1. The spanwise distribution of the principal stiffness direction is therefore formulated as a linear combination of Chebyshev polynomials:

$$\phi(\eta) = \sum_{i=1}^{n} c_{\phi,i} \frac{\left(\eta + \sqrt{\eta^2 - 1}\right)^{n-1} + \left(\eta - \sqrt{\eta^2 - 1}\right)^{n-1}}{2} \tag{3.6}$$

where n denotes the number of polynomials used. The vector of coefficients $\mathbf{c}_\phi = [c_{\phi,1}, c_{\phi,2}, ..., c_{\phi,n}]^T$ is used as the structural tailoring design variable. A similar approach based on B-splines has been used by Stodieck et al. [55] to ensure smooth property variations along the span.

The MLA design space is spanned by a vector of commanded control surface deflections δ_{MLA} for each load case and additionally the roll allocation weights $\bar{\delta}_{\text{MLA,asym}}$ for asymmetric conditions as roll manoeuvres. Finally, the GLA design variables consist of one vector of FIR filter coefficients $\mathbf{h}$ for each control surface pair that is used for dynamic gust load control.

Various constraints $c \in \mathscr{R} > 0$ are used to form the feasible region that is defined as $c \leq 1$ in the design space. For each component of the wingbox structure, i.e. front spar, rear spar, upper skin, and lower skin, one buckling and one strength constraint are formulated for each beam element and flight condition. The constraints resulting from the time histories of all gust analyses, i.e. with the various gust gradients considered, are aggregated to one constraint using the Kreisselmeier-Steinhauser functions [83]. By this, the gust analysis results in one buckling and one strength constraint per beam element and wingbox component.

The maximum and minimum control surface deflections used for MLA are bounded for symmetric flight conditions and formulated as constrains for roll conditions. The control surface rate and deflections occurring during gust encounters are limited by the actuator models resulting in an always feasible GLA feed-forward path. A damping constraint is used at the gust analysis speed, ensuring a stable dynamic system for numerical purposes during the time domain gust analyses.

It should be noted that flutter margins and flutter control are not considered in the course of this work. However, for numerical reasons, static and dynamic stability are constrained at the speeds at which the manoeuvre and gust analyses are carried out.

A single optimisation problem is formulated that consists of structural and control design variables to minimise the wingbox structural mass with respect to the constraints described above. The workflow is shown in the form of an Extended Design Structure Matrix (XDSM, [84]) in Figure 3.6.

An active set algorithm is used to reduce the complexity of the search for the optimal solution by considering only a subset of constraints which are active at the current design point. The gradient-based optimisation algorithm requires the computation of a Jacobian matrix at every optimisation iteration. The sparsity of this Jacobian is exploited by an efficient procedure that runs only the required analyses, e.g. as the GLA design variables do not affect manoeuvre constraints, the respective gradients are zero and do not need to be computed by finite differentiation.

3.4. ANALYSIS AND RESULTS

The previously described models and analysis procedures are now used for the optimisation of an aircraft wing structure. After a description of the test case, eight optimisations are carried out with the individual technologies, i.e. MLA, GLA and structural tailoring, being activated or deactivated. Based on the resulting designs, the interaction of manoeuvre load alleviation, gust load alleviation and passive structural tailoring is investigated next. A study of the sensitivity of the major findings with respect to the knockdown factor applied to the material properties is presented at the end of the section.

3.4.1. TEST CASE DESCRIPTION

The analyses and optimisations presented in this work are conducted on a generic long-haul transport aircraft model. The configuration belongs to category 4E (ICAO/EASA aerodrome reference code) and has a Maximum Take-Off Weight (MTOW) of more than 250,000 kg.

The airframe structure is made from AS4/3501-6 composite material. The individual layers of unidirectional tape are placed in an angle of 0°, 90° and ±45° relative to the reference direction. The layup is also defined by fixed percentages of the individual layer directions. Furthermore, only symmetric and balanced layups are considered. Tailoring is exerted in the wing skins only, the primary stiffness direction of the spars coincides with the beam axis. This means that the desired bending torsion coupling is only achieved by modifying the extension shear coupling in the skins. The maximum number of the Chebyshev polynomials used as shape functions for the distribution of the reference angle ϕ is set to five. The wing structure is discretised using 34 beam elements.

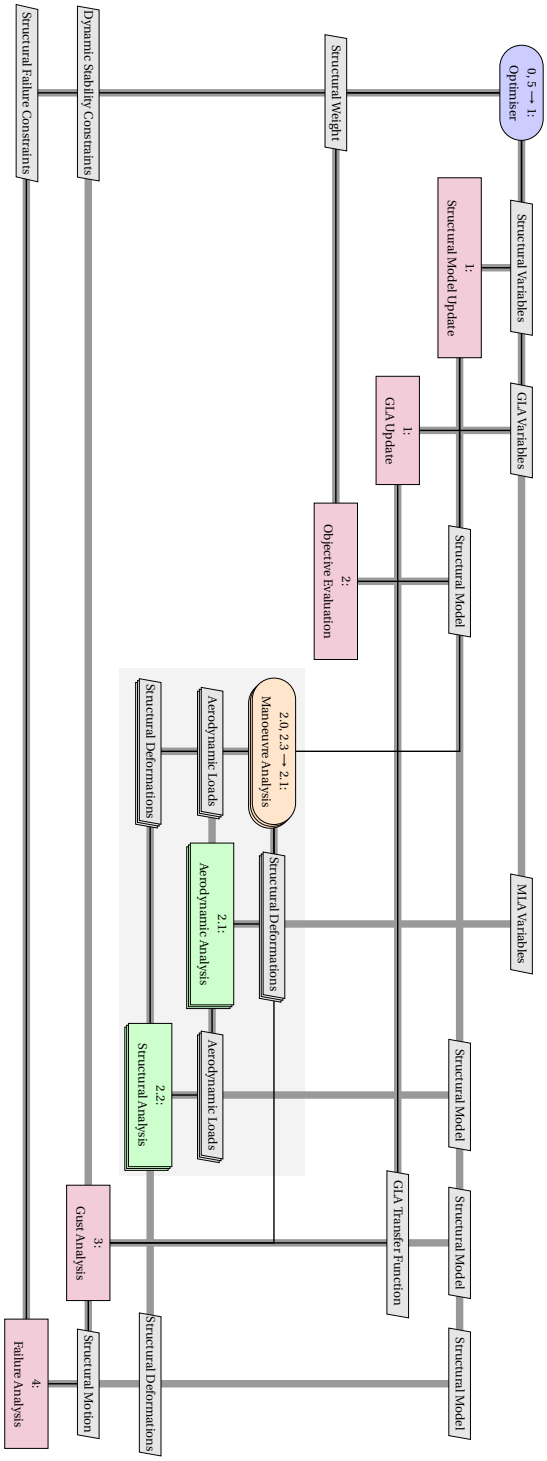

Figure 3.6: XDSM diagram showing the workflow of the optimisations.

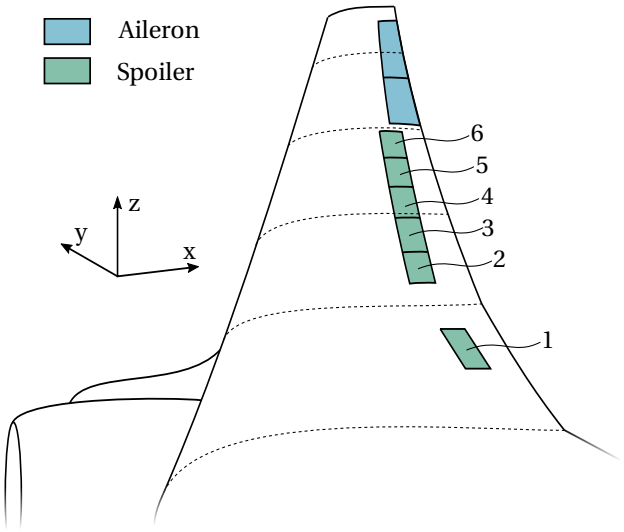

Figure 3.7: Schematic drawing of the used conventional control surface layout consisting of six spoilers and the inner as well as the outer aileron.

Design Variables		
Laminate Thickness (Skins and Spars; $\mathbf{t}$)	$4 \cdot 17$	
Tailoring (Upper and Lower Skin; $\mathbf{c}_\phi$)	$2 \cdot 5$	
MLA ($\delta_{\text{MLA}} + \bar{\delta}_{\text{MLA,asym}}$)	$4 \cdot 8$	
GLA ($\mathbf{h}$)	$16 \cdot 5$	
Total	190	
Constraints		
Manoeuvre Strength (Skins and Spars, Right and Left Wing)		$3 \cdot 4 \cdot 2 \cdot 17$
Manoeuvre Buckling (Skins and Spars, Right and Left Wing)		$3 \cdot 4 \cdot 2 \cdot 17$
Gust Strength (Skins and Spars, Right and Left Wing)		$1 \cdot 4 \cdot 2 \cdot 17$
Gust Buckling (Skins and Spars, Right and Left Wing)		$1 \cdot 4 \cdot 2 \cdot 17$
Roll Case Control Surface Deflection Limits (Upper and Lower limit, Right and Left Wing)		$2 \cdot 2 \cdot 8$
Static Manoeuvre Stability		4
Minimum Damping (Dynamic Stability)		1
Total		1125

Table 3.1: Summary of the design variables and constraints of the given test case.

The employed conventional control surface layout consists of six spoiler control surfaces as well as an inner and an outer aileron as shown in Fig. 3.7. All wing control surfaces are used for manoeuvre load alleviation and roll control while for gust load alleviation, only the outer three spoilers and the ailerons are used. While the actuation characteristics, i.e. maximum rate, natural frequency and damping are the same for the spoilers and the ailerons, the downward deflection limits differ. Aileron deflections are symmetric to the zero position whereas spoilers can only be deflected upwards. An order of 16 is used for the FIR filter of each control surface used for gust load alleviation.

The aerodynamic model includes wing and tail lifting surfaces, and no aerodynamic fuselage is considered. The panel mesh consists of more than 10^4 panels. The configuration is divided into 10 gust zones to account for the delay occurring when the gust moves along the aircraft.

The constraints are evaluated at three, previously selected representative manoeuvre flight conditions: a $2.5g$ pull-up manoeuvre, a $-1g$ push-over manoeuvre and a roll manoeuvre with a predefined roll rate at a load factor of $1.67g$. The gust analysis is carried out at the design speed in the MTOW configuration. The analysis includes 15 discrete gust gradients analysed in a range from nine to 107m as specified by the certification specifications for large aeroplanes [42]. Updraught and downdraught gust conditions are considered. The modal basis used for the dynamic analysis consists of 31 modes, including the six rigid-body modes.

For the given test case, the design space results in 190 design variables that are summarised in Table 3.1 together with the resulting 1125 constraints. The starting point of all optimisations is an over-sized but feasible structure. The design variables associated with MLA, GLA or structural tailoring are initialised with a zero value. Only the wing structure is optimised while the remaining airframe is fixed throughout the optimisation.

The optimisations are stopped when the change in the wingbox mass between two iterations is less than 0.01kg, and the constraints are satisfied within a tolerance of 10^{-4}.

3.4.2. INDIVIDUAL AND COMBINED METHODS FOR MASS REDUCTION

Various optimisations are carried out in which the different methods are active or inactive to investigate the influence of the different technologies on the primary wing structural mass. Table 3.2 shows the various performed optimisations together with the active and inactive subsets of the design variables. The reference (N) is an optimization where neither active control, i.e. MLA and GLA, nor passive structural adaptation is considered. Besides optimisations including the different methods alone (T, M, G), their possible combinations are considered (TM, TG, MG, TMG). In the following, the achieved mass reduction relative to the reference case is normalised to the reduction obtained by the optimisation in which all design variables are active (TMG). The achieved normalised mass reduction in each of the optimisations is also given in Table 3.2. As expected, the maximum achievable reduction in primary wing structural mass is obtained by the TMG optimisation. It can be seen that the sum of the results of the optimisations with the individual methods is smaller than the results of the combined methods. For example, the sum of the results of the T, M and G optimisation yields a normalised mass reduction of 94% being six per cent lower than the result in the concurrent optimisation (TMG, 100 %). This indicates that the various methods interact in a synergistic way that, of course, is

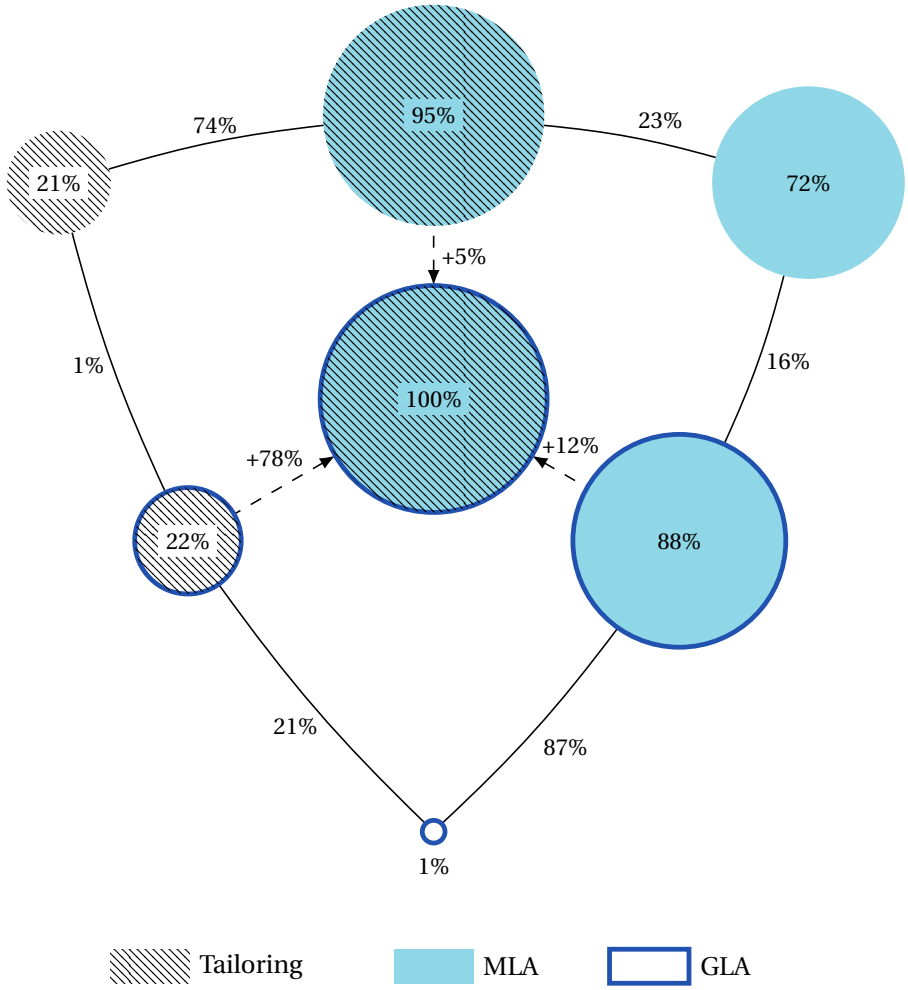

Figure 3.8: Normalised mass reduction obtained in the optimisations and the differences between the various combinations. The area of the circles corresponds to the normalised mass reduction. 100% signifies the maximum achievable mass reduction combining structural tailoring, MLA and GLA.

Setup	Design Variable Subsets				Weight Reduction	
	Thickness	Tailoring	MLA	GLA	Relative	Normalised
N	✓	-	-	-	-	-
T	✓	✓	-	-	-7.5%	20.9%
M	✓	-	✓	-	-25.5%	71.5%
G	✓	-	-	✓	-0.4%	1.1%
TM	✓	✓	✓	-	-31.6%	95.2%
TG	✓	✓	-	✓	-7.7%	21.6%
MG	✓	-	✓	✓	-34.0%	88.4%
TMG	✓	✓	✓	✓	-35.7%	100%

Table 3.2: Description of the various optimisation configurations with active (✓) and inactive (-) subsets of design variables and the resulting mass reduction relative to the primary structural wing weight and normalised to the maximum achievable mass reduction obtained by the concurrent optimisation with all design variables (TMG).

only revealed in simultaneous optimisations.

The results are illustrated in Fig. 3.8 in which the area of each circle corresponds to the obtained normalised mass reduction. Also, the differences between the optimisation results are shown. The most synergistic effect is observed in the combination of active manoeuvre and gust load alleviation. While the sum of normalised mass reduction achieved by the separate use of the active control methods results in 73% (M+G), the combined use yields a 15% higher mass reduction of 88% of the maximum achievable mass reduction. This significant synergistic effect between MLA and GLA has been observed before [62]. A similar though less remarkable trend is visible in the combination of MLA with structural tailoring resulting in a two per cent higher mass saving than the sum of the savings obtained in the optimisations with the individual technologies. In contrast, no synergistic effect is observed by the combination of GLA and structural tailoring. Here the sum of the effects obtained in separate optimisations equals the effect observed in the optimisation with the combined use. It is furthermore worth noting that, the mass reduction obtained by MLA is underestimated when optimised individually compared to a combination with GLA, structural tailoring or both. The same is observed for GLA where the effect in the individual optimisation is only a normalised mass reduction of one per cent compared to for example an added value of 16% (MG-M) in the combined use with MLA or five per cent (TMG-TM) in the combined use with MLA and structural tailoring. For structural tailoring, this does not hold. The added value of tailoring is 12% when combined with active control (TMG-MG) being nine per cent lower than observed in the individual optimisation (T: 21%).

To understand the interaction, in the following, the design driving factors and the resulting designs are investigated more closely. In Fig. 3.9, the normalised mass reduction is therefore first split into the contributions of each of the components of the wingbox. Most of the mass reduction results from the wing skins, the spars play only a small role. However, due to their contribution to the overall stiffness distribution, simultaneous optimisation of spar thicknesses is important. As the major weight saving is resulting from the skin thickness reduction, particular focus is placed on the driving constraints

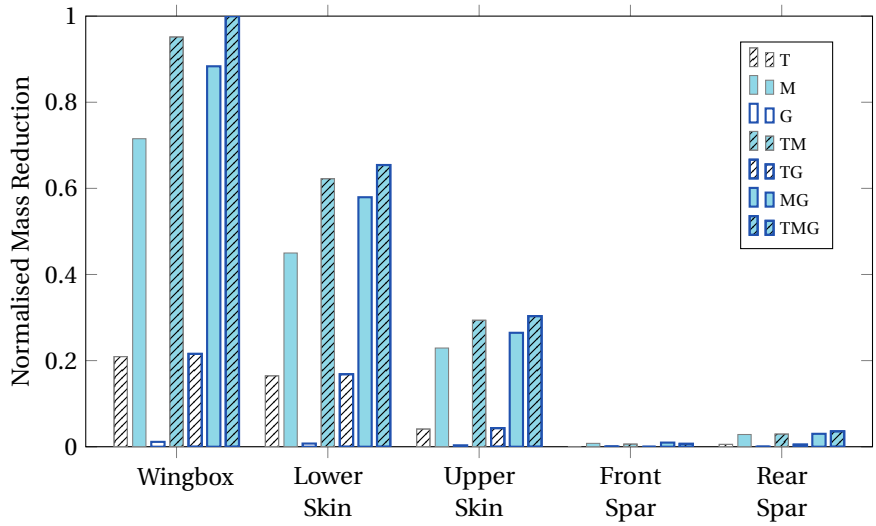

Figure 3.9: Componentwise mass reduction obtained in the optimisations normalised to the achievable mass reduction obtained in the TMG optimisation.

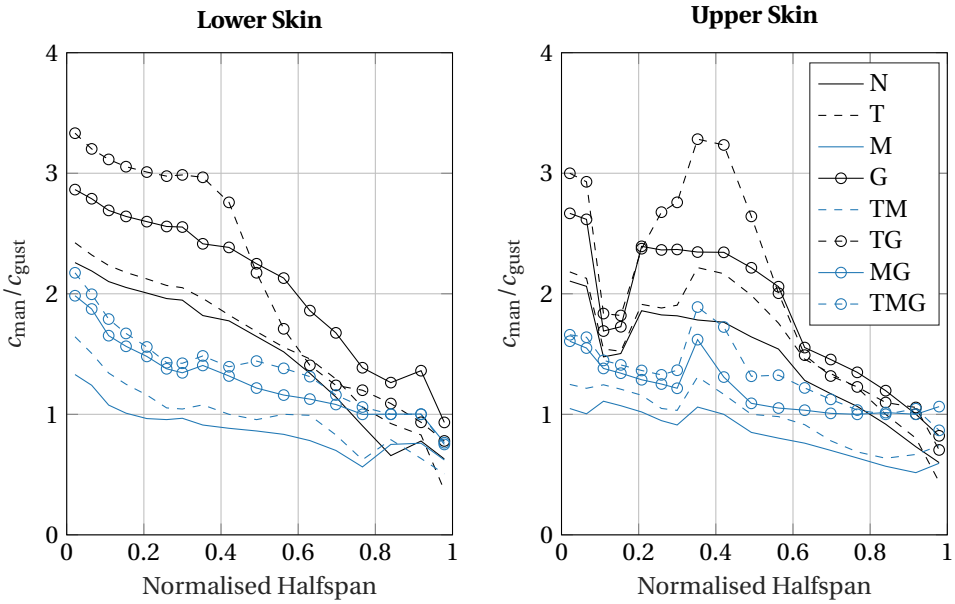

Figure 3.10: Spanwise distribution of the ratio between manoeuvre and gust constraints.

in the skins. The ratio between manoeuvre and gust constraints in the skins over the spanwise position is shown in Fig. 3.10. The ratio between manoeuvre and gust constraints takes values of greater than one in areas where manoeuvres are critical, less than one where gust conditions are dimensioning the wing and equals one for spanwise positions where manoeuvre and gust conditions are equally critical. The wing resulting from the N optimisation is mainly driven by manoeuvre constraints and gust conditions dimension only the outboard quarter. When adding MLA in optimisation M, the manoeuvre constraints are reduced, and gust conditions dominate approximately 80% of the span. In contrast to that, the introduction of GLA in the G optimisation increases the ratio between manoeuvre and gust constraints along the whole span of the lower and upper skin. The result is a wing that is entirely driven by manoeuvre conditions. The values at the tip are not of concern as the thickness reaches the minimum allowable thickness resulting in a locally overdesigned structure where neither gust nor manoeuvre constraints are active. Given these results, the synergy between MLA and GLA can be explained. Each of the methods gives more room for the other, i.e. MLA reduces the manoeuvre constraints giving GLA a more substantial fraction of the wingspan that is driven by the gust constraints. The introduction of bending-torsion coupling by structural tailoring influences both, manoeuvre and gust constraints. The ratio between manoeuvre and gust constraints of the wing resulting from the T optimisation is increased compared to the reference (N). With the lowering effect of structural tailoring on the gust constraints relative to the manoeuvre constraints, the fraction dimensioned by gust conditions is reduced which explains that the addition of GLA (TG vs G) can not lead to more benefits in the combined use compared to the effect observed in the individual optimisation (G vs N). Also, this lowering effect of structural tailoring on the gust constraints relative to the manoeuvre constraints explains the synergistic effect in the combination of MLA and structural tailoring.

The synergistic effect is visible in the thickness difference shown in Fig. 3.11. While tailoring alone (T) requires a thicker upper skin to sustain the manoeuvre conditions, MLA can reduce the deflections in this area so that, in combination (TM), the thickness can be reduced along the whole span. For further analysis of the mechanism of structural tailoring in the presence of active control, the nondimensional bending-torsion coupling ratio as defined by [48] is used:

$$\Psi = \frac{-C_{45}}{\sqrt{C_{44}C_{55}}} \tag{3.7}$$

with C_{44} being the bending stiffness, C_{55} the torsional stiffness and C_{45} the bending-torsion coupling stiffness from the cross-sectional stiffness matrix $\mathbf{C}$ given in Eq. 3.1. Positive values of Ψ indicate a positive bending-torsion coupling, also known as wash-in, i.e. upward bending accompanied by a nose up twist. Negative values relate to wash-out, i.e. upward bending accompanied by a nose-down twist. The tailoring induced bending-torsion coupling is shown in Fig. 3.12. In all cases, the optimiser chooses a negative bending-torsion coupling leading to a wash-out effect shifting the centre of load inboard. Except for the tip, where the thickness of the skins and spars is defined by the minimum allowable thickness, the characteristics of the tailoring induced bending-torsion coupling distribution are similar with and without MLA (T vs TM). Especially notable is that in the presence of MLA, the optimiser increases the amount of wash-out

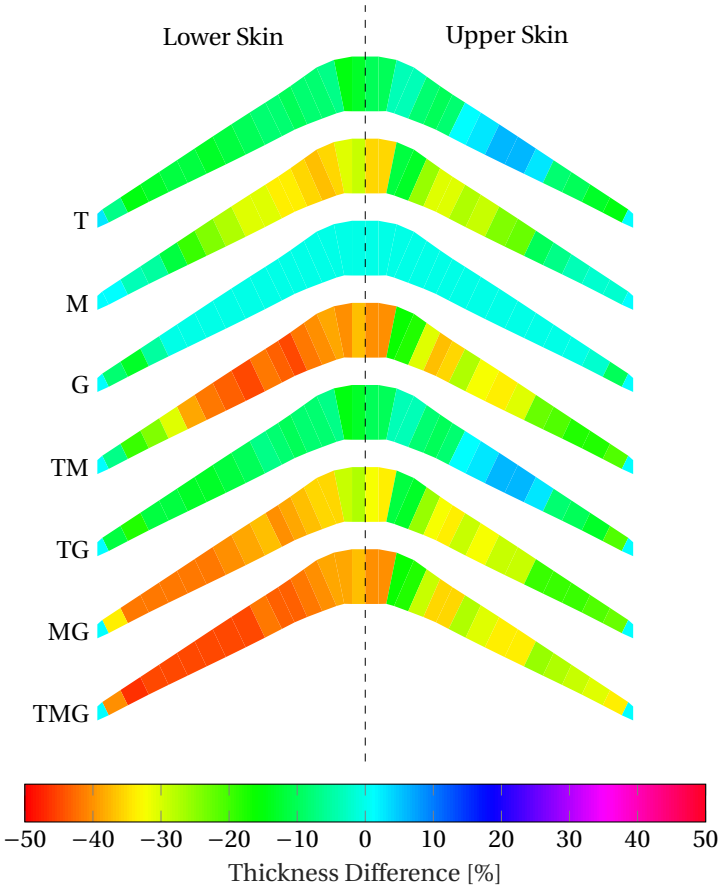

Figure 3.11: Relative difference in the skin thickness distribution resulting from the different optimisations compared to N.

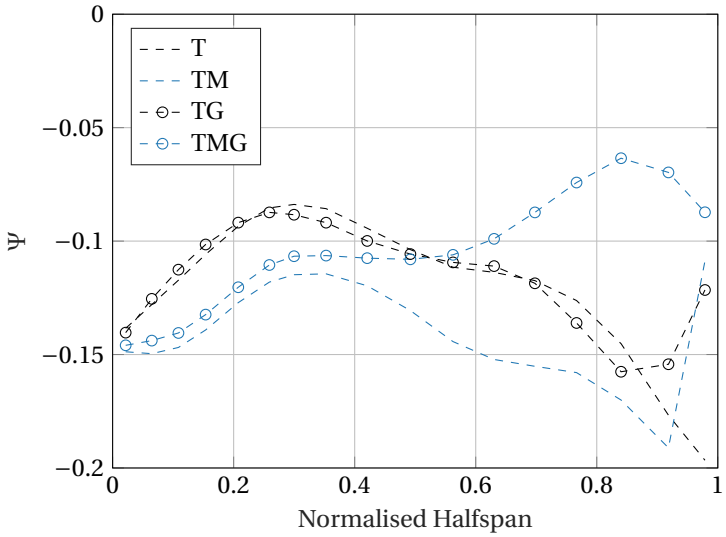

Figure 3.12: Spanwise distribution of the bending-torsion coupling parameter Ψ.

even though the negative bending-torsion coupling has a negative effect on the control surface effectiveness as shown by Weisshaar [48].

It is worth noting that in the TM optimisation, the optimiser intensifies the negative bending-torsion coupling by increasing the principal stiffness direction angle of the laminate of the upper skin inboard and the lower skin outboard compared to the T optimisation, see Fig. 3.13.

With the addition of GLA, the optimiser reduces the amount of negative bending-torsion coupling in the outboard area of the wing as seen in Fig. 3.12. In the TG optimisation, only the very outboard part is affected but comparing TMG and TM, the addition of GLA significantly influences the characteristics of the bending-torsion coupling distribution. As gust conditions strongly drive the design resulting from the TM optimisation, the addition of GLA requires the optimiser to strengthen the control authority of the control surfaces on the gust loads to increase the effectiveness of GLA. The $\mathscr{H}_2$ norm of the transfer function of a control surface input to a bending load output is used as a measure for the load control authority. To characterise the influence of structural tailoring on the load control authority, the $\mathscr{H}_2$ norm is computed with and without structural tailoring, i.e. $\phi_{\text{lo}}, \phi_{\text{up}}$ are set to zero after the optimisation. The relative difference is given by:

$$\Delta_{\mathscr{H}_2} = \frac{\mathscr{H}_2}{\mathscr{H}_{2,\phi=0}} - 1 \tag{3.8}$$

The relative difference in the $\mathscr{H}_2$ norm of transfer functions from the ailerons to various spanwise load outputs is shown in Fig. 3.14. In all cases, structural tailoring reduces the bending load control authority of both ailerons. The outer aileron is more affected than the inner aileron. For both ailerons, the structural tailoring in the TMG optimisation has less detrimental effect on the control authority compared to the TM optimisation.

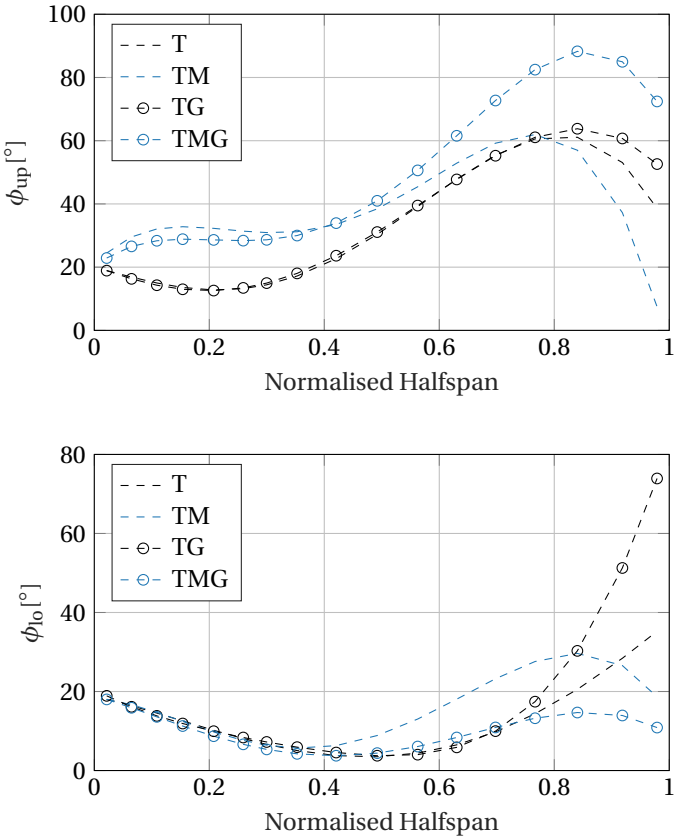

Figure 3.13: Spanwise distribution of the principal stiffness direction in the upper and lower skins' laminate. Positive values of ϕ result in wash-out.

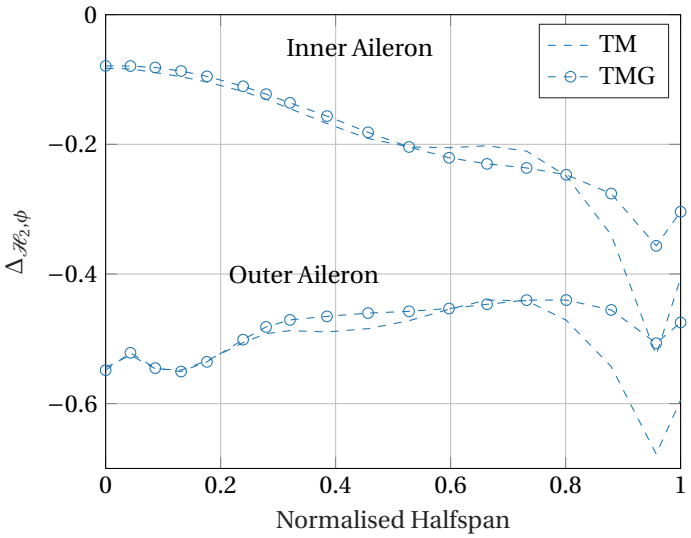

Figure 3.14: Effect of structural tailoring on spanwise load control authority characterized by the relative difference in the $\mathscr{H}_2$ norm of the transfer function from a control surface input to a spanwise bending load output with and without structural tailoring.

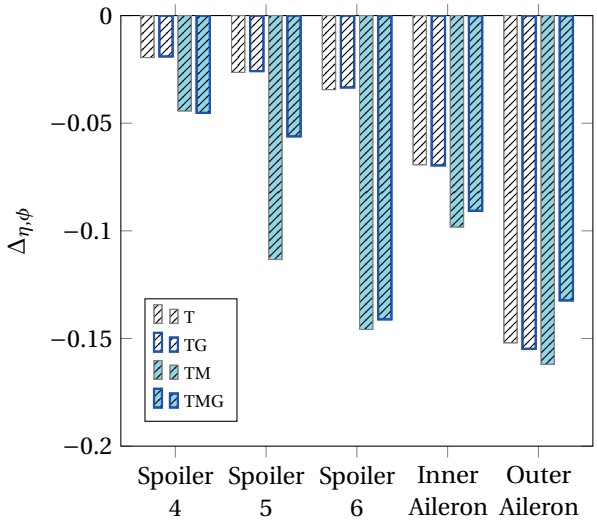

Figure 3.15: Effect of structural tailoring on the effectiveness of the outer control surfaces used for MLA.

This means that the optimiser reduces the amount of negative bending-torsion coupling to strengthen the load control authority of both ailerons in TMG optimisation compared to TM optimisation.

Moreover, with the addition of GLA, the ratio between the manoeuvre and gust constraints is lowered, resulting in a larger area that can be positively influenced by MLA. The optimiser, therefore, reduces the amount of negative bending-torsion coupling in the TMG optimisation to strengthen the efficacy of MLA. To support this thesis, the influence of structural tailoring on the control surface effectiveness is determined. The aeroelastic control surface effectiveness η is defined as the effect of a control surface normalised to the effect of the same control surface without the influence of structural flexibility, i.e. on a rigid wing. For ailerons, the effect of interest is the rolling moment coefficient C_l per deflection δ; For spoilers, the effect corresponds to the change in lift coefficient C_L generated by a deflection δ:

$$\eta_{\text{ail}} = \frac{(\partial C_l/\partial\delta)_{\text{flexible}}}{(\partial C_l/\partial\delta)_{\text{rigid}}} \tag{3.9}$$

$$\eta_{\text{sp}} = \frac{(\partial C_L/\partial\delta)_{\text{flexible}}}{(\partial C_L/\partial\delta)_{\text{rigid}}} \tag{3.10}$$

The control surface effectiveness is computed in the presence of structural tailoring, i.e. η with $\phi_{\text{lo}}, \phi_{\text{up}}$ as obtained in the optimisations, and absence of structural tailoring, i.e. η' with $\phi_{\text{lo}}, \phi_{\text{up}}$ set to zero. The difference, i.e. the influence of the change in principal stiffness direction due to structural tailoring ($\Delta_{\eta,\phi} = \eta - \eta'$) is shown in Fig. 3.15. The principal stiffness direction resulting from all optimisations has a detrimental effect on the control surface effectiveness of up to 16%. As observed in the analysis of the bending-torsion coupling parameter Ψ, the reduction in control surface effectiveness due to structural tailoring is comparable between the T and TG optimisation. The principal stiffness direction has a more significant influence on the control surface effectiveness in the TM optimisation due to the higher inboard bending-torsion coupling, as seen in Fig. 3.12. As initially assumed, the optimiser tries to restore the control surface effectiveness of the control surfaces used in the TMG optimisation. The differences show that an integrated design of structural tailoring with active load alleviation is needed to exploit the synergies of both technologies to the full extent.

The differences in the MLA design are discussed next. As an example, the control surface deflections given by the optimised MLA during the push-over manoeuvre are shown in Fig. 3.16. In the optimisation including only MLA, the -1g push-over manoeuvre constraints are not active, and the control surface deflections are not influencing the design. In the other cases, the -1g manoeuvre plays a more critical role, and the optimiser uses MLA to redistribute the loads, reducing the level of constraints. Except for the outer aileron, which in all cases is deflected downwards to shift the centre of pressure inboard, the characteristics of the MLA deflections are different between the cases with (TM and TMG) and without (MG) structural tailoring. Without tailoring, the deflections increase towards the tip while with tailoring, the deflections are reduced towards the tip. The latter is the expected pattern shifting the load inboard and is similar to the patterns found by Stanford [85] and Krupa et al. [70]. While finding the exact reason for the pattern observed

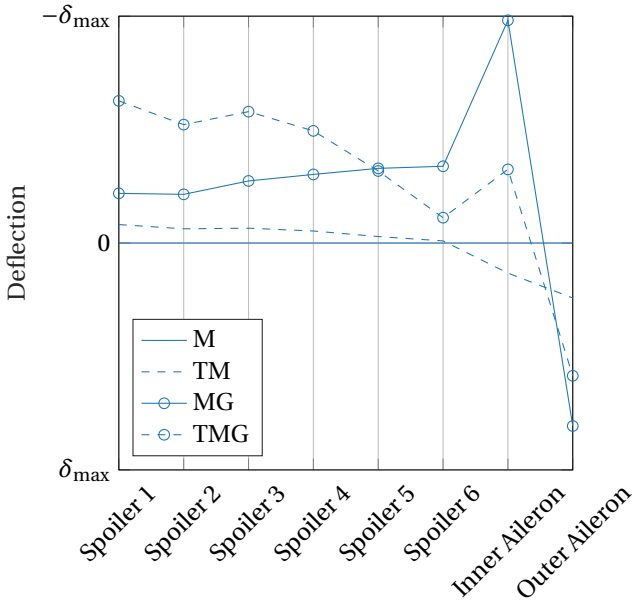

Figure 3.16: Optimised control surface deflections for MLA during the push-over manoeuvre.

in the MG optimisation would require further analysis, the different characteristics justify the need for an integrated design of MLA together with the variables of the structural tailoring to make optimal use of both technologies.

It is expected that besides the observed differences in structural tailoring and MLA, different properties of the GLA system result from the various optimisations. Due to the dynamic nature of gust encounters, the differences are even more challenging to grasp. However, the primary influence on the control law can be linked to the first symmetric bending mode frequency that, for the given type of configuration, governs the dynamic gust loads [86].

The variation observed in the first bending frequency shown in Table. 3.3 indicates that different control deflections during gust encounters are to be expected. The frequency response of the FIR filter associated with the fifth spoiler, including the high-pass filter of the AOA probe is shown in Fig. 3.17. The frequency response characteristics of the filter, e.g. the peak position, resulting from the various optimisations are different due to the variation of the structural eigenfrequencies. For each control surface pair used for gust load alleviation, rate and deflection limits are reached for at least one analysed gust length. The resulting control surface deflections of the fifth spoiler are exemplary shown in Fig. 3.18 for different gust lengths after the filtered signal is fed through the nonlinear actuator model. The deflection histories resulting from updraught and downdraught type gust conditions differ as spoilers can be deflected in only one direction. For control surfaces with the symmetric limits on positive and negative deflections, the deflection histories resulting from updraught and downdraught gusts differ only in the sign.

The difference in the resulting GLA mechanism is analysed by a comparison of the

Optimisation	First Sym. Bending Frequency Difference
T	-9.2%
M	-12.4%
G	-0.1%
TM	-25.2%
TG	-9.4%
MG	-15.8%
TMG	-25.9%

Table 3.3: Relative difference in the first symmetric bending frequency of the resulting wing structures obtained in the different optimisations compared to N.

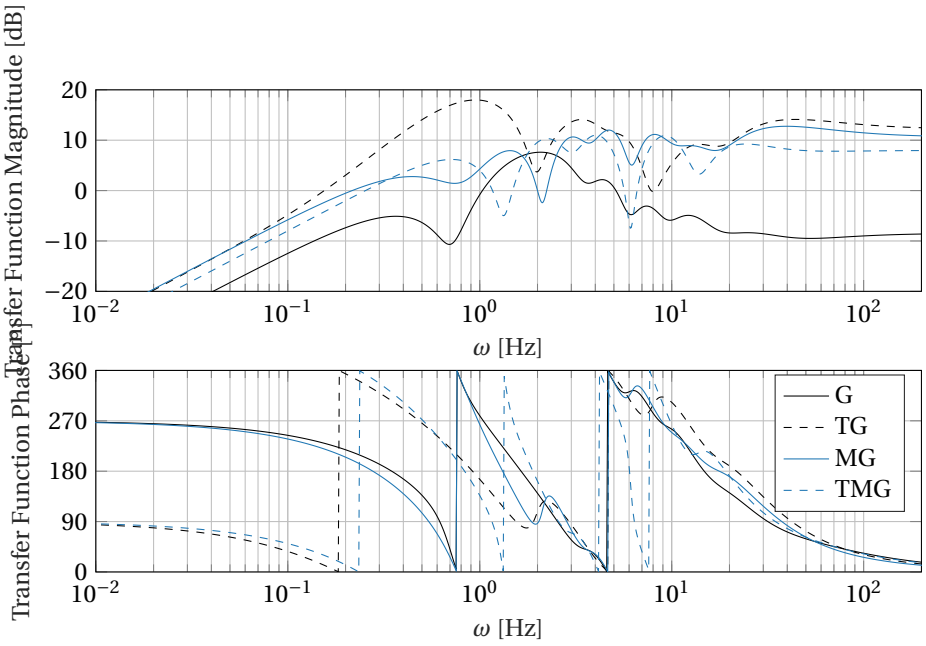

Figure 3.17: Bode plot of the frequency response of the optimal FIR filter associated to the fifth spoiler as optimised in the different setups including GLA.

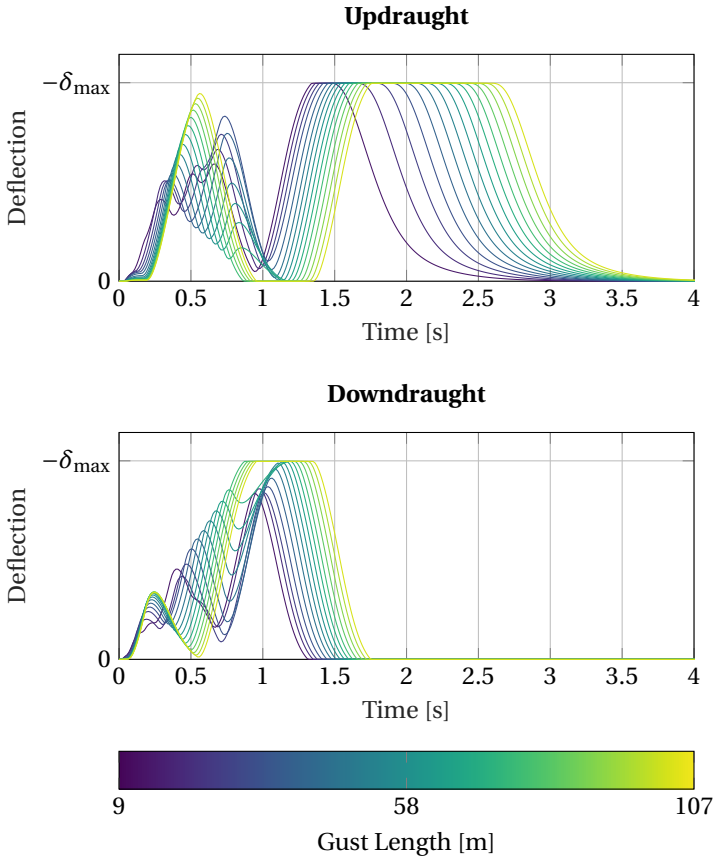

Figure 3.18: Spoiler deflections during updraught and downdraught gusts for the gust lengths considered in the gust analysis. The deflection histories result from fifth spoiler in the TMG optimisation.

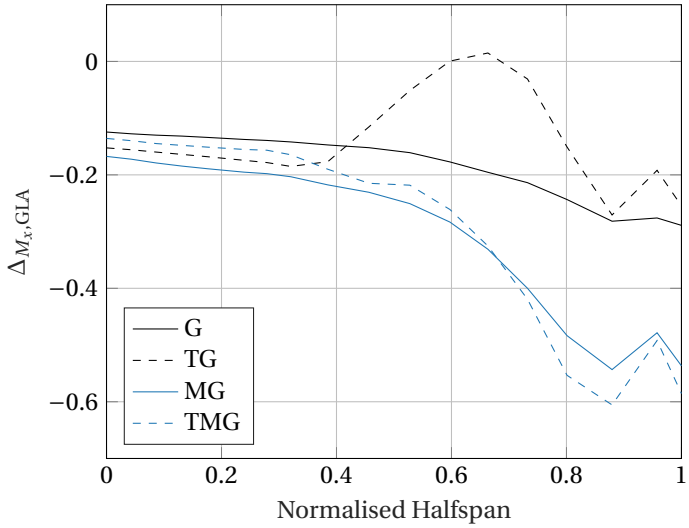

Figure 3.19: Relative difference between the open and closed loop spanwise maximum bending moment distribution during gust encounters.

relative difference on the maximum bending moment around the longitudinal axis x between open loop and closed loop gust loads defined as:

$$\Delta_{M_x,\mathrm{GLA}} = \frac{\max(M_{x,\mathrm{gust,open\,loop}})}{\max(M_{x,\mathrm{gust,closed\,loop}})} - 1 \tag{3.11}$$

The relative difference in the maximum bending moment distribution is shown in Fig. 3.19 for the different controllers resulting from the optimisations G, TG, MG and TMG. A significant difference is visible between the cases with and without manoeuvre load alleviation (G and TG vs MG and TMG). Due to the reduced stiffness, the controller is much more effective in reducing the gust loads. Another interesting point is that in the TG optimisation, the optimiser even allows the controller to increase the bending loads at a mid-wing position of 60-70% of the normalised halfspan, as this region is not dimensioned by gust loads, see Fig. 3.10. This means the optimiser adopts the mechanism to the prevailing load hierarchy.

In conclusion, only the simultaneous design of GLA with MLA and structural tailoring can exploit the full potential.

3.4.3. SENSITIVITY OF MATERIAL PROPERTIES KNOCKDOWN FACTOR

In the design of safety-critical aircraft structures, the nominal allowables are significantly reduced by knockdown factors accounting for low-speed impact damage, material scatters and environmental effects as temperature, moist and UV light [87]. A variety of knockdown factors is investigated because new design paradigms and materials are envisioned in the future. The inclusion of fatigue models in the optimisation problem could replace the respective knockdown factors allowing for more flexible wing designs

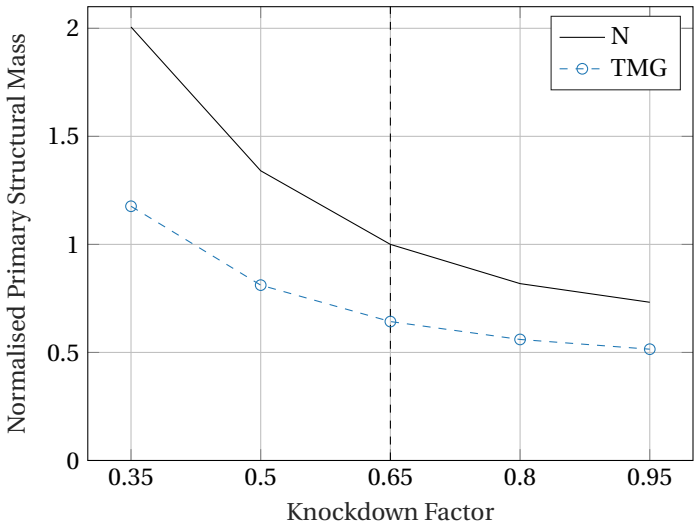

Figure 3.20: Influence of the material knockdown factor on resulting objective function, namely primary structural mass, normalised to the objective resulting from the N optimisation with a knockdown factor of 0.65.

[21]. Also, the development of materials with significantly higher allowables, e.g. carbon nanotubes, can reduce the stiffness of future wing structures drastically [88].

While most of the examples listed in the introduction give no information on the applied knockdown factor, there are also studies which do not consider any knockdown factor [89] [90]. Other studies use maximum strain allowables that are more conservative [70].

The results shown in the previous section were produced with a knockdown factor of 0.65 applied to the material strength properties, i.e. longitudinal/transverse tension/compression strength as well as the in-plane shear strength. In this section, the knockdown factor is gradually changed from 0.35 to 0.95 to investigate the effect of the material properties on the main findings of the previous section.

Fig. 3.20 shows the resulting primary structural mass for various knockdown factors normalised to the primary structural mass obtained in the N optimisation using a knockdown factor of 0.65. As expected, the knockdown factor has a significant impact on the objective, i.e. the resulting primary structural mass. A reduction of the knockdown factor from 0.65 to 0.35 results in an increase of the optimised mass of 100% in the absence of active control and structural tailoring (N). The sensitivity is less pronounced when all technologies are present (TMG). It is worth noting that, an increase in the material knockdown factor of 0.01 corresponds to a mass reduction of 1.60% in the N optimisations compared to 0.75% in the TMG optimisations. The net benefit of new material technologies should therefore always be assessed with taking into account all system and technologies that influence the loads on the wing structure.

The influence of the material knockdown factor on the mass reduction achievable by the individual technologies and their combinations is given in Fig. 3.21. The mass reduction achievable by structural tailoring is increasing with higher knockdown factors,

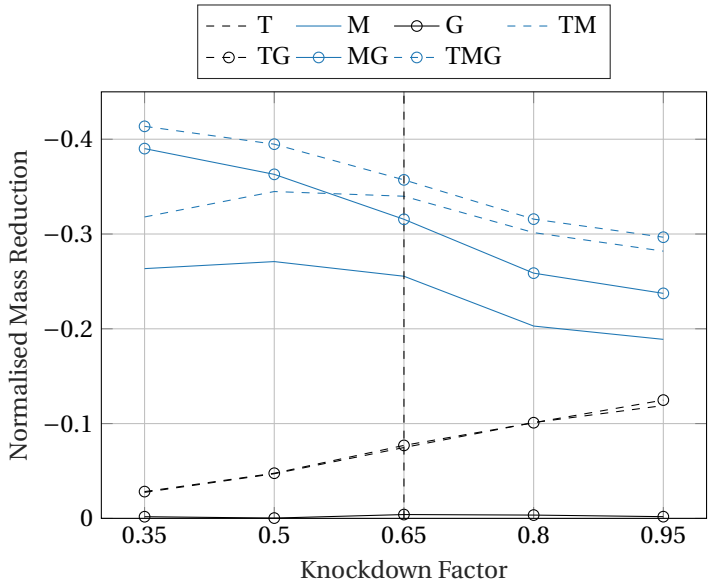

Figure 3.21: Influence of the material knockdown factor on the mass reduction normalised with respect to the N optimisations.

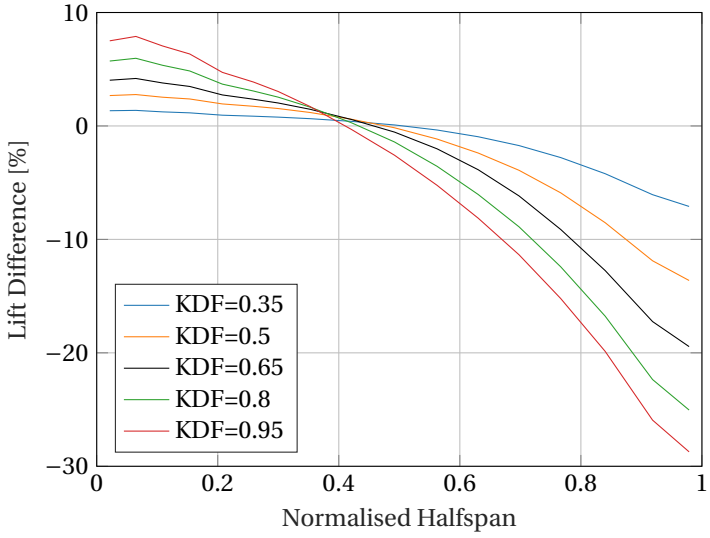

Figure 3.22: The difference in the lift distribution during the 2.5g manoeuvre due to structural tailoring (T vs N) for different knockdown factors.

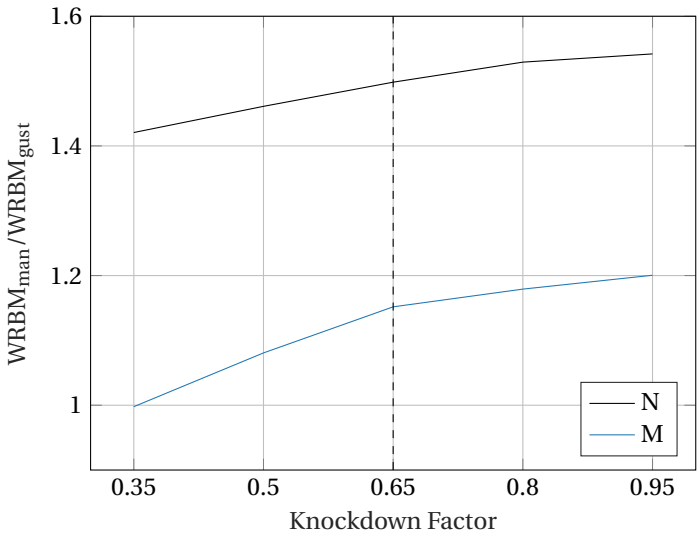

Figure 3.23: Ratio between the maximum wing root bending moment (WRBM) encountered during manoeuvre and gust for various knockdown factors.

i.e. more flexible and hence less stiff structures. The effect of the knockdown factor on the tailoring-induced difference in the pull-up manoeuvre lift distribution (T vs N) is given in Fig. 3.22. With higher knockdown factors and less bending stiffness, the bending-torsion coupling induced by structural tailoring is resulting in more wash-out by higher deflecitons.

Manoeuvre load alleviaiton is, as expected, negatively affected by reduced stiffness resulting from higher knockdown factors as the conrtrol surface effectiveness is reduced. The reduction of the stiffness furthermore increases the ratio between manoeuvre and gust loads, as can be seen in the maximum wing root bending moment ratio shown in Fig. 3.23 both for the N and M optimisations.

For the investigated range of knockdown factors, the individual application of GLA is not leading to any mass reduction as for all N optimisations the gust constraints are below the manoeuvre constraint level.

For all used knockdown factors, tailoring is increasing the ratio between the manoeuvre and gust constraints, i.e. tailoring is lowering the gust loads more than the manoeuvre loads. In combination with the increase of the ratio between manoeuvre to gust loads for higher knockdown factors, this explains the observed lower synergistic behaviour between tailoring and MLA. The increase in the ratio between manoeuvre and gust constraints by structural tailoring also explains that no interaction with GLA is observed in the absence of MLA. For all knock factors, GLA only has added value if MLA is active. The interplay of MLA and GLA observed in the MG and TMG optimisations is improved for lower knockdown factors, which can be linked to the higher control surface effectiveness that comes with stiffer wings.

In total, a substantial shift of effectiveness from active GLA to passive structural

tailoring is observed with increasing structural flexibility. For a knockdown factor of 0.35, the combination of MLA and GLA can lead to 94% of the possible mass reduction reducing the added value of structural tailoring to six per cent. For knockdown factors higher than 0.65, the added value of active GLA shrinks down to less than five per cent of the achievable mass reduction. That means that with the trend of increasing material allowables and the industrialisation of structural tailoring, the mass saving potential of GLA is reduced. However, the added value of MLA is still significant.

3.5. CONCLUSIONS

The interaction between the three technologies of active manoeuvre load alleviation, gust load alleviation and structural tailoring has been investigated. The simultaneous design optimisation of a wing structure together with the control system was carried out on the example of a typical long-haul transport aircraft configuration. The optimisations with the individual technologies and their combinations reveal, that, as expected, the maximum reduction in primary wing structural mass is achieved by a concurrent optimisation of all three technologies. Design differences are observed in the individual and combined optimisations as the technologies adapt to the respective prevailing load hierarchy. The results indicate that combined optimisation is required to exploit the synergies of active control and structural tailoring to the full extent and to assess the potential of each of the technologies correctly. Conversely, the separate design of active control and structural tailoring leads to suboptimal results.

A variation of the knockdown factor applied to the material properties allowed the study of the influence of structural flexibility on the results found. The study revealed that the interplay between active control and structural tailoring is strongly dependent on the material properties. A substantial shift of effectiveness from active gust load control to passive structural tailoring is observed with increasing structural flexibility. While the increasing material allowables and the exploitation of the anisotropic material properties promise significant mass savings, the relative potential of the active gust load control is reduced. The net benefit of new material technologies should, therefore, be assessed by taking into account active control.

As the present work involves a generally idealised approach for active load alleviation and structural tailoring, future studies would benefit from a more refined implementations. These enhancements could include stacking sequence optimisation, manufacturing constraints, chordwise thickness variation or stringer shape and geometry optimisation as well as failure scenarios and more detailed constraints, e.g. including continuous turbulence load conditions. Especially the consideration of low speed handling qualities is essential as they are defining the required control surface effectiveness of the outboard aileron. The aerodynamic modelling approach would benefit from the consideration of compressible and transonic effects enabling the inclusion of stability constraints that are important for high aspect ratio wing designs. With the introduction of flutter constraints, flutter suppression methods need to be considered alongside.

To assess the transferability of the main findings of this work to other aircraft configurations, future studies investigate configurations comprising wingtip devices and different control surface layouts.

4

Implications for Preliminary Design of Future Aircraft

Abstract This chapter examines the effects of the observed interaction of active and passive load alleviation on the preliminary design of future aircraft. First, alternative optimisation approaches more suitable for the preliminary design are examined and compared to the results of simultaneous optimisation. Besides the investigation of a separate design approach, an approach is proposed where subspaces of the overall parameter space are optimised iteratively. The results confirm that simultaneous optimisation is the only way to find the optimal solution. However, the proposed iterative approach offers the possibility to separate certain subspaces of the optimisation and still reach results close to the optimum.

In addition to the initial sizing of novel concepts, one task of the preliminary design is the rapid assessment of configurational changes. A change of the control surface layout is examined as an example to demonstrate the suitability of the given framework for the preliminary design of future aircraft. Furthermore, a comparison with the results presented in the previous chapter determines the extent to which the interactions and synergies are configuration-specific.

In the further course of the chapter, a non-planar configuration with an active winglet is examined. The results are compared again with those of the previous chapter. Especially for cases of high allowables, the winglet configuration tends to be more prone to flutter. The results show that the effectiveness of structural tailoring is limited, as its mechanism of action changes from load alleviation to flutter stabilisation.

4.1. Comparison of Separate, Iterative and Concurrent Design Procedures

Separate Design In the preceding chapter, design differences were observed when the different technologies were optimised individually or combined. In this section, the designs resulting from the individual optimisations of structural tailoring (T) and active

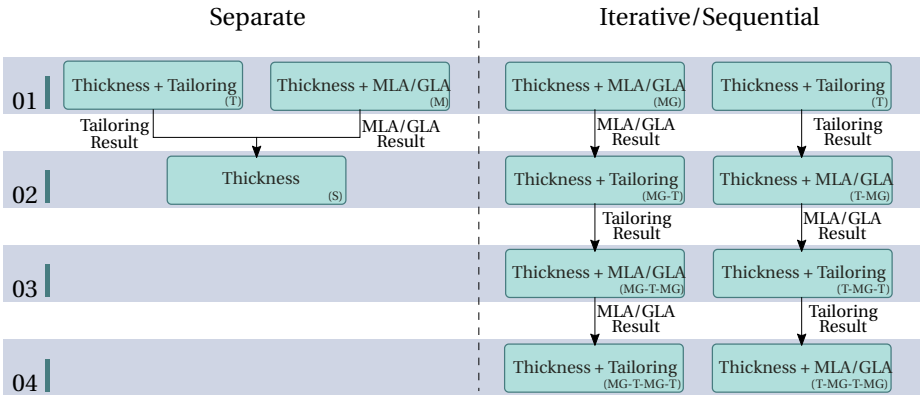

Figure 4.1: Visualisation of the separate and iterative optimisation approaches as alternative to a concurrent optimisation of active and passive load alleviation.

Table 4.1: Description and weight reduction (normalised and relative) obtained by a separate design (S) in comparison the concurrent optimisation (TMG).

Setup	Design Variable Subsets			Weight Reduction	
	Thickness	Tailoring	MLA and GLA	Relative	Normalised
N	✓	-	-	-	-
T	✓	✓	-	-7.5 %	20.9%
MG	✓	-	✓	-31.6%	88.4%
S	✓	fixed (T)	fixed (MG)	-32.9%	92.1%
TMG	✓	✓	✓	-35.7%	100%

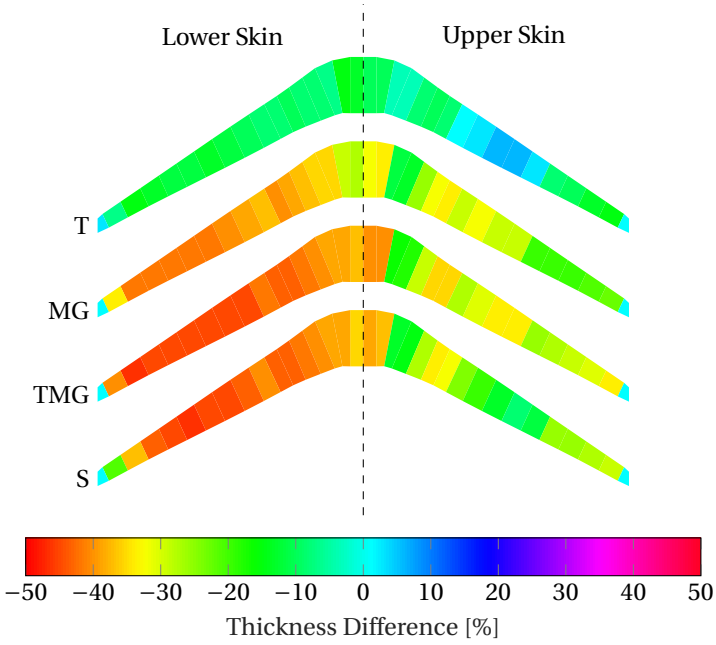

Figure 4.2: Relative difference in the skin thickness distribution resulting from the individual optimisations with structural tailoring (T), active control (MG) as well as the separate (S) and concurrent (TMG) optimisation (compared to N).

aeroelastic control by MLA and GLA (MG) are combined in one design, and the result is compared to the concurrent optimisation (TMG). Therefore the tailoring design variables are frozen at the design point obtained from the T optimisation, and the active control design variables (MLA and GLA) are frozen as obtained in the MG optimisation as shown in Table 4.1 and Figure 4.1. Subsequently, only the skin and spar thicknesses are optimised, starting from an overdesigned thickness distribution. This approach is referred to as a separate design (S).

The results shown in Table 4.1 indicate that, as expected, the separate approach is inferior to concurrent optimization, leading to an eight per cent lower normalised mass reduction. The added value of structural tailoring in a separate design is only less than four per cent and thus reduced by two-thirds compared to the 12% that can be observed in the concurrent optimisation. The differences in the skin thickness of the various configurations compared to the N optimisation are shown in Fig. 4.2. The optimiser is not able to reduce the thickness to the same extent compared to the TMG optimisation. This is especially visible in the mid-upper skin as well as the tip area of the lower skin. The mid-upper skin of the design resulting from the S optimisation is driven by the constraints of the push-over manoeuvre that are shown in Fig. 4.3. Contrary to the MLA in the TMG optimisation, the MLA deflections obtained from the MG optimisation are not effectively reducing the constraints in the S optimisation. Similarly, the GLA controller parameters

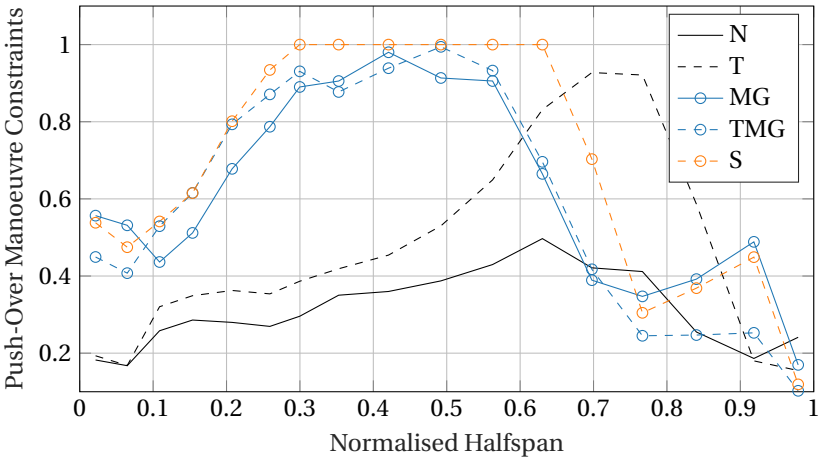

Figure 4.3: Distribution of the structural constraints in the upper skin resulting from the push-over manoeuvre flight condition.

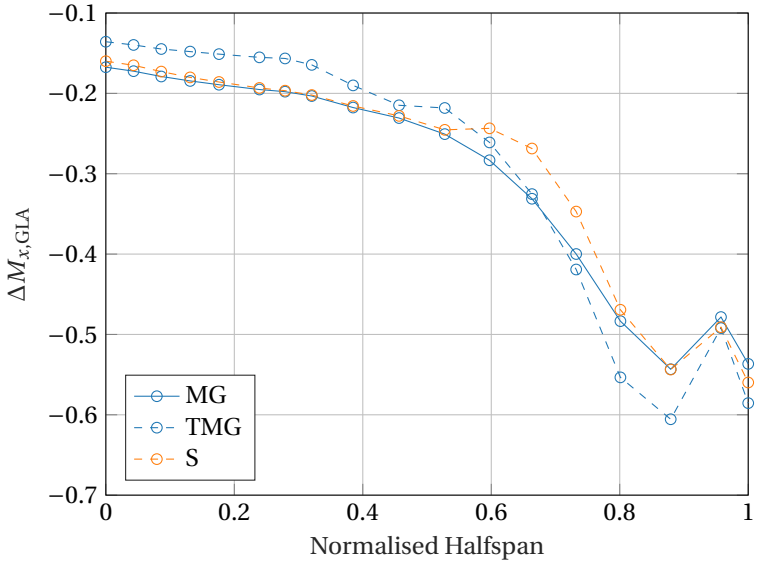

Figure 4.4: Influence of GLA on the distribution of the maximum bending moment induced by gusts.

obtained in the MG optimisation are suboptimal for the structure obtained in the S optimisation. The difference in the gust induced bending-moment between open and closed loop gust loads is shown in Fig. 4.4. The GLA cannot reduce the gust loads in the outboard wing area to the extent that is observed by GLA in the design resulting from the TMG optimisation.

The observed trend is expected as the active control properties are obtained from the MG optimisation in which structural tailoring was not considered. As structural tailoring changes the load distributions and structural dynamics, including the eigenfrequencies and the controllability of the aeroelastic behaviour, the control laws are not optimally tuned for the structural design resulting from the S optimisation. On the other hand, the structural tailoring has been optimised in the absence of active control and is thereby suboptimal for the actively controlled structure. The optimal designs of both technologies for weight minimisation can only be obtained by a concurrent optimisation in which their synergies are fully exploited. However, as integrated optimisation requires considerable computational effort as well as close collaborations of the disciplines involved, the next section examines to what extent iterations between the disciplines can improve the design.

Iterative Design Motivated by the trade-off between low drag and low structural mass, early applications of integrated design focussed on the optimisation of aerodynamic, e.g. planform or twist, and structural parameters. Grossman et al. compared the integrated approach to an iterative or sequential approach in the aerostructural design of a sailplane wing [91]. Different objectives are used for the two disciplines in the sequential optimisation. The goal of the aerodynamic planform optimisation is increasing aerodynamic performance while he structural optimisation targets the reduction of structural mass. In the integrated design, the optimiser makes use of the planform parameters to establish a lift distribution that creates lower structural loads and thereby a lower wing weight resulting in a slightly higher overall performance compared to the iterative approach.

The discipline of control engineering was usually addressed in later stages of the aircraft design process after an initial concept of the aerodynamics and structures was created [92].

Differences in the outcome of the iterative and concurrent design of control algorithms and aircraft structures have been studied by Zink et al. in the design of a generic fighter aircraft structure [93]. Different objective functions, namely hinge moment and structural weight, are applied in the optimisations of the two disciplines of trim and structures. Again, the iterative optimisation method does not achieve the results of the integrated approach. The author mentions, however, that the outcome of the sequential optimisation process is dependent on the choice of the objective functions and thus, an essential advantage of the integrated approach is that it frees the user from defining the objective function for the trim discipline.

Since the mentioned comparisons of iterative and simultaneous design use different objectives for the disciplines involved, the designs resulting from the iterative approach are not optimal in terms of the overall objective. Additionally, the optimisation algorithm in one of the discipline is not aware of the effect the parameters have on the objective of

Table 4.2: Definition and result of the optimisation runs performed in the analysis of the sequential approach iterating between the optimisation of structural tailoring and active aeroelastic control.

Setup	Design Variable Subsets			Weight Reduction	
	Thickness	Tailoring	MLA and GLA	Relative	Normalised
N	✓	-	-	-	-
T	✓	✓	-	-7.5%	20.9%
MG	✓	-	✓	-31.6 %	88.4%
MG-T	✓	✓	fixed (MG)	-34.1%	95.5%
MG-T-MG	✓	fixed (MG-T)	✓	-34.5%	96.7%
MG-T-MG-T	✓	✓	fixed (MG-T-MG)	-35.2%	98.5%
T-MG	✓	fixed (T)	✓	-35.0%	98.1%
T-MG-T	✓	✓	fixed (T-MG)	-35.5%	99.5%
T-MG-T-MG	✓	fixed (T-MG-T)	✓	-35.5%	99.5%
TMG	✓	✓	✓	-35,7%	100%

the other discipline.

The technologies considered in this thesis, namely structural tailoring and active aeroelastic control, pursue the same objective of reducing the wing structural weight. Thus, the iterative approach applied in this work differs from the examples mentioned above, as both disciplines have the same objective function. In both optimisations, the purely structural optimisation and the active aeroelastic control optimisation, the skin and spar thicknesses are design parameters and optimised alongside the structural tailoring parameters or the active control parameters, see Figure 4.1. Thereby, the optimiser in both optimisations is aware of the influence it has on the shared weight objective and all the constraints. This approach of iteratively optimising a subspace of the overall design space converges to the same result of the concurrent optimisation when the overall objective function is convex in the design space spanned by all design variables.

Starting with an iteration of active control (MG) or structural tailoring (T), three outside iterations are carried out in the iterative design. The different optimisation design space definitions, as well as the obtained normalised mass reductions, are shown in Table 4.2. The iterative optimisations converge to a difference from the optimal result of less than one per cent after only two iterations starting with the active control optimisation (MG) or three outside iterations starting with structural tailoring optimisation (T). The convergence of the deviation from the optimal result obtained by the concurrent optimisation (TMG) is shown in Fig. 4.5 with the convergence history of the TMG optimisation for comparison. Compared to the concurrent optimisation, significantly more inner iterations are required in the iterative design to reach the one per cent deviation from the optimal result. However, these inner optimisation iterations are less computationally expensive as the number of function evaluations required for the finite differences is proportional to the number of design variables. It is interesting to note that, even though the individual optimisation of structural tailoring (T) results in less mass reduction compared to the individual optimisation of active control (MG), the iterative optimisation starting

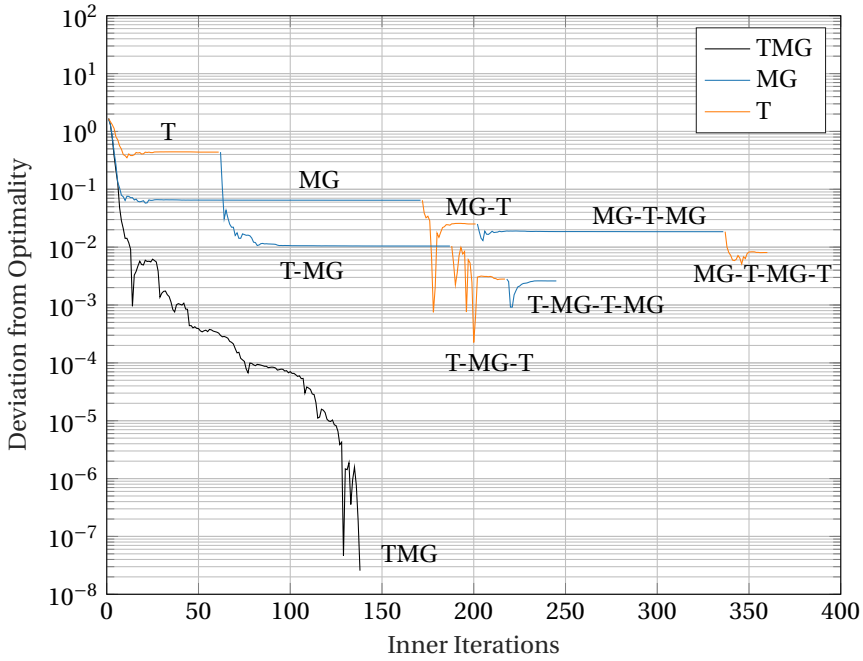

Figure 4.5: Convergence history of the iterative optimisation runs compared to the convergence history of the concurrent optimisation (TMG).

from T converges faster to a deviation of one per cent from the optimum (TMG). While the iterative approach is not suitable to find the exact optimum it is useful for problems in which the concurrent optimisation is computationally not tractable (due to the size of the design space) or different optimisation architectures or algorithms are required for the design variables from the different disciplines. However, the given iterative approach requires the possibility of defining a shared objective function. In the present case, this is only possible by simultaneously optimising the parameters of one of the technologies together with the thickness variables.

In total, the study reveals that an iterative design approach can lead to similar results compared to an integrated design. However, it is observed that the convergence behaviour depends on the choice of which technology is optimised first, in this case, structural tailoring or active control.

4.2. ANALYSIS OF A CONTROL SURFACE LAYOUT VARIATION

The results of Chapter 3 show that a strong interaction between structural tailoring and active aeroelastic control is observed when the technologies are applied together. The differences in the mechanism of structural tailoring resulting from optimisations with and without active control suggest that the layout, i.e. placement and location of the individual control surfaces affects the effectiveness and interaction of both technologies.

In the past, two different control surface layouts were widely used for the type of aircraft used as an example in this work. The control surface layouts mainly differ in the arrangement and position of the primary control surfaces for roll control. The first layout employs two or more ailerons located at the wingtip. The second type consists of a combination of one aileron located at the tip of the wing and a flaperon (flap + aileron) located at an intermediate wing position, usually close to the pylon-wing junction or trailing edge kink. Ailerons are primarily used for roll control for which an antisymmetric deflection of the left and right control surface produces a rolling moment. For flaperons, an additional symmetrical deflection can be superimposed to increase the overall lift.

The following study aims to investigate the impact the type of control layout has on the interaction of structural tailoring and active aeroelastic control in the mass optimisation of wing structures. Therefore, in addition to the split aileron control surface layout studied in the previous chapter, a control surface layout employing a flaperon is investigated. The flaperon control surface layout consisting of five spoilers, one aileron and a flaperon is shown in Fig. 4.6.

For a fair comparison, the area of the flaperon is chosen to match the area of the inner aileron of the split aileron control surface layout. Furthermore, the position and size of the aileron in the flaperon control surface layout correspond to the position and size of the outer aileron used in the split aileron control surface layout. In addition, the arrangement and size of the spoilers are chosen to be similar to common control surface layouts employing a flaperon control surface.

All control surfaces are used for manoeuvre load alleviation. The aileron, flaperon and the three outermost spoilers are used for gust load alleviation. For simplicity, the deflection limits used for the flaperon and aileron are set to the aileron deflection limits used in the split aileron control surface layout described in Section 3.4.1.

Besides a concurrent optimisation of structural tailoring, active manoeuvre load

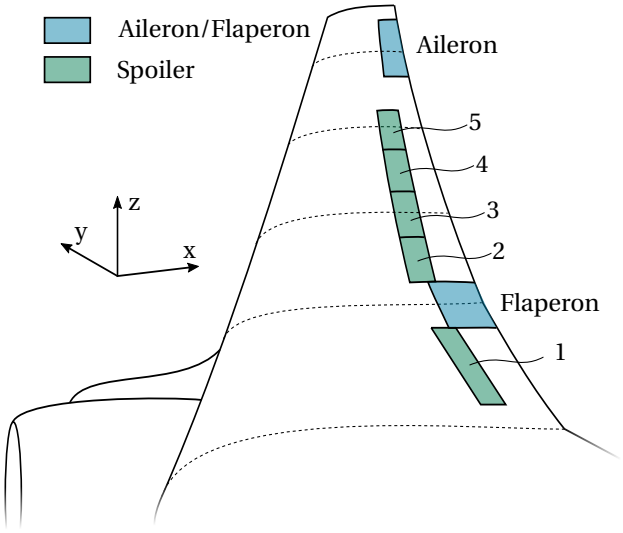

Figure 4.6: Schematic drawing of the flaperon control surface layout consisting of five spoilers (numbering as indicated), aileron and flaperon.

Table 4.3: Relative reduction in primary structural mass obtained in the different optimisation setups and for both control surface layouts.

Setup	Control Surface Layout	
	Split Aileron	Flaperon
N	Reference	
T	-7.5%	-7.5%
M	-25.5%	-22.9%
G	-0.4%	-0.5%
TM	-31.6%	-28.9%
TG	-7.7%	-7.7%
MG	-34.0%	-31.5%
TMG	-35.7%	-33.7%

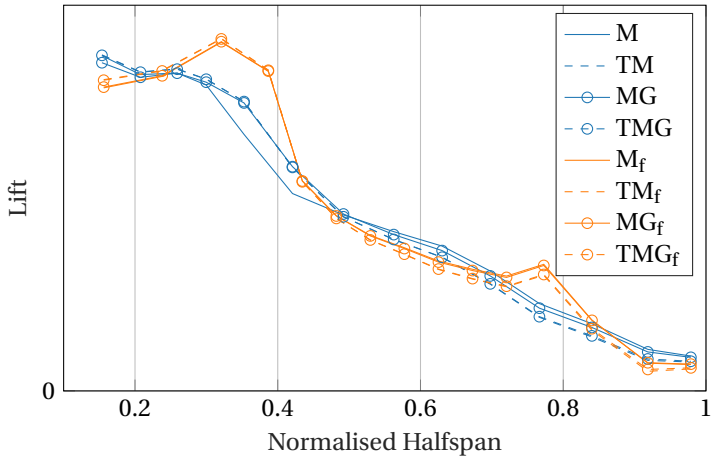

Figure 4.7: Lift distribution during the pull-up manoeuvre resulting from the optimisations including manoeuvre load alleviation (M, TM, MG and TMG) for both control surface layouts. The subscript f refers to the flaperon control surface layout.

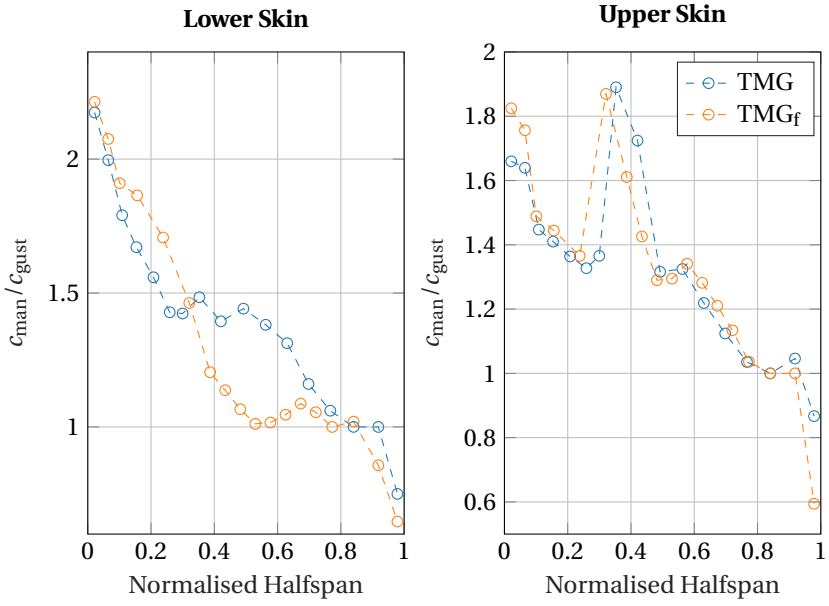

Figure 4.8: Spanwise distribution of the ratio between manoeuvre and gust constraints resulting in the TMG optimisation for both control surface layouts. The subscript f refers to the flaperon control surface layout.

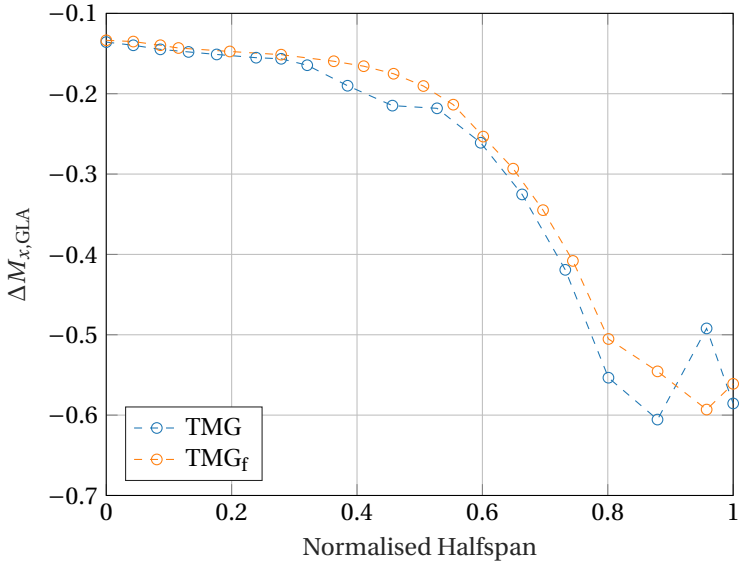

Figure 4.9: Relative difference between the open and closed loop spanwise maximum bending moment distribution during gust encounters for both control surface layouts. The subscript f refers to the flaperon control surface layout.

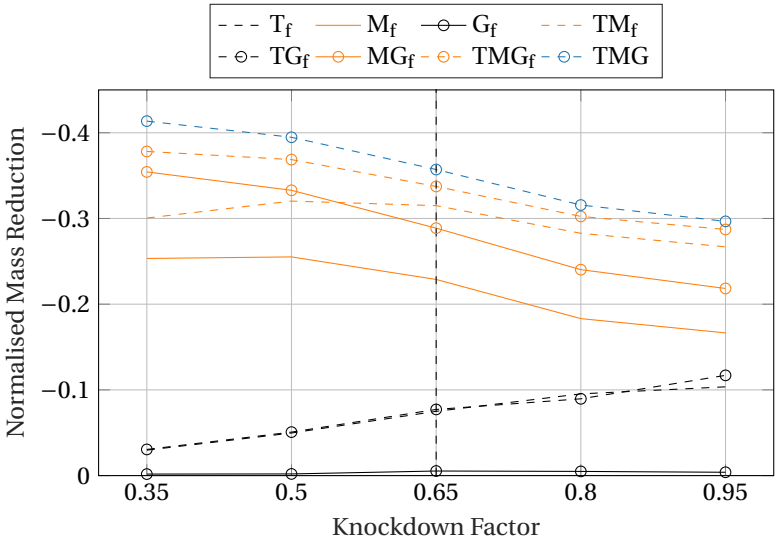

Figure 4.10: Influence of the material knockdown factor on the mass reduction normalised with respect to the N optimisations. The results of the TMG optimisation using the split aileron control surface layout are shown for comparison (no subscript).

alleviation and gust load alleviation, all combinations are considered. The resulting weight reduction normalised to the primary structural mass obtained by the optimisation without structural tailoring or active control (N) are shown in Table 4.3. As expected, individual structural tailoring is leading to the same weight reduction as the control surface layout does not affect the stiffness distribution in the absence of active control. Significant differences are only observed for the optimisations involving MLA (M, TM, MG and TMG). Here, the configuration with the split aileron control surface layout achieves a 2.0-2.7% higher normalised weight reduction. The main difference in the resulting designs is visible in the MLA deflections during the pull-up manoeuvre. In the split aileron configuration, both ailerons and the spoilers 2-6 are fully deflected upwards. In the flaperon configuration, the outer aileron and the spoilers 2-5 are fully deflected upwards to reduce the lift produced on the outer wing. The flaperon is fully deflected downwards to increase the lift produced close to the wing root. The difference in the resulting MLA design is visible in the lift distribution during the pull-up manoeuvre shown in Fig. 4.7. The downward deflection of the flaperon produces more lift in the area of the flaperon. Moreover, due to the gap between the outermost spoiler and the aileron, the lift at the outer wing cannot be reduced the same extent as observed with the split aileron configuration. The differences lead to a centre of pressure which is located more outboard for the flaperon configuration resulting in a higher bending moment close to the wing root. As it can be seen in Fig. 4.8 this higher bending moment increases the manoeuver to gust constraint ratio close to the wing root. Interestingly, for the upper skin fewer differences are observed. More outboard, the manoeuvre and gust constraints are more balanced compared to the split aileron configuration. This indicates that the gust loads in the outer wing area play a more critical role in the flaperon concept. As the underlying structural dynamics are nearly the same between the two configurations, the reason can be explained by the effectiveness of the resulting GLA system. The difference between the maximum gust induced bending moment between open and closed loop gust analysis is shown in Fig. 4.9. The split aileron concept is more effective in reducing the gust loads along the whole span.

Especially because of the following two reasons, the presented results should be handled with care. First, no maximum lift constraint is considered in the present study. The amount of lift produced by angle of attack in the split aileron configuration might be overestimated. A maximum lift constraint reduces the extent to which the centre of pressure is shifted inboard. Furthermore, as no aerodynamic model of the fuselage has been considered, the lift distribution close to the wing root is not realistic.

Nevertheless, the following examines the extent to which the results vary with a change in the material allowables. The influence of the material knockdown factor on the mass reduction achievable by the individual technologies and their combinations is given in Fig. 4.10. Besides all results of the flaperon concept, the results of the concurrent optimisation with the split aileron configuration are shown for comparison. In general, the results are comparable to the results obtained with the split aileron concept shown in the previous chapter in Fig. 3.21. The above discussed lower efficacy of the active control methods using the flaperon control surface layout is particularly noticeable at small knockdown factors (stiffer wing structures). This is in line with the results of the previous chapter where it was found that the added value of active control is most significant for

stiff structures where the efficacy of structural tailoring is less. With the variation in the knockdown factor from 0.35 to 0.95, the difference in the weight reduction achievable by concurrent optimisation between the two control surface layouts is reduced from 3.5% to 1.0%.

The results indicate that the main statements regarding the interaction of structural tailoring and active control made in the previous chapter are valid for different arrangements of the control surfaces. However, to fully exploit the potentials of active and passive methods for load alleviation, the integrated design of structural parameters, the control system and the control surface layout is required. Since incorporating the control surface layout in the design space requires appropriate constraints on the low speed handling qualities as well as high lift performance, the complexity of the optimisation problem will increase rapidly.

4.3. THE INFLUENCE OF AN ACTIVE WINGTIP DEVICE

Aerodynamically optimised winglets can significantly increase the lift-to-drag ratio by induced drag reduction. The benefit obtained by increased aerodynamic performance, however, is put in perspective by a higher structural wing weight that is required to sustain the increased loads during manoeuvres turbulent flight conditions [94]. An active winglet that comprises a trailing edge control surface offers the possibility to increase the overall benefit of the wingtip device. Among others, past studies covered the use of active winglets for primary flight control [95], mission performance improvement [96] or active load alleviation [94]. Within the recently concluded research project SARISTU, several aspects of design, manufacturing and full-scale testing of an active winglet were investigated to demonstrate it's technical feasibility [9]. The aim of the active winglet was twofold: reducing aerodynamic drag and optimising structural loads (fatigue and vibrational load control, turbulence, gusts and manoeuvre load alleviation, and wing load protection).

Due to mass, inertia and the additional required structure, large winglets significantly change the aeroelastic behaviour of aircraft wings. It is thereby expected that active winglets affect the interaction of structural tailoring and active aeroelastic control in the concurrent optimisation of wing structures. Only few application of structural tailoring on nonplanar configurations exist [97] [98]. Furthermore, no application of structural tailoring on a configuration comprising an active winglet has been found by the author.

Thus, the following presents an analysis of the interaction of structural tailoring and active aeroelastic control in the preliminary design of aircraft wings equipped with an active winglet. The results of Section 3.4 are serving as a baseline to which the new results are compared to.

A schematic drawing of the winglet is shown in Fig. 4.4 alongside with the control surface layout description. The span of the winglet corresponds to approximately eight per cent of the halfspan of the main wing. The winglet has a dihedral of 45° and can be considered as a non-horizontal span extension. The control surface (tab) spanning the whole winglet will be used for roll control, manoeuvre and gust load alleviation in the following optimisations. For simplicity, the same rate and deflection constraints are used for the tab as for the ailerons. The remainder of the control surface layout matches the control surface layout of the configuration without winglet.

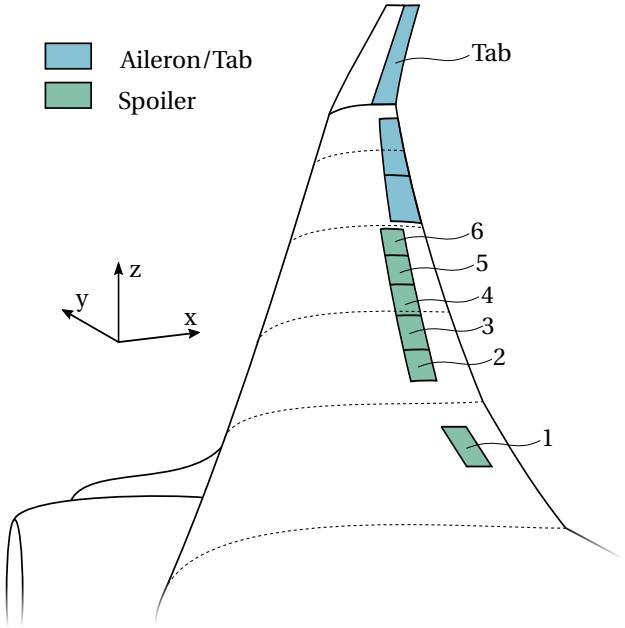

Figure 4.11: Schematic drawing of the control surface layout of the winglet configuration consisting of six spoilers (numbering as indicated), two ailerons (inner and outer) and a winglet tab.

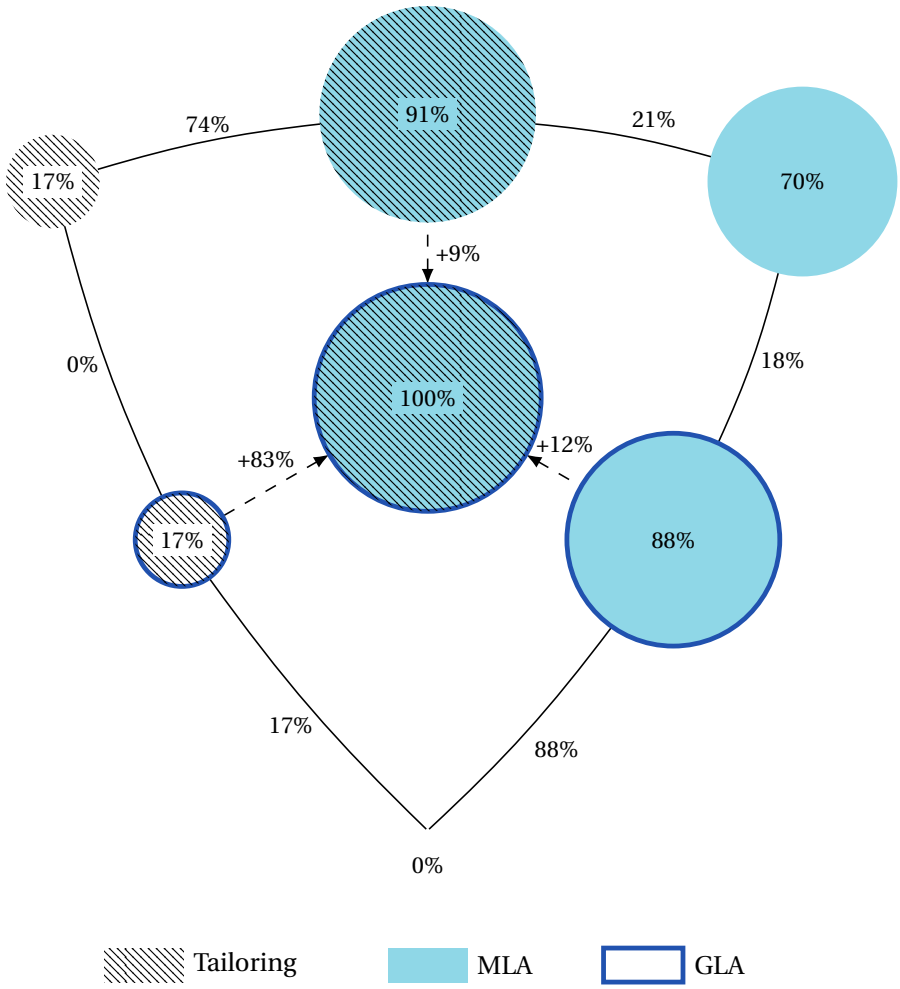

Figure 4.12: Normalised achievable mass reduction obtained in the optimisations of the configuration with winglet. The area of the circles corresponds to the normalised mass redution. 100% signifies the maximum achievable mass reduction combining structural tailoring, MLA and GLA.

Table 4.4: Reduction in primary structural mass obtained in the different optimisation setups and for the configuration with and without winglet. The reference for each configuration is the optimisation without structural tailoring and active control (N).

Setup	Configuration	
	without Winglet	with Winglet
N	Reference	
T	-7.5%	-5.9%
M	-25.5%	-24.7%
G	-0.4%	-0.0%
TM	-34.0%	-31.9%
TG	-7.7%	-6.0%
MG	-31.6%	-31.0%
TMG	-35.7%	-35.2%

Besides a concurrent optimisation of structural tailoring, active manoeuvre load alleviation and gust load alleviation, all combinations are considered. The normalised achievable mass reduction of the different optimisations is visualised in Fig. 4.12. Compared to the configuration without winglet 3.8, only minor differences are observed. The most significant difference is that GLA plays a more crucial role in the concurrent optimisation. The added value of GLA is nine per cent (TMG-TM) compared to four per cent that have been observed in the optimisations without active winglet. This effect can be partially explained by the additional control surface used in the configuration with the active winglet (tab).

The resulting weight reductions normalised to the primary structural mass obtained by the optimisations without structural tailoring or active control (N) are shown in Table 4.4. In general, the results with winglet are in good agreement with the results without winglet. It is notable that even though the configuration with winglet has an additional control surface (tab), the normalised weight reduction of the optimisation with active control (MG) is slightly lower. However, the effect of the winglet on the primary structural mass reduces the relative difference. In the optimisation without structural tailoring and active control (N), the primary structural mass of the winglet configuration is six per cent higher.

More notable differences are observed in the design driving constraints. Fig. 4.13 shows the ratio between the manoeuvre and gust constraints of the designs resulting from the concurrent optimisations with (TMG_w) and without winglet (TMG). With the winglet, the ratio of manoeuvre to gust constraints is decreased across the whole span of the wing, increasing the area of the wings' skins that are dimensioned by gust constraints. This explains the earlier mentioned effect that GLA is more effective when combined with structural tailoring and MLA (added value of GLA in TMG: nine per cent compared to five per cent without winglet).

Additionally, the dynamic damping constraint imposed at the design speed described in Section 3.3.2 is active for nearly all optimisations of the configuration with winglet. The resulting flutter speed margin is shown in Table 4.5. The flutter speed margin varies in the range of 0.1-1% for the cases where the damping constraint is active as the flutter speed

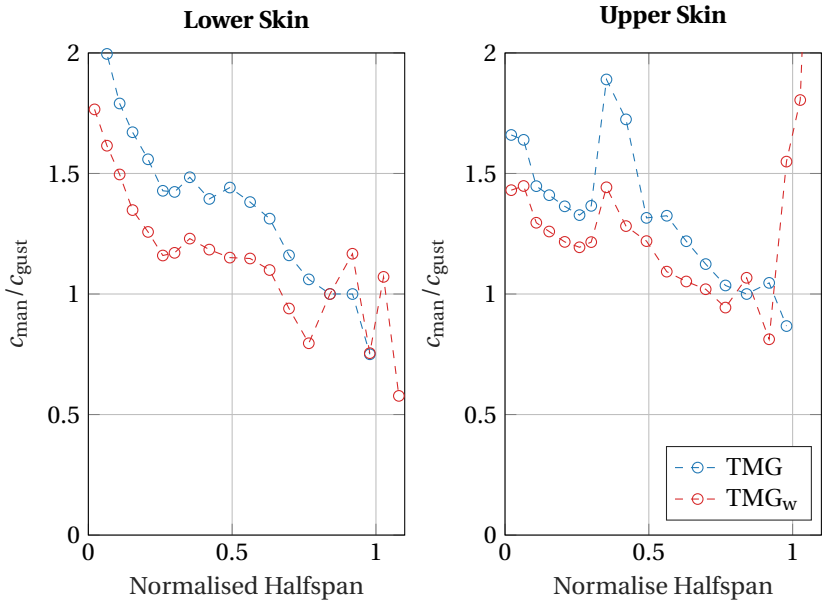

Figure 4.13: Spanwise distribution of the ratio between manoeuvre and gust constraints resulting in the TMG optimisation for both configurations with and without winglet. The subscript w refers to the configuration with winglet.

Table 4.5: Flutter speed margin normalised to the design speed V_{des}; Optimisations in which the damping constraint is active are highlighted

Setup	Configuration	
	without Winglet	with Winglet
N	27.9%	3.3%
T	27.1%	**1.0%**
M	29.9%	**0.4%**
G	23.7%	3.3%
TM	19.3%	**0.1%**
TG	26.3%	**1.0%**
MG	6.4%	**0.4%**
TMG	7.5%	**0.1%**

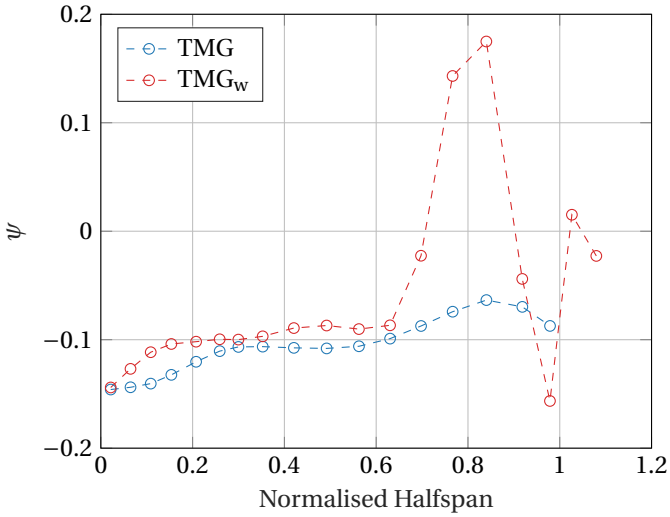

Figure 4.14: Spanwise distribution of the bending-torsion coupling parameter Ψ resulting from the TMG optimisations with (subscript w) and without winglet (no subscript).

is dependent on the damping gradient at the design speed. Also, the applied method of constraint aggregation for the damping constraints of all structural modes influences the resulting flutter speed margin slightly. In the optimisations with the winglet, the flutter speed margin is reduced by up to 30% of the design speed (M).

A possible reason for the reduced efficacy of structural tailoring in terms of weight reduction is, that a forward swept principal stiffness direction required for passive load alleviation might lead to an aeroelastic destabilisation. Hence, the optimiser can only utilise the passive load alleviation effect by structural tailoring until the flutter constraint becomes active. The spanwise distribution of the nondimensional bending-torsion coupling ratio Ψ of the designs resulting from the concurrent (TMG) optimisations with and without winglet is shown in Fig. 4.14. The amount of negative bending-torsion coupling is especially reduced between 70% and 90% of the normalised halfspan. To illustrate the difference in the mechanism of tailoring, Fig. 4.15 and 4.16 show the results of a flutter analysis of the designs resulting from the concurrent optimisations with and without winglet. The variation of the damping and frequency of the first six structural eigenmodes is therefore plotted over the velocity ratio V/V_{des}. Additionally, the flutter analysis is carried out with the principal stiffness direction angle set to zero ($\phi = 0$). It can be seen that, with winglet, the structural tailoring by changing the principal stiffness direction has a stronger stabilising effect. With winglet, structural tailoring increases the flutter speed more than 20% of the design speed compared to around seven per cent without winglet.

It should be emphasised that, for the optimisations carried out in this thesis, one chordwise design region was considered. Optimisations with more than one chordwise design region usually result in thickness distribution with the maximum thickness forward of the centre of the wingbox. This distribution has a stabilising effect on the dynamic

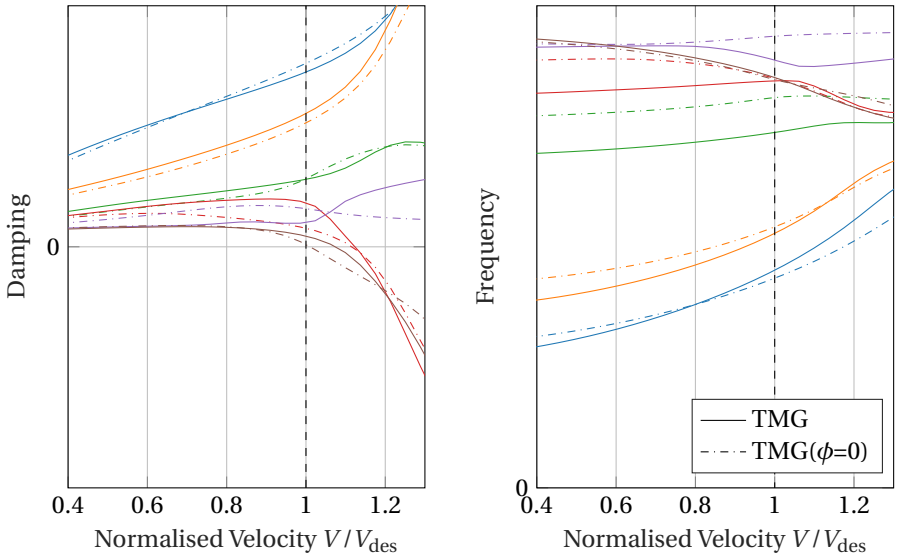

Figure 4.15: Damping and frequency of the first six structural eigenmodes over the flight velocity normalised by the design speed V/V_{des} for the configuration without winglet. Positive damping values indicate a flutter instability. Results are shown with and without the effect of structural tailoring in the structure resulting from the TMG optimisation.

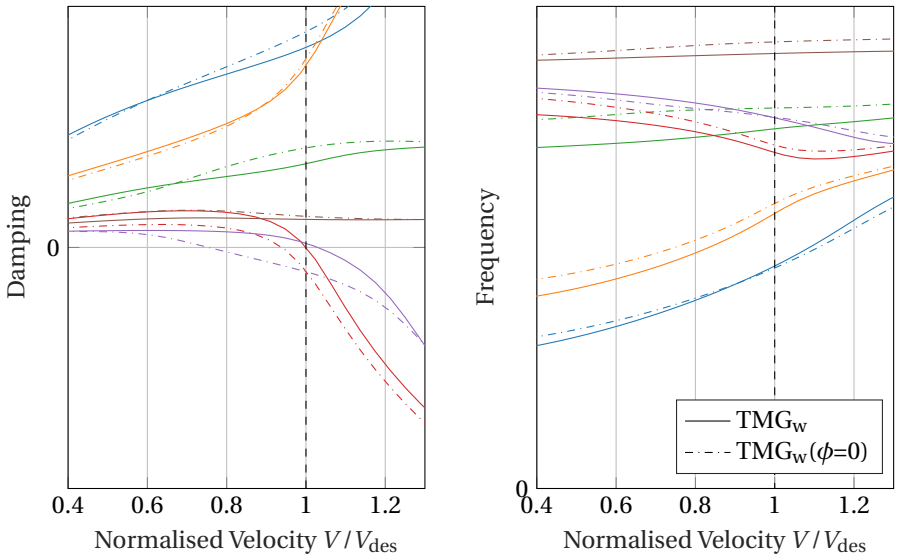

Figure 4.16: Damping and frequency of the first six structural eigenmodes over the flight velocity normalised to the design speed V/V_{des}) for the configuration with winglet. Positive damping values indicate a flutter instability. Results are shown with and without the effect of structural tailoring in the structure resulting from the TMG optimisation.

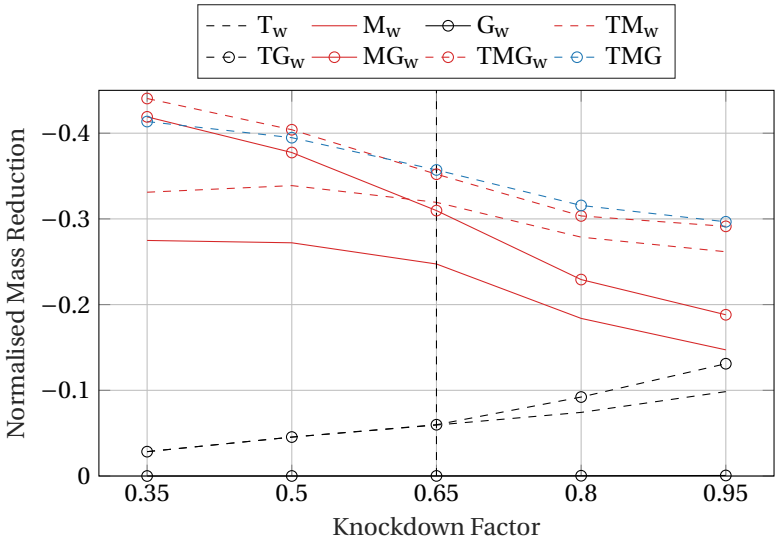

Figure 4.17: Influence of the material knockdown factor on the mass reduction normalised with respect to the N optimisations. The results of the TMG optimisation of the configuration without winglet are shown for comparison (no subscript).

aeroelastic behaviour. Furthermore, no damping augmentation system or flutter control law was considered. The inclusion of both increases the efficacy of structural tailoring in terms of weight reduction.

The extent to which the results vary with a change in the material allowables is examined in the following. The influence of the material knockdown factor on the mass reduction achievable by the individual technologies and their combinations is given in Fig. 4.17. For comparison, the results of the concurrent optimisation with the configuration without winglet are shown besides all results of the configuration with winglet.

While the trends agree well to the results of the configuration without winglet shown in Fig. 3.21, the shift from active to passive efficacy with the increasing knockdown factor is more pronounced. For lower knockdown factors, the active winglet results in a higher normalised mass saving compared to the standard configuration without winglet. This means that the active winglet can partially compensate the additional mass required for the winglet. For knockdown factors of 0.65 and higher, the achievable mass reduction obtained by the TMG optimisation with winglet is slightly below the level without winglet. With increasing flexibility, i.e. higher knockdown factors, the added value of GLA is significantly raised. This results from the increased vulnerability of the configuration with winglet to gust encounters. It is furthermore notable that for knockdown factors above 0.65, a synergistic effect of the combination of structural tailoring and GLA is observed. This means that opposed to the configuration without winglet, the individual structural tailoring does not increase the ratio between manoeuvre to gust constraints and gust conditions increasingly dimension the wing for higher knockdown factors. Thereby, the addition of GLA in the TG optimisation results in a higher weight reduction, which was

not the case for the configuration without winglet.

The analyses shown in this section reveal that a wingtip device influences not only the prevailing load hierarchy but also the mechanism of structural tailoring. In total, the added value of structural tailoring of wing structures becomes more significant with increasing flexibility. In the present case of an active winglet, the added value of active control (MLA and GLA) is particularly high for structures with lower flexibility, i.e. lower knockdown factors.

It should be noted, however, that in the optimisations of the winglet configuration, especially at high knockdown factors, more non-convexity of the objective function was observed. Several starting points were required to achieve the presented results. It can not be guaranteed that the results correspond to the respective global optima.

5

CONCLUSIONS

The most relevant results are summarized, and conclusions are drawn in order to answer the research question that is repeated here for the sake of clarity:

> *What is the benefit of including parameters of active manoeuvre and gust load control systems in the multidisciplinary design optimisation of aeroelastically tailored composite wing structures in the preliminary phases of aircraft design?*

Recommendations for further research activities resulting from the findings and open questions are subsequently given. Finally, a concluding remark is formulated to give an outlook on how the observed results will affect the future of preliminary aircraft design.

5.1. CONCLUSIONS

One of the core elements of this thesis was the development of an optimisation framework suitable for the preliminary design of actively controlled and aeroelastically tailored wing structures. An initial assessment of the existing tools and methods suggested that two existing toolchains should be combined in order to efficiently build a starting point and avoid time-consuming code reimplementation. The cross-sectional modelling capabilities of Proteus, a tool developed for the structural optimisation of aeroelastically tailored wing structures, were integrated into dAEDalus, a tool initially developed to investigate the effects of aeroelasticity on handling qualities during preliminary aircraft design. The resulting combination formed the basis for further developments.

The targeted simultaneous optimisation of aircraft structures and active control systems requires reduced order unsteady aerodynamic models to enable lower turnaround times that are needed in the preliminary design of aircraft. Ideally, these low order aerodynamic models can be used throughout the entire optimisation process and are therefore robust against changes in the respective design parameters. A method for the generation of aerodynamic models of reduced order was developed based on the combination of a

proven method for model order reduction of aerodynamic systems, the balanced proper orthogonal decomposition, and the concept of synthetic modes. Together with the model-order reduction algorithm, three different types of synthetic mode shapes for the use of input and output blending of the full-order model were formulated and then compared. It was shown that the use of synthetic mode shapes based on radial basis functions leads to the highest reduction of states of about two orders of magnitude compared to the full order model, and 77% compared to the model order reduction without prior input transformation using synthetic mode shapes. Only a handful of synthetic modes is sufficient to build one aerodynamic model that is accurate enough for preliminary aircraft design purposes, where radical changes of the structural characteristics and the control surface layout are frequent. From these results, it was concluded that only one previously created aerodynamic reduced order model is required that can be used for the application in the course of an entire aeroservoelastic optimisation carried out in the preliminary design phases of aircraft.

The second major part of the work on the optimisation framework was the integration of the active load control capabilities. Steady control surface deflections, which redistribute the aerodynamic loads during manoeuvres, were used for manoeuvre load alleviation. For gust load alleviation, a feed-forward control law was integrated by passing angle of attack measurements forward to the control surfaces. The consideration of boundary conditions of the actuation system, namely deflection and rate saturation, were included in the form of nonlinear constraint functions to enable the optimisation of the active control laws. By using the scheduling of the control surface deflections for manoeuvre load alleviation and the feed-forward filter properties as design variables, the controller functions were concurrently designed with the structural design parameters.

A third development of the toolchain was the improvement of the aerodynamic modelling of spoiler control surfaces. The proposed method improves the accuracy of low order aerodynamic models by employing a generalised spatial distribution law of the boundary condition that was derived from simulation data with higher accuracy. In the preliminary design of an aircraft, this methodology allows the investigation of multifunctional and innovative control surface layouts consisting of all types of control surfaces already used in current aircraft generations.

The developments resulted in the creation of an open-source preliminary design framework that allows the efficient optimisation of composite wing structures, including both, active and passive load alleviation. In particular, the possibility of using spoiler control surfaces for active load control extends state of the art. The applicability of the developed toolchain to preliminary aircraft design problems was demonstrated by performing various wing structure optimisations, which led to the findings and implications about the interaction between active and passive load control that is discussed in the following.

As mentioned in the introduction, not only the existing studies available in the literature but also the similarities in the effects and mechanisms of active and passive load alleviation indicate substantial interference and interaction when applied together in a single active adaptive wing concept.

Several optimisations of the wing structural mass of a conventional long-haul aircraft

configuration were performed to investigate the interaction thoroughly. The three load alleviation techniques, i.e. manoeuvre load alleviation, gust load alleviation and structural tailoring were, therefore, applied both individually, in pairs, and all together. To the author's knowledge, this is the first report of an integrated analysis that applied the three technologies to a configuration with a conventional control surface layout consisting of trailing edge control surfaces and spoilers.

The available results confirm the initial assumption that the simultaneous design optimisation of all three technologies leads to a higher mass reduction than any design incorporating only one or two of the technologies. Besides, it was shown that significant differences in the design of the technologies could be observed. From a detailed analysis of each of the resulting designs, it was concluded that the technologies adapt to the respective prevailing load hierarchy and active constraints driving the design. This important finding was particularly observed in the effect that structural tailoring has on the control surface efficiency: only when gust induced constraints are active and thus dominate the design, structural tailoring contributes to the efficiency of active gust load alleviation by reducing the bending torsional coupling to increase the efficiency of the outboard control surfaces.

With this finding, it can be concluded that the inclusion of parameters of active manoeuvre and gust load control systems in the multidisciplinary design optimisation of aeroelastically tailored composite wing structures (i) allows the exploitation of synergies between the technologies and (ii) reveals intuitively ungraspable mechanisms that are beneficial for the overall concept. A further conclusion, which mainly concerns the preliminary design of aircraft, is that the potential of each of the technologies can only be adequately assessed if other technologies are also considered in the optimisation process. If each of the technologies is assessed individually, their effect on mass reduction is substantially overestimated in the case of passive load alleviation by structural tailoring and underestimated in the case of active manoeuvre or gust load alleviation.

The stiffness of future aircraft structures will be significantly reduced, on the one hand by further exploiting the material properties due to more precise failure and environmental impact predictions and on the other hand by utilising advanced materials such as carbon nanotubes. The question of the extent to which the results found are influenced by the increased allowables and thereby increased flexibility was investigated by varying the knockdown factor applied to the material properties.

The variation of the knockdown factor showed that the interaction between active control and structural tailoring is, in fact, strongly dependent on the material properties. Especially concerning gust conditions, a substantial shift of effectiveness from active aeroelastic control to passive structural tailoring was observed in the less stiff wing designs resulting from increased allowables. While an increase in material allowables together with the utilisation of anisotropic material properties promises considerable mass savings, the added value of active gust load control is significantly reduced with the resulting increased flexibility.

The presented results further support the already concluded indispensability of an integrated preliminary design of active adaptive wings for two reasons. First, the interaction is strongly influenced by the overall flexibility of the structural concept that itself is

sometimes considered as a design decision taken at an early stage of the design process. Second, the use of new materials could exacerbate the overestimation of the effectiveness of structural tailoring observed when optimised without active control.

The promising perspectives resulting from an integrated design of active adaptive wings are contrasted by considerable computational effort and intensive cross-divisional collaboration. For this reason, the standard practice in preliminary design is still based on a separate or partially sequential and iterative development. The different approaches were compared to discuss possible differences in the resulting designs. In addition to a separate design approach, a semi-sequential design approach was proposed where subspaces are iteratively optimized in which the focus is placed on either active or passive load alleviation.

While the sequential design was inferior, the disciplines involved could be partially decoupled by the subdivision of the design space allowing a parallel development with iterative updates. This approach can be seen as an intermediate step which the preliminary design offices of aircraft manufacturers could take in order to gradually transition from their established way of working to integrated processes.

The result section ends with the investigation of the influence of two configurational changes that are characteristic for the preliminary design of aircraft: an alternative control surface layout and the incorporation of a large active winglet extending the span by 10%.

In terms of the control surface layout, the introduction of a flaperon control surface between the inboard and outboard flap led to very similar results compared to the conventional double aileron concept initially analysed. As expected, the effectiveness of active gust load control was slightly reduced in the flaperon concept, where only one aileron is attached to the wingtip. This was particularly noticeable with lower knock-down factors and stiffer structures, where active gust load alleviation was previously found to be of greater importance. However, the main findings of the interaction between active and passive load alleviation observed with the baseline configuration were confirmed.

The second configurational change was the addition of a large winglet with an additional control surface. The analyses showed that the winglet influences not only the prevailing load hierarchy but also the mechanism of structural tailoring. With the occurrence of a flutter instability, the optimiser not only utilises structural tailoring for weight reduction. It was shown that, when the flutter constraint was active the optimiser utilised the directional stiffness properties also to aeroelastically stabilise the design by reducing bending-torsion coupling that is beneficial for load alleviation. Thereby, with the winglet reducing the flutter speed, the possibility of aeroelastic tailoring for weight reduction, i.e. by increasing the wash-out generating bending-torsion coupling, is limited.

It is an important finding that the mechanism of structural tailoring can change depending on whether other technologies are included in the optimisation or not. From that, it was concluded that integrated design is required to allow each technology to adapt to the actual critical requirements during the design process.

5.2. RECOMMENDATIONS AND OUTLOOK

Recommendations for Future Work The developed optimisation framework provides a valuable basis for continuing studies on the field of integrated active adaptive wing design. However, the tool would benefit from several further developments and improvements, which are outlined here.

The studies with the active winglet showed that flutter is indeed a design constraining phenomenon that reduces the operational envelope of the resulting aircraft. Reliable aeroelastic analyses at this boundary of flight envelope require a precise consideration of compressible and transonic aerodynamic effects. The use of more accurate aerodynamic models or the application of correction methods would allow a more precise flutter prediction and thus the formulation of more accurate aeroelastic stability conditions Although it is expected that the developed method for generating reduced order aerodynamic models can also be applied to higher-order models, the verification of this assumption is the subject of further research.

With the possibility of accurate flutter point prediction, the natural next step is to include active flutter suppression controller functions in the collection of technologies to be optimised. Also, more considerable attention is recently devoted to actively adapting the lift distribution to improve performance in the various phases of flight. The integration of this technology in the optimisation would undoubtedly be beneficial for the resulting concept. Integrating active damping augmentation and cruise performance control extends the function catalogue of innovative multifunctional control surface layouts which are indispensable in the design of future active adaptive wing concepts.

With the integration of further technologies and the associated increase in the complexity of the optimisation problem, it becomes necessary to express further constraint functions and to detail the constraint functions already in use. According to the author's recommendation, these include in particular controller failure cases, continuous turbulence load conditions and low speed handling quality constraints. The latter becomes especially important when the resulting structural stiffness is reduced to a level that significantly reduces the effectiveness of control surfaces or when even control reversal occurs.

In addition to further developments in the field of aerodynamic modelling and active control, several further developments in the field of structural modelling are recommended. The distribution of the primary stiffness direction, approximated using Chebyshev polynomials, can lead to designs that are not manufacturable. This shortcoming can be eliminated by introducing blending constraints. By using more design zones, the effectiveness of structural tailoring can be improved, especially by realizing a variable thickness distribution in the chordwise direction. To further increase efficiency, the shape and geometry of stringers can be included in the design parameter space. On the other hand, a possibly not negligible design constraint is the consideration of the jig shape.

In addition to the extensions to the framework, further studies of the interaction between active and passive load alleviation can be carried out with the existing toolchain.

A prominent idea in terms of innovative control surface layouts is the use of small control surfaces or tabs with inversed effectiveness that when deflected twist a significant fraction of the wing and thus achieve a more substantial overall effect. None of the

optimisations performed in this thesis resulted in control surfaces with heavily inversed effectiveness. Initialising the optimisation with a design having inversed control surface effectiveness in one or more control surfaces could lead to different results indicating a non-convex design problem. While such concepts are in themselves an interesting area for future research, this would conversely require the use of gradient-free optimisation algorithms. Once again, the modelling of the optimisation problem for the gradient-free simultaneous optimisation of active adaptive wings forms an interesting field of research in its own.

In the conception of novel active adaptive wing concepts, other technologies not directly related to the structural concept or the field of active control might be considered as well. An interesting synergy between natural laminar flow with active load control was already found by Xu and Kroo [62]. The combination with the concept of structural tailoring might reveal interesting new aspects relevant for the design of future aircraft.

Outlook In order to be able to use the described potentials of current adaptive wing concepts resulting from integrated design, a rethinking in the minds of engineers of the different disciplines is necessary for addition to the technical developments recommended in the previous paragraph. The necessary transition from silo thinking to cooperative interdisciplinary work can take place using existing digital methods as soon as the people sitting behind the silos are readily taking the step. It is therefore not only increasing development costs due to the growing complexity but also human aspects that are delaying the introduction of intelligent adaptive wing concepts in modern aircraft design and production. Due to the almost unchecked climate change, the use of this and other potentials will not only be essential but necessary for the future of civil aviation.

A

Control Surface Deflection and Rate Signals

As mentioned in Section 3.4 this appendix presents the control surface deflections that result from the optimised gust load controller of the TMG optimisation. The deflection and rate signals are obtained after the filtered controller command signal is fed through the nonlinear actuator model.

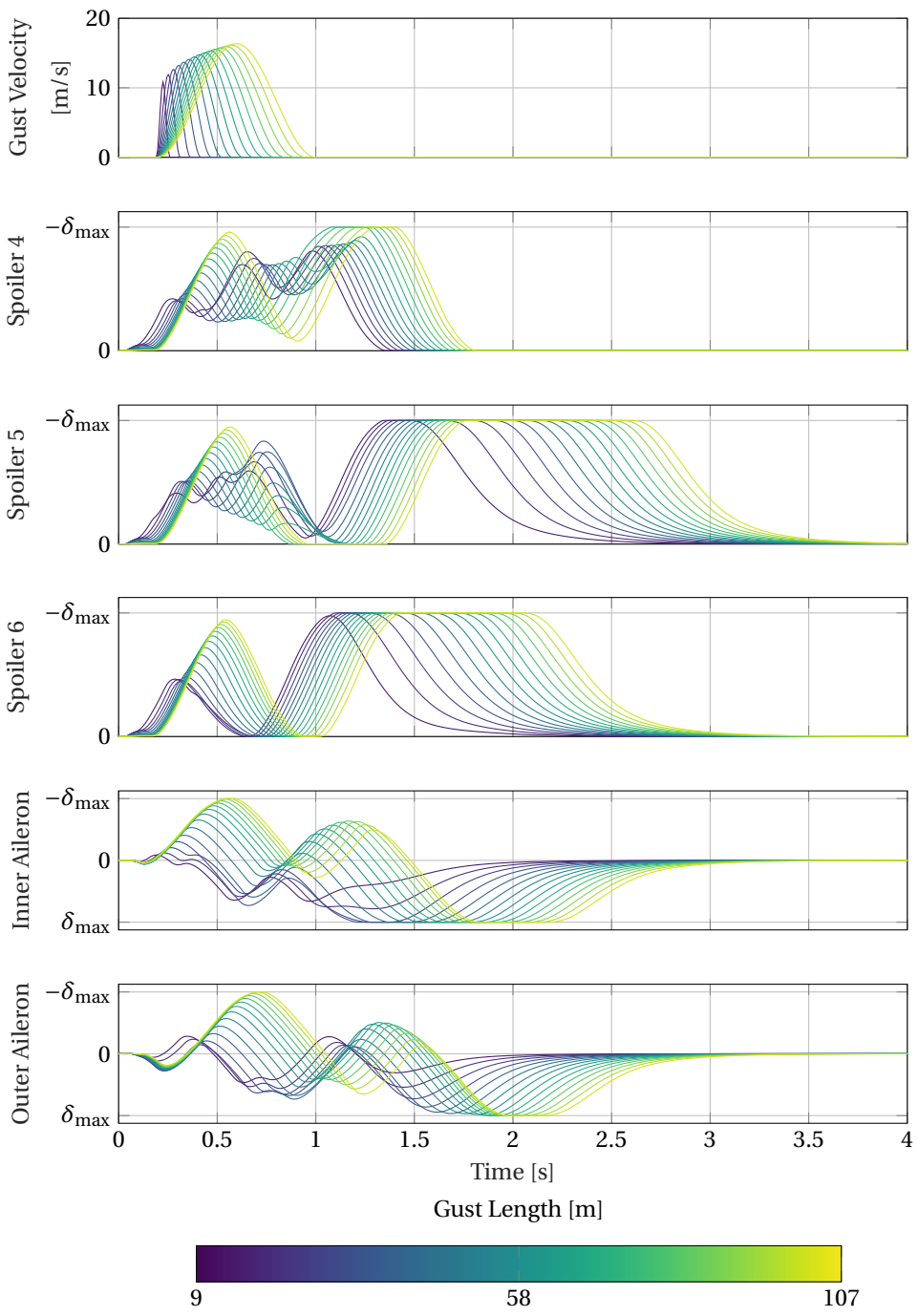

Figure A.1: Control surface deflections during updraught gusts for the gust lengths considered in the gust analysis. The deflection histories result from the TMG optimisation.

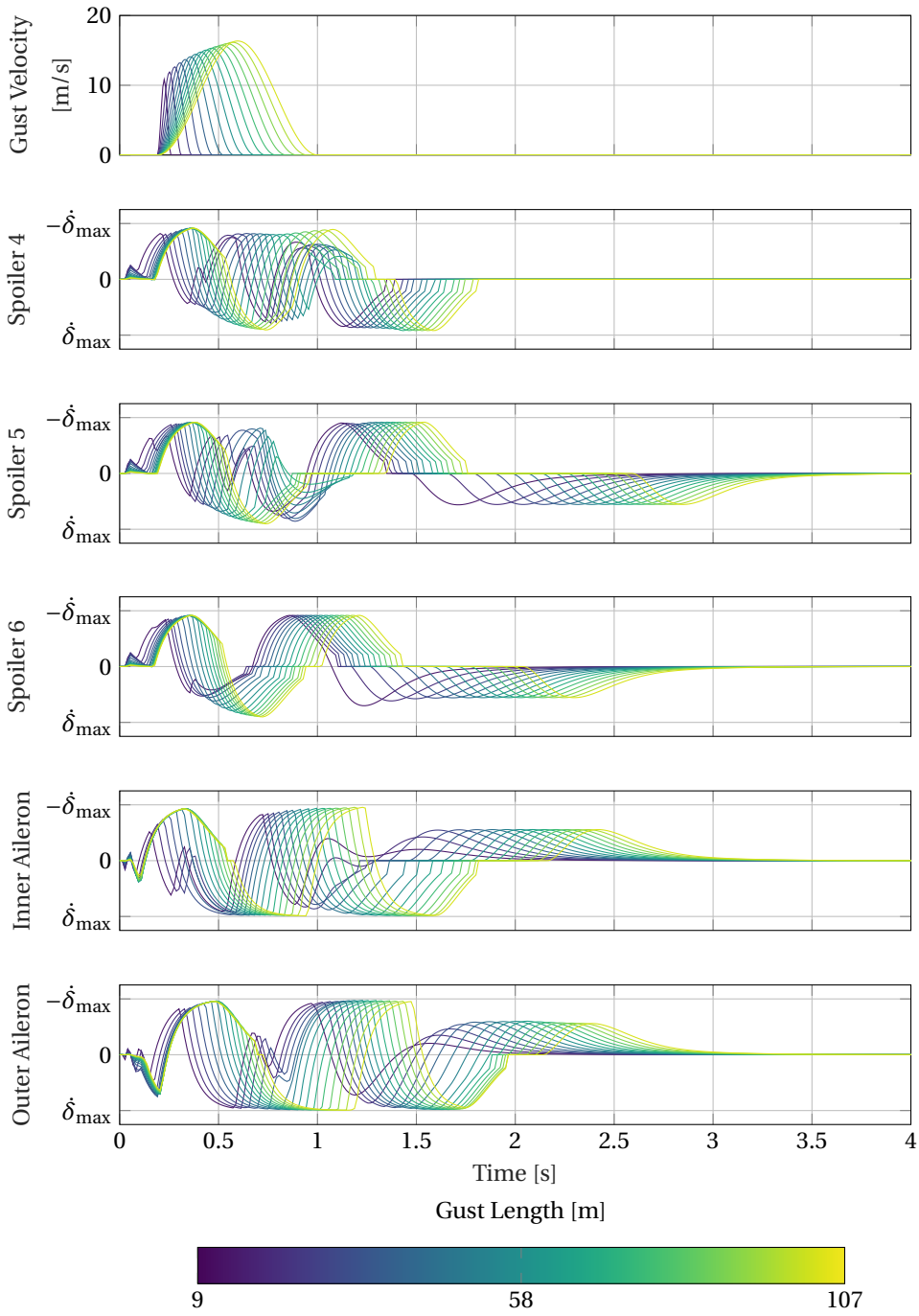

Figure A.2: Control surface rate signals during updraught gusts for the gust lengths considered in the gust analysis. The deflection histories result from the TMG optimisation.

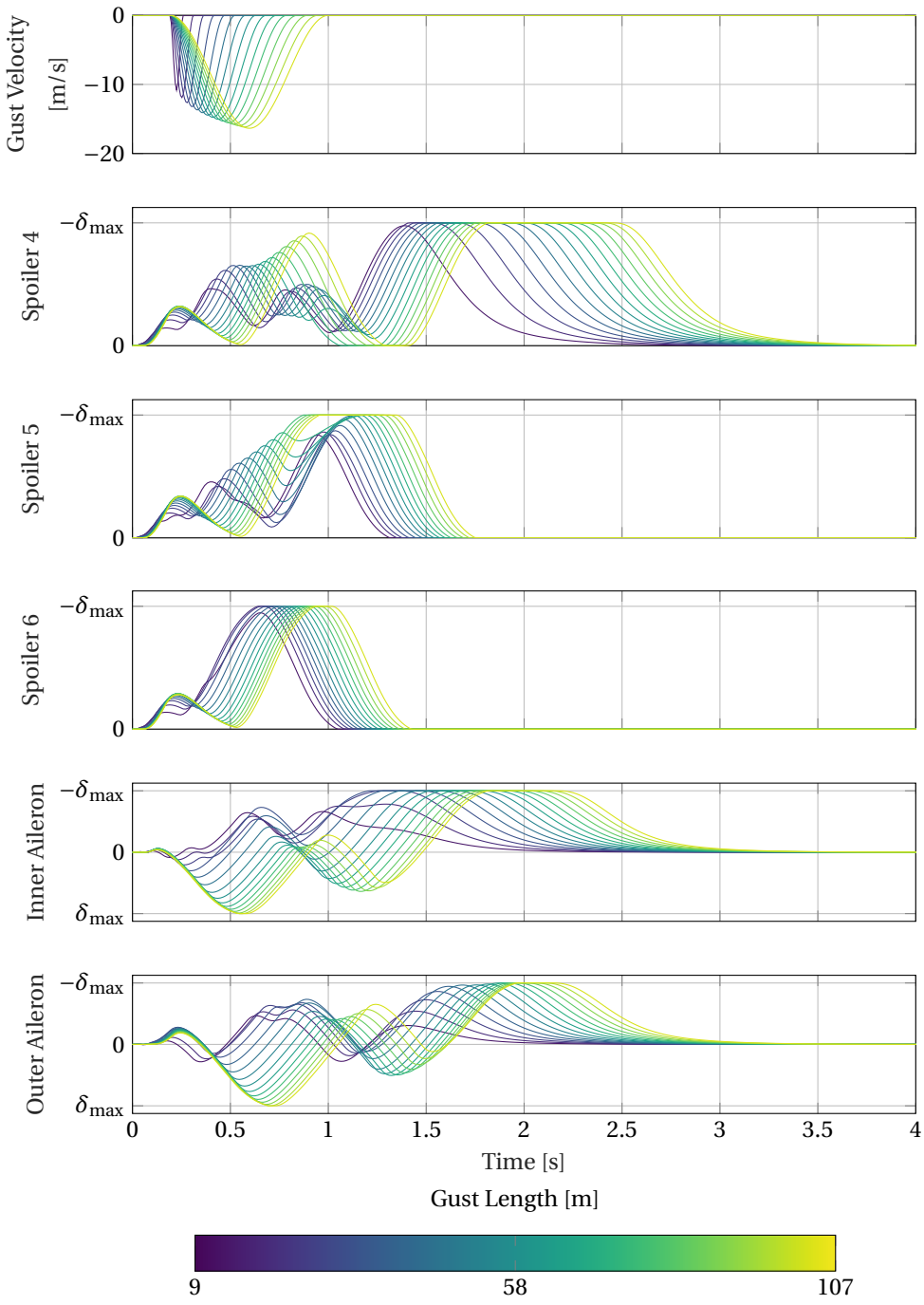

Figure A.3: Control surface deflections during downdraught gusts for the gust lengths considered in the gust analysis. The deflection histories result from the TMG optimisation.

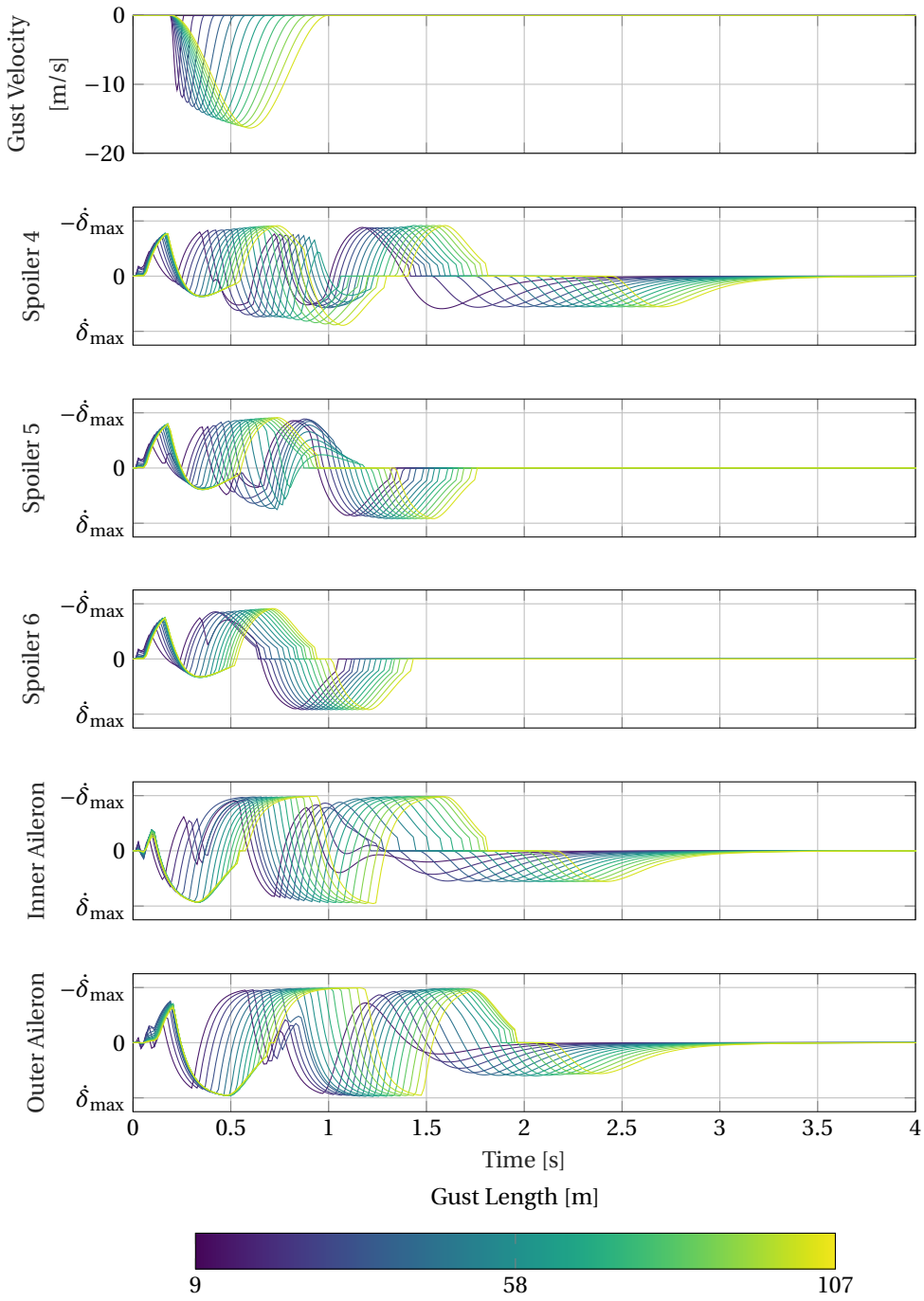

Figure A.4: Control surface rate signals during downdraught gusts for the gust lengths considered in the gust analysis. The deflection histories result from the TMG optimisation.

REFERENCES

[1] Airbus S.A.S., "Cities, airports & aircraft: Global market forecast 2019-2038," 2019.

[2] Boeing, "Commercial market outlook: 2019-2038," 2019.

[3] B. Graver, K. Zhang, and D. Rutherford, "Co2 emissions from commercial aviation 2018: Working paper 2019-16," *The International Council on Clean Transportation*, 2019.

[4] European Comission, "Flightpath 2050: Europes vision for aviation," 2011.

[5] International Energy Agency, "Transport, energy and co2: Moving toward sustainability," 2009. ISBN: 978-92-64-07316-6.

[6] D. Reckzeh, "Technologies for the future: Focusing on aircraft configuration design perspectives," *Deutscher Luft- und Raumfahrtkongress (DLRK)*, 2018.

[7] Boeing, "777x by design," http://www.boeing.com/commercial/777x/by-design/#/777-8-characteristics Accessed: 2020-04-29.

[8] M. M. Munk, "Laminated propeller: U.s. patent no. 2,599,718," 1949.

[9] P. C. Wölcken and M. Papadopoulos, *Smart Intelligent Aircraft Structures (SARISTU): Proceedings of the Final Project Conference*. Springer, 2016. https://doi.org/10.1007/978-3-319-22413-8.

[10] T. Wilson, J. Kirk, J. Hobday, and A. Castrichini, "Small scale flying demonstration of semi aeroelastic hinged wing tips," *International Forum on Aeroelasticity and Structural Dynamics*, 2019.

[11] D. Reckzeh, "Multifunctional wing movables: Design of the a350xwb and the way to future concepts," *29th Congress of the International Council of the Aeronautical Sciences (ICAS)*, 2014.

[12] M. Richardson, "Building things with wings," 2019. https://www.aero-mag.com/airbus-aircraft-wing-manufacturing-developments/ Accessed: 2020-04-29.

[13] K. Seywald, *Impact of Aeroelasticity on Flight Dynamics and Handling Qualities of Novel Aircraft Configurations: PhD Thesis*. 2016. ISBN: 978-3-8439-3076-5.

[14] N. P. M. Werter and R. De Breuker, "A novel dynamic aeroelastic framework for aeroelastic tailoring and structural optimisation," *Composite Structures*, vol. 158, pp. 369–386, 2016. https://doi.org/10.1016/j.compstruct.2016.09.044.

[15] B. Moore, "Principal component analysis in linear systems: Controllability, observability, and model reduction," *IEEE Transactions on Automatic Control*, vol. 26, no. 1, 1981. https://doi.org/10.1109/TAC.1981.1102568.

[16] E. Livne, "Integrated aeroservoelastic optimization: Status and direction," *Journal of Aircraft*, vol. 36, no. 1, pp. 122–145, 1999. https://doi.org/10.2514/2.2419.

[17] G. Berkooz, P. Holmes, and J. L. Lumley, "The proper orthogonal decomposition in the analysis of turbulent flows," *Annual Review of Fluid Mechanics*, vol. 25, no. 1, 1993. https://doi.org/10.1146/annurev.fl.25.010193.002543.

[18] C. W. Rowley, "Model reduction for fluids using balanced proper orthogonal decomposition," *International Journal of Bifurcation and Chaos*, vol. 15, no. 03, pp. 997–1013, 2005. https://doi.org/10.1142/S0218127405012429.

[19] Z. Ma, S. Ahuja, and C. W. Rowley, "Reduced order models for control of fluids using the eigensystem realization algorithm," *Theoretical and Computational Fluid Dynamics*, vol. 25, no. 1-4, pp. 233–247, 2011. https://doi.org/10.1007/s00162-010-0184-8.

[20] T. B. Thanh and K. Willcox, "Model reduction for large-scale cfd applications using balanced proper orthogonal decomposition," *17th AIAA Computational Fluid Dynamics Conference*, 2005. https://doi.org/10.2514/6.2005-4617.

[21] D. Rajpal, C. Kassapoglou, and R. De Breuker, "Aeroelastic optimization of composite wings subjected to fatigue loads," in *AIAA/ASCE/AHS/ASC Structures, Structural Dynamics, and Materials Conference*, 2018. https://doi.org/10.2514/6.2018-0227.

[22] C. L. Fenwick, D. P. Jones, and A. L. Gaitonde, "Consideration of reduced order model interpolation for aeroelastic design using structural modification," *18th AIAA Computational Fluid Dynamics Conference*, 2007. https://doi.org/10.2514/6.2007-3831.

[23] M. Karpel, "Multidisciplinary optimization of aeroservoelastic systems using reduced-size models," *Journal of Aircraft*, vol. 29, no. 5, pp. 939–946, 1992. https://doi.org/10.2514/3.46266.

[24] M. Karpel and D. Raveh, "Fictitious mass element in structural dynamics," *AIAA Journal*, vol. 34, no. 3, pp. 607–613, 1996. https://doi.org/10.2514/3.13111.

[25] M. Karpel, "Efficient vibration mode analysis of aircraft with multiple externalstore configurations," *Journal of Aircraft*, vol. 25, no. 8, pp. 747–751, 1988. https://doi.org/10.2514/3.45653.

[26] M. Karpel and B. Moulin, "Models for aeroservoelastic analysis with smart structures," *Journal of Aircraft*, vol. 41, no. 2, pp. 314–321, 2004. https://doi.org/10.2514/3.20514.

[27] R. Voss, L. Tichy, and R. Thormann, "A rom based flutter prediction process and its validation with a new reference model," *International Forum of Aeroelasticity and Structural Dynamics*, 2011.

[28] W. Zhang, K. Chen, and Z. Ye, "Unsteady aerodynamic reduced-order modeling of an aeroelastic wing using arbitrary mode shapes," *Journal of Fluids and Structures*, vol. 58, pp. 254–270, 2015. https://doi.org/10.1016/j.jfluidstructs.2015.07.007.

[29] M. Winter, F. M. Heckmeier, and C. Breitsamter, "Cfd-based aeroelastic reduced-order modeling robust to structural parameter variations," *Aerospace Science and Technology*, vol. 67, pp. 13–30, 2017. https://doi.org/10.1016/j.ast.2017.03.030.

[30] W. H. A. Schilders, H. Van Der Vorst, and J. Rommes, *Model Order Reduction: Theory, Research Aspects and Applications*. Springer, 2008. https://doi.org/10.1007/978-3-540-78841-6.

[31] M. G. Safonov and R. Y. Chiang, "A schur method for balanced-truncation model reduction," *IEEE Transactions on Automatic Control*, vol. 34, no. 7, pp. 729–733, 1989. https://doi.org/10.1109/9.29399.

[32] S. Gugercin and A. C. Antoulas, "A survey of model reduction by balanced truncation and some new results," *International Journal of Control*, vol. 77, no. 8, pp. 748–766, 2004. https://doi.org/10.1080/00207170410001713448.

[33] S. Lall, J. E. Marsden, and S. Glavaski, "Empirical model reduction of controlled nonlinear systems," *IFAC Proceedings Volumes*, vol. 32, no. 2, pp. 2598–2603, 1999. https://doi.org/10.1016/S1474-6670(17)56442-3.

[34] K. Pearson, "On lines and planes of closest fit to systems of points in space," *The London, Edinburgh, and Dublin Philosophical Magazine and Journal of Science*, vol. 2, no. 11, pp. 559–572, 1901. https://doi.org/10.1080/14786440109462720.

[35] L. Sirovich, "Turbulence and the dynamics of coherent structures. part 1: Coherent structures," *Quarterly of applied mathematics*, vol. 45, no. 3, pp. 561–571, 1987. https://doi.org/10.1090/qam/910462.

[36] P. Holmes, J. L. Lumley, G. Berkooz, and C. W. Rowley, *Turbulence, coherent structures, dynamical systems and symmetry*. Cambridge: Cambridge university press, 2012. https://doi.org/10.1017/CBO9780511919701.

[37] M. Ilak and C. W. Rowley, "Modeling of transitional channel flow using balanced proper orthogonal decomposition," *PHYSICS OF FLUIDS*, vol. 20, no. 3, 2008. https://doi.org/10.1063/1.2840197.

[38] F. T. Boesch and H. Prodinger, "Spanning tree formulas and chebyshev polynomials," *Graphs and Combinatorics*, vol. 2, no. 1, pp. 191–200, 1986. https://doi.org/10.1007/BF01788093.

[39] N. P. M. Werter, R. De Breuker, and M. M. Abdalla, "Continuous-time state-space unsteady aerodynamic modeling for efficient loads analysis," *AIAA Journal*, vol. 56, no. 3, pp. 905–916, 2018. https://doi.org/10.2514/1.J056068.

[40] S. Binder, A. Wildschek, and R. De Breuker, "Extension of the continuous time unsteady vortex lattice method for arbitrary motion, control surface deflection and induced drag calculation," *International Forum on Aeroelasticity and Structural Dynamics*, 2017.

[41] M. R. Waszak and D. K. Schmidt, "Flight dynamics of aeroelastic vehicles," *Journal of Aircraft*, vol. 25, no. 6, pp. 563–571, 1988. https://doi.org/10.2514/3.45623.

[42] European Union Aviation Safety Agency, "Certification specifications and acceptable means of compliance for large aeroplanes (cs-25): Amendment 23," 2019.

[43] D. Petersson and J. Löfberg, "Model reduction using a frequency-limited h2-cost," *Systems & Control Letters*, vol. 67, pp. 32–39, 2014. https://doi.org/10.1016/j.sysconle.2014.02.004.

[44] P. V. Kokotovic, R. E. O'Malley Jr., and P. Sannuti, "Singular perturbations and order reduction in control theory - an overview," *Automatica*, vol. 12, no. 2, pp. 123–132, 1976. https://doi.org/10.1016/0005-1098(76)90076-5.

[45] R. J. Allemang, "The modal assurance criterion – twenty years of use and abuse," *Sound and vibration*, vol. 37, no. 8, pp. 14–23, 2003.

[46] H. Rösner and K. Jockel-Miranda, "Airbus airframe – new technologies and management aspects," *Materialwissenschaft und Werkstofftechnik*, vol. 37, no. 9, pp. 768–772, 2006. https://doi.org/10.1002/mawe.200600062.

[47] M. H. Shirk, T. J. Hertz, and T. A. Weisshaar, "Aeroelastic tailoring - theory, practice, and promise," *Journal of Aircraft*, vol. 23, no. 1, pp. 6–18, 1986. https://doi.org/10.2514/3.45260.

[48] T. A. Weisshaar, "Aeroelastic tailoring - creative uses of unusual materials," in *AIAA/ASME/ASCE AHS 28th Structures, Structural Dynamics and Materials Conference*, 1987. https://doi.org/10.2514/6.1987-976.

[49] T.-U. Kim and I. H. Hwang, "Optimal design of composite wing subjected to gust loads," *Computers & Structures*, vol. 83, no. 19-20, pp. 1546–1554, 2005. https://doi.org/10.1016/j.compstruc.2005.02.002.

[50] G. K. W. Kenway and J. R. R. A. Martins, "Multipoint high-fidelity aerostructural optimization of a transport aircraft configuration," *Journal of Aircraft*, vol. 51, no. 1, pp. 144–160, 2014. https://doi.org/10.2514/1.C032150.

[51] J. K. S. Dillinger, M. M. Abdalla, T. Klimmek, and Z. Gürdal, "Static aeroelastic stiffness optimization and investigation of forward swept composite wings," in *World Congress on Structural and Multidisciplinary Optimization*, 2013.

[52] G. J. Kennedy and J. R. R. A. Martins, "A comparison of metallic and composite aircraft wings using aerostructural design optimization," in *AIAA Aviation Technology, Integration, and Operations (ATIO) Conference and 14th AIAA/ISSM*, 2012. https://doi.org/10.2514/6.2012-5475.

[53] T. Farsadi, D. Asadi, and H. Kurtaran, "Flutter improvement of a thin walled wing-engine system by applying curvilinear fiber path," *Aerospace Science and Technology*, vol. 93, p. 105353, 2019. https://doi.org/10.1016/j.ast.2019.105353.

[54] A. Viglietti, E. Zappino, and E. Carrera, "Free vibration analysis of variable angle-tow composite wing structures," *Aerospace Science and Technology*, vol. 92, pp. 114–125, 2019. https://doi.org/10.1016/j.ast.2019.05.068.

[55] O. Stodieck, J. E. Cooper, P. M. Weaver, and P. Kealy, "Aeroelastic tailoring of a representative wing box using tow-steered composites," *AIAA Journal*, vol. 55, no. 4, pp. 1425–1439, 2017. https://doi.org/10.2514/1.J055364.

[56] C. D. Regan and C. V. Jutte, "Survey of applications of active control technology for gust alleviation and new challenges for lighter-weight aircraft: Nasa/tm-2012-216008."

[57] T. A. Weisshaar, "Aeroelastic tailoring of forward swept composite wings," *Journal of Aircraft*, vol. 18, no. 8, pp. 669–676, 1981. https://doi.org/10.2514/3.57542.

[58] T. A. Zeiler and T. A. Weisshaar, "Integrated aeroservoelastic tailoring of lifting surfaces," *Journal of Aircraft*, vol. 25, no. 1, pp. 76–83, 1988. https://doi.org/10.2514/3.45544.

[59] L. Librescu, L. Meirovitch, and O. Song, "Integrated structural tailoring and control using adaptive materials for advanced aircraft wings," *Journal of Aircraft*, vol. 33, no. 1, pp. 203–213, 1996. https://doi.org/10.2514/3.46923.

[60] T. A. Weisshaar and D. K. Duke, "Induced drag reduction using aeroelastic tailoring with adaptive control surfaces," *Journal of Aircraft*, vol. 43, no. 1, pp. 157–164, 2006. https://doi.org/10.2514/1.12040.

[61] T. A. Weisshaar, D. K. Duke, and A. Dobbins, "Active aeroelastic tailoring with adaptive continuous control surfaces," in *AIAA Structures, Structural Dynamics, and Materials Conference and Exhibit*, 2000. https://doi.org/10.2514/6.2000-1619.

[62] J. Xu and I. Kroo, "Aircraft design with active load alleviation and natural laminar flow," *Journal of Aircraft*, vol. 51, no. 5, pp. 1532–1545, 2014. https://doi.org/10.2514/1.C032402.

[63] B. K. Stanford, C. D. Wieseman, and C. V. Jutte, "Aeroelastic tailoring of transport wings including transonic flutter constraints," in *AIAA/ASCE/AHS/ASC Structures, Structural Dynamics, and Materials Conference*, 2015. https://doi.org/10.2514/6.2015-1127.

[64] B. K. Stanford, "Optimization of an aeroservoelastic wing with distributed multiple control surfaces," *Journal of Aircraft*, vol. 53, no. 4, pp. 1131–1144, 2016. https://doi.org/10.2514/1.C033613.

[65] B. K. Stanford, "Static and dynamic aeroelastic tailoring with variable-camber control," *Journal of Guidance, Control, and Dynamics*, vol. 39, no. 11, pp. 2522–2534, 2016. https://doi.org/10.2514/1.G000413.

[66] B. K. Stanford, "Aeroservoelastic optimization under stochastic gust constraints," in *AIAA Applied Aerodynamics Conference*, 2018. https://doi.org/10.2514/6.2018-2837.

[67] D. A. Burdette and J. R. R. A. Martins, "Design of a transonic wing with an adaptive morphing trailing edge via aerostructural optimization," *Aerospace Science and Technology*, vol. 81, pp. 192–203, 2018. https://10.1016/j.ast.2018.08.004.

[68] V. H. Handojo, P. Lancelot, and R. De Breuker, "Implementation of active and passive load alleviation methods on a generic mid-range aircraft configuration," in *AIAA Multidisciplinary Analysis and Optimization*, 2018. https://https://doi.org/10.2514/6.2018-3573.

[69] N. P. M. Werter, *Aeroelastic Modelling and Design of Aeroelastically Tailored and Morphing Wings: PhD Thesis*. 2017. https://doi.org/10.4233/uuid:74925f40-1efc-469f-88ee-e871c720047e.

[70] E. P. Krupa, J. E. Cooper, A. Pirrera, and R. Nangia, "Improved aerostructural performance via aeroservoelastic tailoring of a composite wing," *The Aeronautical Journal*, vol. 122, no. 1255, pp. 1442–1474, 2018. https://doi.org/10.1017/aer.2018.66.

[71] E. A. Ferede and M. M. Abdalla, "Cross-sectional modelling of thin-walled composite beams," in *AIAA/ASME/ASCE/AHS/ASC Structures, Structural Dynamics, and Materials Conference*, 2014. https://doi.org/10.2514/6.2014-0163.

[72] S. G. Hedman, "Vortex lattice method for calculation of quasi steady state loadsings on thin elastic wings in subsonic flow: Ffa report 105," *The Aeronautical Research Institute of Sweden*, no. FFA Report 105, 1966.

[73] M. Mohammadi-Amin, B. Ghadiri, M. M. Abdalla, H. Haddadpour, and R. De Breuker, "Continuous-time state-space unsteady aerodynamic modeling based on boundary element method," *Engineering Analysis with Boundary Elements*, vol. 36, no. 5, pp. 789–798, 2012. https://doi.org/10.1016/j.enganabound.2011.12.007.

[74] N. P. M. Werter, R. De Breuker, and M. M. Abdalla, "Continuous-time state-space unsteady aerodynamic modeling for efficient loads analysis," in *International Forum on Aeroelasticity and Structural Dynamics*, 2015.

[75] S. Binder, A. Wildschek, and R. De Breuker, "Extension of the continuous time unsteady vortex lattice method for arbitrary motion, control surface deflection and

induced drag calculation," in *International Forum on Aeroelasticity and Structural Dynamics*, 2017.

[76] J. Vassberg, M. Dehaan, M. Rivers, and R. Wahls, "Development of a common research model for applied cfd validation studies," in *26th AIAA Applied Aerodynamics Conference*, ([Reston, VA]), p. 2001, [American Institute of Aeronautics and Astronautics], 2008. https://doi.org/10.2514/6.2008-6919.

[77] D. Rajpal, E. Gillebaart, and R. De Breuker, "Preliminary aeroelastic design of composite wings subjected to critical gust loads," *Aerospace Science and Technology*, vol. 85, pp. 96–112, 2019. https://doi.org/10.1016/j.ast.2018.11.051.

[78] S. Binder, A. Wildschek, and R. De Breuker, "Unsteady aerodynamic model order reduction for aeroservoelastic optimisation by balanced proper orthogonal decomposition and the use of synthetic mode shapes," *Journal of Aeroelasticity and Structural Dynamics*, vol. 6, no. 1, pp. 43–72, 2018. https://doi.org/10.3293/asdj.2018.49.

[79] S. Binder, A. Wildschek, and R. De Breuker, "Aeroelastic stability analysis of the flexop demonstrator using the continuous time unsteady vortex lattice method," in *AIAA/ASCE/AHS/ASC Structures, Structural Dynamics, and Materials Conference*, 2018. https://doi.org/10.2514/6.2018-0950.

[80] S. J. Elliot, *Signal Processing for Active Control*. Elsevier, 2001. https://doi.org/10.1016/B978-0-12-237085-4.X5000-5.

[81] S. T. IJsselmuiden, M. M. Abdalla, and Z. Gürdal, "Implementation of strength-based failure criteria in the lamination parameter design space," *AIAA Journal*, vol. 46, no. 7, pp. 1826–1834, 2008. https://doi.org/10.2514/1.35565.

[82] J. K. S. Dillinger, T. Klimmek, M. M. Abdalla, and Z. Gürdal, "Stiffness optimization of composite wings with aeroelastic constraints," *Journal of Aircraft*, vol. 50, no. 4, pp. 1159–1168, 2013. https://doi.org/10.2514/1.C032084.

[83] G. Kreisselmeier and R. Steinhauser, "Systematic control design by optimizing a vector performance index," *Computer aided design of control systems*, pp. 113–117, 1980. https://doi.org/10.1016/B978-0-08-024488-4.50022-X.

[84] A. B. Lambe and J. R. Martins, "Extensions to the design structure matrix for the description of multidisciplinary design, analysis, and optimization processes," *Structural and Multidisciplinary Optimization*, vol. 46, no. 2, pp. 273–284, 2012. https://doi.org/10.1007/s00158-012-0763-y.

[85] B. K. Stanford, "Optimal control surface layout for an aeroservoelastic wingbox," *AIAA Journal*, vol. 55, no. 12, pp. 4347–4356, 2017. https://doi.org/10.2514/1.J056070.

[86] A. Wildschek, *An Adaptive Feed-Forward Controller for Active Wing Bending Vibration Alleviation on Large Transport Aircraft: PhD Thesis*. 2008.

[87] C. Kassapoglou, *Design and Analysis of Composite Structures: With Applications to Aerospace Structures*. John Wiley & Sons, 2013. https://doi.org/10.1002/9781118536933.

[88] G. J. Kennedy, G. K. W. Kenway, and J. R. R. A. Martins, "High aspect ratio wing design: Optimal aerostructural tradeoffs for the next generation of materials," in *AIAA Aerospace Sciences Meeting*, 2014. https://doi.org/10.2514/6.2014-0596.

[89] T. R. Brooks and J. R. R. A. Martins, "High-fidelity multipoint aerostructural optimization of a high aspect ratio tow-steered composite wing," in *AIAA/ASCE/AHS/ASC Structures, Structural Dynamics, and Materials Conference*, 2017. https://doi.org/10.2514/6.2017-1350.

[90] K. R. B. Bramsiepe, V. H. Handojo, Y. M. Meddaikar, M. Schulze, and T. Klimmek, "Loads and structural optimisation process for composite long range transport aircraft configuration," in *AIAA Multidisciplinary Analysis and Optimization*, 2018. https://doi.org/10.2514/6.2018-3572.

[91] B. Grossman, Z. Gürdal, R. T. Haftka, G. J. Strauch, and W. M. Eppard, "Integrated aerodynamic/structural design of a sailplane wing," *Journal of Aircraft*, vol. 25, no. 9, pp. 855–860, 1988. https://doi.org/10.2514/3.45670.

[92] J. Sobieszczanski-Sobieski and R. T. Haftka, "Multidisciplinary aerospace design optimization survey of recent developments," in *AIAA Aerospace Sciences Meeting and Exhibit*, 1996. https://doi.org/10.2514/6.1996-711.

[93] S. P. Zink, D. E. Raveh, and D. N. Mavris, "Integrated trim and structural design process for active aeroelastic wing technology," *Journal of Aircraft*, vol. 40, no. 3, pp. 523–531, 2003. https://doi.org/10.2514/2.3126.

[94] A. Wildschek, "Concurrent optimization of a feed-forward gust loads controller and minimization of wing box structural mass on an aircraft with active winglets," in *AIAA/ISSMO Multidisciplinary Analysis and Optimization Conference*, 2015. https://doi.org/10.2514/6.2015-2490.

[95] P. Bourdin, A. Gatto, and M. I. Friswell, "The application of variable cant angle winglets for morphing aircraft control," in *AIAA Applied Aerodynamics Conference*, 2006. https://doi.org/10.2514/6.2006-3660.

[96] N. M. Ursache, T. Melin, A. T. Isikveren, and M. I. Friswell, "Morphing winglets for aircraft multi-phase improvement," in *AIAA Aviation Technology, Integration and Operations Conference (ATIO)*, 2007. https://doi.org/10.2514/6.2007-7813.

[97] D. Gimmestad, "Aeroelastic tailoring of a composite winglet for kc-135," in *Dynamics Specialists Conference*, 1981. https://doi.org/10.2514/6.1981-607.

[98] T. A. Weisshaar, "Aeroelastic tailoring of joined-wing configurations," in *AIAA/ASME/ASCE/AHS/ASC Structures, Structural Dynamics, and Materials Conference*, 2002. https://doi.org/10.2514/6.2002-1207.

CURRICULUM VITÆ

Simon BINDER

01-08-1988	Born in Filderstadt, Germany.

EDUCATION

1998–2007	Grammar School Ludwing-Uhland Gymnasium, Kirchheim unter Teck, Germany
2007–2013	Diploma in Aerospace Technische Universität München, Munich, Germany
2011–2012	Course Study in Flight Vehicle Design Beihang University, Beijing, China
2015–2021	PhD in Aerospace Technical University of Delft, Delft, Netherlands *Thesis:* Simultaneous Optimisation of Composite Wing Structures and Control Systems for Active and Passive Load Alleviation *Promotor:* Dr. R. De Breuker Prof. Dr. C. Bisagni

PROFESSIONAL EXPERIENCE

2013–2015	Aerodynamicist KLK Motorsport GmbH, Hohenthann, Germany
2015–2019	PhD Student and Research Engineer Airbus Group Innovations, Munich, Germany
2019–present	Research Associate German Aerospace Center, Munich, Germany

LIST OF PUBLICATIONS

6. **S. Binder**, A. Wildschek, R. De Breuker *The Interaction Between Active Aeroelastic Control and Structural Tailoring in Aeroservoelastic Wing Design*, Aerospace Science and Technology, Vol. 110, No. 106516, 2021, DOI:10.1016/j.ast.2021.106516

5. **S. Binder**, A. Wildschek, R. De Breuker *Unsteady Aerodynamic Model Order Reduction for Aeroservoelastic Optimisation by Balanced Proper Orthogonal Decomposition and the use of Synthetic Mode Shapes*, Journal of Aeroelasticity and Structural Dynamics, Vol.6 No.1 pp. 43-72, 2018, DOI: 10.3293/asdj.2018.49

4. **S. Binder**, A. Wildschek, R. De Breuker *Aeroelastic Stability Analysis of the FLEXOP Demonstrator using the Continuous Time Unsteady Vortex Lattice Method*, AIAA/ASCE/AHS/ASC Structures, Structural Dynamics, and Materials Conference, Orlando, Florida, USA 2018, DOI: 10.2514/6.2018-0950

3. R. De Breuker, **S. Binder**, A. Wildschek *Combined Active and Passive Loads Alleviation through Aeroelastic Tailoring and Control Surface/Control System Optimization*, AIAA Aerospace Sciences Meeting, Orlando, Florida, USA 2018, DOI: 10.2514/6.2018-0764

2. **S. Binder**, A. Wildschek, R. De Breuker *Extension of the Continuous Time Unsteady Vortex Lattice Method for Arbitrary Motion, Control Surface Deflection and Induced Drag Calculation*, International Forum on Aeroelasticity and Structural Dynamics, Como, Italy 2017

1. D. Paulus, **S. Binder**, Ö. Petersson, H. Baier, M. Hornung *The Integration of an Efficient High Lift System in the Design Process of a Blended Wing Body Aircraft*, 12th AIAA Aviation Technology, Integration, and Operations (ATIO) Conference and 14th AIAA/ISSMO Multidisciplinary Analysis and Optimization Conference, Indianapolis, USA 2012, DOI: 10.2514/6.2012-5650